Modelling transport through biological environments that contain obstacles

A THESIS SUBMITTED TO

THE SCIENCE AND ENGINEERING FACULTY

OF THE QUEENSLAND UNIVERSITY OF TECHNOLOGY

IN FULFILMENT OF THE REQUIREMENTS FOR THE DEGREE OF

DOCTOR OF PHILOSOPHY

Adam James Ellery *BAppSc BMath (Hons)*

School of Mathematical Sciences

Science and Engineering Faculty

The Queensland University of Technology

March 2017

Statement of Original Authorship

The work contained in this thesis has not been previously submitted to meet requirements for an award at this or any other higher education institution. To the best of my knowledge and belief, the thesis contains no material previously published or written by another person except where due reference is made.

Signature:

Date:

To my family

Abstract

Transport through biological environments that are densely crowded with obstacles is often classified as anomalous, rather than Fickian diffusion. Researchers often describe these transport processes using either a random walk model or a fractional order differential equation model. To explore these ideas, we simulate a single agent migrating through a crowded environment that is populated by impenetrable immobile obstacles and examine averaged mean squared displacement data. We also simulate the transport of a population of such agents through a similar crowded environment and attempt to match population density data to the solution of a related fractional order differential equation. Our work suggests that it may be inappropriate to model the transport of either a single agent, or a population of agents through a crowded environment using these standard approaches. We conclude that, despite the ubiquitous use of fractional differential equations, that these modelling frameworks must be used with care. To build on our simulation-based results, we also develop a new analytical method, based on the theory of Markov chains, for modelling the transport of an agent through a crowded environment. Using our new method, we calculate the exact long-time diffusivity as well as the crossover time, which is the time scale required for the transport process to effectively become Fickian. Finally, we extend our new model to include interactions between the motile agent and the obstacles such as adhesion and repulsion.

Acknowledgments

I would like to express my appreciation and gratitude to PROFESSOR MATTHEW SIMPSON. You have been a tremendous mentor to me and I am grateful for your guidance throughout my doctoral studies as well as the generosity with which you have offered your time to further my education.

I would also like to thank PROFESSOR SCOTT MCCUE and PROFESSOR RUTH BAKER for their help, assistance and their invaluable insights over the years of my studies, PROFESSOR TROY FARRELL, PROFESSOR IAN TURNER and DR STEVEN HUGHES for their help and inspiration with other projects, all the staff in the QUT School of Mathematics, who work so hard to help the post-graduate and under-graduate communities, as well as the student body. I also acknowledge assistance and resources provided by the High Performance Computing and Research Support group at QUT. Fellow PhD students who have offered comradeship: MR. RAVINDRA PETHIYAGODA, MR. WANG JIN, MR. MICHAEL JACKSON and my various peers.

I am also grateful to several professional associations, especially the CSIRO and ANZIAM, for offering me financial assistance so that I could travel to the ANZIAM conferences and relate my research to the wider mathematical community in Australia and New Zealand. I would like to thank the Australian Commonwealth, whose generous APA scholarship financed my doctoral research. Finally, I appreciate support from the Australian Research Council (DP140100249, FT130100148) which contributed to the content of Chapters 2–7 as well as several publications [1–3].

Thank you to friends outside the academic world for their support and advice. I am extremely grateful to my family, especially my MUM, DAD and JASON and KRISTY. Your continual love and support means the world to me.

Table of Contents

Nomenclature

Acronyms

CTRW   Continuous time random walk

FDE   Fractional order differential equation

PDE   Partial differential equation

MAT   Mean action time

MSD   Mean squared displacement

RW   Random walk

Chapter 1

Introduction

1.1 Overview

It is well known in the literature [4–9] that the transport of cells through environments that are densely crowded by obstacles is not linear Fickian diffusion because the obstacles act as blockages that hinder the rate at which transport can take place [4, 7, 10]. Because biological environments are densely crowded with cells and macromolecules, it is believed that crowding may play an important role in the motion of cells and some macromolecules, such as proteins [4, 6]. At present, the quantitative effect that crowding has on transport through biological environments is poorly understood [4]. As a result, there is great interest in accurate mathematical models of crowding and of transport through crowded environments within the mathematical biology community, as these models may provide valuable insights into the physical behaviour of motile agents in these systems [8]. Previous studies have sought to describe transport through crowded environments using either lattice–based time random walk (RW) models [11–17] or fractional order differential equation (FDE) models [8, 10, 18–20].

Early RW models of transport in crowded environments were motivated by the problem of modelling the transport of charge in complex amorphous solids. Montroll and Weiss [21] and Scher and Lax [22] instigated a investigation of this problem and developed a continuous–time random walk (CTRW) model that laid the theoretical foundation for many future studies. Their model also motivated Saxton [11, 12] to study stochastic simulations of transport through crowded environments. More recently, the main results of Saxton's studies have been confirmed by Wedemeier [23–26] and by Vilaseca and Isvoran [13–17]. Wedemeier also demonstrated

that a similar effect is observed if the motile agent adheres to the obstacles [25]. In RW models, crowding effects are modelled by randomly occupying lattice sites with obstacles prior to the commencement of the simulation and then enforcing an exclusion principle [27] by aborting potential motility events that would lead to the motile agent occupying the same site as an obstacle as the simulation progresses [11–17]. In these simulations, it is generally assumed that the mean squared displacement (MSD) of the motile agent evolves in time as a power law,

$$\left\langle r^2 \right\rangle = (2d)\bar{D}\, t^\alpha, \tag{1.1}$$

where r represents the displacement, d is the dimension of the system, t is time and $\langle \cdot \rangle$ represents an average over a large ensemble of observations. We note that several random systems exhibit non-ergodicity and that, for these systems, the ensemble and time averages are not always equivalent [10]. The exponent α describes the type of transport process taking place, with $\alpha = 1$ being associated with Fickian diffusion and $\alpha < 1$ being associated with subdiffusion†. All cases in which $\alpha \neq 1$ are referred to as *anomalous* diffusion.

Other investigators such as Yuste and Lindenberg [18, 28–30], Metzler and Klafter [10] and Henry and Langlands [20] have modelled transport through crowded environments using FDE models. An FDE model is related to a CTRW whose the master equation utilises either a long–tailed waiting time distribution or a long–tailed jump step distribution [10]. Assuming that the waiting times are exponentially distributed leads to an FDE with the basic form

$$\frac{\partial^\alpha u}{\partial t^\alpha} = \bar{D}\, \nabla^2 u, \tag{1.2}$$

where $u(\mathbf{x}, t)$ represents the concentration of agents at $\mathbf{x}$, $\bar{D}$ is a generalised diffusivity with units $[L^2/T^\alpha]$ and $\partial^\alpha/\partial t^\alpha$ represents a Caputo fractional derivative [31, 32] of order α. The parameter α has the same meaning in Equation (1.2) as it does in Equation (1.1).

More recently, experimentalists have shown that the MSD of an agent undergoing transport through a crowded environment does not evolve in time as a linear power law [9, 33–35]. Banks and Fradin used fluorescence correlation spectroscopy to demonstrate experimentally that the MSD of proteins moving through a solution of dextran (a polysaccharide made of glucose

---

†If the master equation contains a long–tailed jump–step distribution then this parameter assumes values in the domain $1 < \alpha \leq 2$ in the associated FDE model. The domain $1 < \alpha < 2$ is termed "superdiffusion" and $\alpha = 2$ is termed "ballistic" transport. These unique cases do not occur in crowded environments and we do not consider them in this thesis.

molecules) does not evolve as a linear power law, even at very low obstacle concentrations [34]. These results were confirmed and extended by Sanabria et al. [33]. More recently, Dix and Verkman have demonstrated experimentally that the MSD of lipids and proteins undergoing transport through a membrane does not follow a linear power law [9] but were unsure whether this was the result of crowding effect, intracellular interactions or some combination of both effects. Experimental developments have lead some biologists [4, 5] to propose that crowding may play a significant role in protein and nucleic acid synthesis and that the persistent neglect of crowding by biochemists desperately needs to be remedied.

Numerical data from RW simulations [11, 12] demonstrate that in the long time limit, as $t \to \infty$, the transport process becomes Fickian. This effect has not been demonstrated for FDE models. The time that an experimentalist must wait until the transport process has transitioned from anomalous to Fickian diffusion is called the *crossover* time [11, 12]. The determination of the crossover time as well as the long–time diffusivity in the long–time limit are both of great interest. This behaviour has motivated some experimentalists to attempt to model crowded transport using a Fickian diffusion equation with a time dependent diffusivity [6].

1.2 Research questions

This thesis will examine and answer the following questions:

1. **Can the transport of cells through crowded environments be accurately modelled using fractional order differential equations?**

   In the literature it is common to assume, without justification, that all transport processes that occur in crowded environments are anomalous subdiffusion and can be accurately modelled using an FDE [7, 10, 18, 20, 28–30, 36–38]. Unfortunately, many studies do not consider the underlying RW that correspond to these models. Additionally, it can be difficult to compare FDE models to experimental data due to practical difficulties in the collection of this data that limits the size of most appropriate datasets [39, 40]. One way to access the accuracy of FDE models is by comparing the quantitative predictions of an FDE model with density information collected from a related RW model. We endeavour to do so in the first stage of this project.

2. **What effect do different obstacles shapes and sizes have on the transport process**

taking place?

Electron microscopy photographs indicate that cells can vary greatly in both their size and shape [41]. It is known that these details can affect the transport process taking place [13–17] but it is not clear how to include this information in an FDE model [7, 10]. Nor is it clear how to quantify the effect that the presence of multiple cell types has on the parameter α that describes the type of process taking place. However, it is relatively simple to include this level of detail in a CTRW model. By comparing a standard FDE model to a related CTRW model which includes these details, the effect that including multiple obstacles of different sizes and shapes has on the FDE and the parameter α can be ascertained.

3. **How can the diffusivity in the long time limit of the system be calculated?**

   Studies of the MSD of a single agent undergoing transport in a crowded environment demonstrate that in the long time limit, as $t \to \infty$, the transport tends to become Fickian [11, 12]. However, the diffusivity in the long time limit is not the same as the diffusivity of an analogous random walk on an empty lattice [11, 12]. There is great interest in determining the value of this reduced diffusivity $\bar{D}$ in the long time limit for different obstacle combinations [42–44]. A new algorithm for exactly calculating this value is developed and outlined in this thesis.

4. **How long must we wait until we can reasonably assume that the transport has become Fickian?**

   There is interest in determining the length of time an experimentalist must wait until the system has transitioned from the anomalous regime to the Fickian regime. This quantity is called the *crossover* time and was studied by Saxton who proposed a method to calculate it [11, 12]. Unfortunately, the application of Saxton's method requires stochastic data which is computationally expensive and, subsequently, very time consuming to generate. Saxton's method also requires that an investigator make several subjective choices that can affect reproducibility [11, 12].

   An alternative method of estimating this time is to use the Mean Action Time (MAT) proposed by McNabb and Wake [45, 46]. MAT is an objective "rule–of–thumb" measurement of the time that one must wait until a diffusion process can be considered to be *effectively* at its steady state distribution [45–51] that can be applied to any process that

tends to its steady state exponentially quickly [47–50].

In this thesis, McNabb and Wake's theory and methodology are extended in a way that allows their application to this new problem. This leads us to develop an explicit closed form expression for the MAT of an agent undergoing transport through a crowded environment.

The average displacement that a motile agent after one MAT is also of interest, however, a thorough examination of this length is beyond the scope of this thesis.

5. **How can we extend this new model to include cellular interactions such as adhesion and repulsion?**

   The motion of cells and molecules through *in vivo* biological environments is affected by the presence of other cells and scaffolds that can act as obstacles [11, 52–54]. Interactions between cells and obstacles can include both crowding effects [55, 56], as well as adhesion/repulsion effects [57, 58]. A great deal of theoretical progress has been made in terms of developing mathematical insight into how adhesion between motile cells impacts *in vitro* experiments without any obstacles present [59–62]. However, mathematical models describing the impacts of both crowding and adhesion/repulsion *in vivo*, with obstacles present, are predominantly based on simulation studies, without any underlying analysis [11, 13, 25, 55].

   While it is anticipated that both crowding and adhesion act to impede the motion of cells *in vivo*, it is not possible to quantify the relative roles of these two mechanisms based on intuition alone. Although it is possible to perform simulations that include both crowding and adhesion, simulation studies can be time consuming, and can fail to provide more general insight. To address these limitations, a stochastic, lattice-based model is considered that describes the motion of an agent (e.g. a cell or biological molecule) through an environment that is randomly populated by immobile obstacles at density $\phi \in [0, 1]$. The motion of the agent is affected by crowding and adhesion/repulsion between the agent and the obstacles. The strength of adhesion/repulsion is given by $\zeta \in [-1, 1]$. Setting $\zeta = 0$ corresponds to pure crowding with no adhesion/repulsion; $\zeta > 0$ corresponds to combined adhesion and crowding; and, $\zeta < 0$ corresponds to combined repulsion and crowding. An exact method that can be used to quantify the relative roles of crowding and adhesion/repulsion by producing exact calculations of the

long time Fickian diffusivity of the motile agent is presented in this thesis. This method is used to quantify the roles of both crowding and adhesion/repulsion in terms of the long time Fickian diffusivity $D(\phi, \zeta)$.

1.3   Aims and outcomes of this thesis

The principal aim of this thesis is to use mathematical modelling to identify and quantify transport processes that occur in crowded biological environments.

This thesis consists of the following aims:

- Compare an FDE with population density data from a CTRW to determine the role that crowding plays in determining the type of transport process taking place.

- Extend this model to include environments densely crowded with obstacles of different shapes, sizes and densities to determine how different distributions of obstacles affect the transport process.

- Develop a new modelling methodology that describes the early time behaviour of an agent undergoing transport through a crowded environment.

- Develop a new modelling methodology that allows the calculation of the long time diffusivity of an agent undergoing transport through a crowded environment as well as the calculation of the crossover time associated with a crowded environment.

This thesis is presented by publication and consists of five peer reviewed publications. Four of these publications have been published in Q1 journals and one has been published in a Q2 journal[†]. The PhD candidate has contributed significantly to all five publications and is the primary author of all five publications. The work presented in the thesis fulfils the Queensland University of Technology requirements for the award of thesis by publication.

This thesis comprises the following publications:

- A.J. Ellery, M.J. Simpson, S.W. McCue and R.E. Baker (2014). Characterizing transport through a crowded environment with different obstacle sizes. The Journal of Chemical

---

[†]Journal rankings are taken from `http://www.scimagojr.com`, which calculates rankings based on information contained in the Scopus database.

Physics. 140, 054108. Rank Q1. (Chapter 2.)

`http://dx.doi.org/10.1063/1.4864000`

- A.J. Ellery, R.E. Baker, S.W. McCue and M.J. Simpson (2016). Modeling transport through an environment crowded by a mixture of obstacles of different shapes and sizes. Physica A: Statistical Mechanics and its Applications. Rank Q2. (Chapter 4.)

  `http://dx.doi.org/10.1016/j.physa.2015.12.123`

- A.J. Ellery, R.E. Baker and M.J. Simpson (2015). Calculating the Fickian diffusivity for a lattice-based random walk with agents and obstacles of different shapes and sizes. Physical Biology. 12: 066010. Rank Q1. (Chapter 5.)

  `http://dx.doi.org/10.1088/1478-3975/12/6/066010`

- A.J. Ellery, R.E. Baker and M.J. Simpson (2016). Distinguishing between short-time non-Fickian diffusion, and long-time Fickian diffusion for a random walk on a crowded lattice. The Journal of Chemical Physics. 144, 171104. Rank Q1. (Chapter 7.)

  `http://dx.doi.org/10.1063/1.4948782`

- A.J. Ellery, R.E. Baker and M.J. Simpson (2016). An analytical method for disentangling the roles of adhesion and crowding for random walk models on a crowded lattice. Physical Biology. 13: 05LT02. Rank Q1. (Chapter 10).

  `http://dx.doi.org/10.1088/1478-3975/13/5/05LT02`

1.4 Structure of this thesis

Each chapter of this thesis corresponds to a publication. Because each paper is an independent publication there is some overlap in ideas between the chapters. The contribution that each member of the research team made to each publication is indicated in Section 1.5. All team members have read the contents of Section 1.5 and have consented to the inclusion of our publications in this document.

In the literature [7, 10, 18, 20, 28–30, 36–38], CTRW models and FDE models are often assumed, without justification, to be equivalent and interchangeable. In Chapter 2 this assumption is explored by comparing both single agent and population data from a CTRW, implemented using the Gillespie algorithm [63], with the analytical solution of a related FDE. Specifically,

the MSD of a motile agent undergoing a nearest neighbour random walk on a lattice which contains obstacles is used to provide an estimate of the parameter α. Then, the transport of a population of motile agents through a related crowded environment is modelled using the same CTRW model and used to calculate population density data. Matching the solution of a related FDE to this data provides an alternative estimate of α. The relationship between these two independent estimates of α is examined and used to determine the properties of the obstacle field for both a single agent and a population of agents; and for both types of models; and in both cases, α decreases as the obstacle density increases and that the rate of decrease is greater for smaller obstacles than for larger obstacles.

In Chapter 4 a similar analysis is performed in which there are several different types of obstacles present on the lattice, of various shapes and sizes. Three different combinations of obstacle types, which are referred to as *distributions*, are considered: (i) the first contains relatively more smaller obstacles than larger ones; (ii) the second contains relatively more larger obstacles than smaller ones and; (iii) the third contains the same number of occupied lattice sites for each type of obstacle considered. By comparing two independent estimates of α it is shown that the distribution of obstacle shapes and sizes also plays an important role in determining the type of transport process taking place and investigate these effects.

The algorithm proposed by Mercier and Slater [42–44] for calculating the long time diffusivity in a crowded environment is modified and extended in Chapter 5 so that it can be applied to this new system. We show that in the long time limit as $t \rightarrow \infty$, the transport process becomes Fickian and that it is possible to use the Nerst–Einstein equation, a special case of the fluctuation–dissipation theorem [64], to exactly calculate the long time diffusivity, $\bar{D}$ for our new system. We use this new method to confirm and extend our results from Chapter 2–4.

In Chapter 7 a Markov chain is developed and used to model the early time behaviour of our system. A new method, based on the MAT proposed by McNabb and Wake [45, 46] and expanded by others [47–51], is used to calculate the crossover time [11, 12], the amount of time an experimentalist must wait until they can consider the transport process to be *effectively* Fickian diffusion. Unlike the crossover time proposed by Saxton [11, 12], our new definition of the crossover time does not require stochastic simulations to be evaluated and is exact, objective and always reproducible.

The Mercier–Slater algorithm is then extended to examine the role of cellular interactions

such as adhesion and repulsion in Chapter 10. Our model indicates that there is a threshold density of obstacles ($\phi \approx 0.30$) below which the affect of adhesion and repulsion has a negligible affect on the transport process in the long time limit as $t \to \infty$.

Finally, in Chapter 12, the main conclusions of this study are outlined and some possible directions for future work are explored and discussed.

1.5 Statements of joint authorship

In this section, we outline the joint contributions of the PhD candidate and the coauthors to each paper. All coauthors have consented to the presentation of this material in this thesis.

1.5.1 Chapter 2: Characterising transport through a crowded environment with different obstacle sizes

The associated reference for this chapter is:

Ellery, Adam J and Simpson, Matthew J and McCue, Scott W and Baker, Ruth E, Characterizing transport through a crowded environment with different obstacle sizes. *J Chem Phys* **140**, 054108 (2014)

Abstract Transport through crowded environments is often classified as anomalous, rather than normal (Fickian) diffusion. Several previous studies have sought to describe such transport processes using either a continuous time random walk model or fractional order differential equation model. For both these models the transport mechanism is characterised by a parameter α, where $\alpha = 1$ is associated with normal diffusion and $\alpha < 1$ is associated with anomalous subdiffusion. Here, we simulate a single agent migrating through a crowded environment that is populated by impenetrable immobile obstacles and estimate α from averaged mean squared displacement data. We also simulate the transport of a population of such agents through a similar crowded environment and match population density data to the solution of a related fractional order differential equation to obtain an alternative estimate of α. Our results allow us to examine the relationship between our estimate of α and the properties of the obstacle field for both a single agent and a population of agents; and we show that in both cases, α decreases as the obstacle density increases, and that the rate of decrease is greater for smaller obstacles than for larger obstacles. Our work suggests that it may be inappropriate to model

the transport of both a single agent and a population of agents through a crowded environment using standard approaches. In particular, despite the ubiquitous use of fractional differential equations to describe the transport of populations of agents through crowded environments, this modelling framework must be used with care.

Statement of joint authorship

The work is divided as follows:

- **Ellery, A. J. (Candidate)** developed and programmed the numerical algorithms used to simulate and model the process considered, performed the data analysis, derived algebraic solutions to the fractional differential equation model, composed all figures and wrote and critically reviewed the manuscript during the peer-review process.

- Simpson, M. J. initiated the concept for the manuscript, oversaw and supervised the research, oversaw the drafting and redrafting of the manuscript prior to publication, wrote the cover and revision letters, critically reviewed and revised the manuscript during the peer-review process and acted as corresponding author.

- McCue, S. W. oversaw and supervised the research, oversaw the drafting and redrafting of the manuscript prior to publication, critically reviewed and revised the manuscript during the peer-review process.

- Baker, R. E. oversaw the drafting and redrafting of the manuscript prior to publication, critically reviewed and revised the manuscript during the peer-review process.

1.5.2 Chapter 4: Modelling transport through an environment crowded by a mixture of obstacles of different shapes and sizes

The associated reference for this chapter is:

Ellery, Adam J and Baker, Ruth E and McCue, Scott W and Simpson, Matthew J, Modeling transport through an environment crowded by a mixture of obstacles of different shapes and sizes. *Physica A: Statistical Mechanics and its Applications* **449** 74 (2016).

Abstract Many biological environments are crowded by macromolecules, organelles and cells which can impede the transport of other cells and molecules. Previous studies have sought to describe these effects using either random walk models or fractional order differential

equations. Here we examine the transport of both a single agent and a population of agents through an environment containing obstacles of varying size and shape, whose relative densities are drawn from a specified distribution. Our simulation results for a single agent indicate that smaller obstacles are more effective at retarding transport than larger obstacles, and these findings are consistent with our simulations of the collective motion of populations of agents. In an attempt to explore whether these kinds of stochastic random walk simulations can be described using a fractional order differential equation framework, we calibrate the solution of such a differential equation to our averaged agent density information. Our approach suggests that these kinds of commonly used differential equation models ought to be used with care since we are unable to match the solution of a fractional order differential equation to provide a meaningful interpretation of our averaged discrete results.

Statement of joint authorship

The work is divided as follows:

- **Ellery, A. J. (Candidate)** developed and programmed the numerical algorithms used to simulate and model the process considered, performed the data analysis, derived algebraic solutions to the fractional differential equation model, composed all figures and wrote and critically reviewed the manuscript during the peer-review process.

- Baker, R. E. oversaw the drafting and redrafting of the manuscript prior to publication, critically reviewed and revised the manuscript during the peer-review process.

- McCue, S. W. oversaw and supervised the research, oversaw the drafting and redrafting of the manuscript prior to publication, critically reviewed and revised the manuscript during the peer-review process.

- Simpson, M. J. initiated the concept for the manuscript, oversaw and supervised the research, oversaw the drafting and redrafting of the manuscript prior to publication, wrote the cover and revision letters, critically reviewed and revised the manuscript during the peer-review process and acted as corresponding author.

1.5.3 Chapter 5: Calculating the Fickian diffusivity for a lattice based random walk with agents and obstacles of different shapes and sizes

The associated reference for this chapter is:

Ellery, Adam J and Baker, Ruth E and Simpson, Matthew J, Calculating the Fickian diffusivity for a lattice-based random walk with agents and obstacles of different shapes and sizes. *Physical Biology* **12** 066010 (2015).

Abstract Random walk models are often used to interpret experimental observations of the motion of biological cells and molecules. A key aim in applying a random walk model to mimic an in vitro experiment is to estimate the Fickian diffusivity (or Fickian diffusion coefficient), D. However, many in vivo experiments are complicated by the fact that the motion of cells and molecules is hindered by the presence of obstacles. Crowded transport processes have been modelled using repeated stochastic simulations in which a motile agent undergoes a random walk on a lattice that is populated by immobile obstacles. Early studies considered the most straightforward case in which the motile agent and the obstacles are the same size. More recent studies considered stochastic random walk simulations describing the motion of an agent through an environment populated by obstacles of different shapes and sizes. Here, we build on previous simulation studies by analysing a general class of latticebased random walk models with agents and obstacles of various shapes and sizes. Our analysis provides exact calculations of the Fickian diffusivity, allowing us to draw conclusions about the role of the size, shape and density of the obstacles, as well as examining the role of the size and shape of the motile agent. Since our analysis is exact, we calculate D directly without the need for random walk simulations. In summary, we and that the shape, size and density of obstacles has a major influence on the exact Fickian diffusivity. Furthermore, our results indicate that the difference in diffusivity for symmetric and asymmetric obstacles is significant.

Statement of joint authorship

The work is divided as follows:

- **Ellery, A. J. (Candidate)** jointly developed the concept, developed and programmed the numerical algorithms used to model the stochastic process considered, performed the data analysis, simplified the solution methodology, composed all figures and wrote and critically reviewed the manuscript both prior to and during the peer-review process.

- Baker, R. E. oversaw the drafting and redrafting of the manuscript prior to publication, critically reviewed and revised the manuscript during the peer-review process.

- Simpson, M. J. jointly developed the concept, prepared the cover and response letters, critically reviewed and revised the manuscript both prior to and during the peer-review process.

1.5.4 Chapter 7: Distinguishing between short-time non-Fickian diffusion, and long-time Fickian diffusion for a random walk on a crowded lattice

The associated reference for this chapter is:

Ellery, Adam J and Baker, Ruth E and Simpson, Matthew J, Distinguishing between short-time non-Fickian diffusion, and long-time Fickian diffusion for a random walk on a crowded lattice. *The Journal of Chemical Physics* **144** 171104 (2016).

Abstract The motion of cells and molecules through biological environments is often hindered by the presence of other cells and molecules. A common approach to modelling this kind of hindered transport is to examine the mean squared displacement (MSD) of a motile tracer particle in a lattice-based stochastic random walk in which some lattice sites are occupied by obstacles. Unfortunately, stochastic models can be computationally expensive to analyse because we must average over a large ensemble of identically-prepared realisations to obtain meaningful results. To overcome this limitation we describe an exact method for analysing a lattice-based model of the motion of an agent moving through a crowded environment. Using our approach we calculate the exact MSD of the motile agent. Our analysis confirms the existence of a transition period where, at first, the MSD does not follow a power law with time. However, after a sufficiently long period of time, the MSD increases in proportion to time. This latter phase corresponds to Fickian diffusion with a reduced diffusivity owing to the presence of the obstacles. Our main result is to provide a mathematically motivated, reproducible and objective estimate of the amount of time required for the transport to become Fickian. Our new method to calculate this crossover time does not rely on stochastic simulations.

Statement of joint authorship

The work is divided as follows:

- **Ellery, A. J. (Candidate)** jointly developed the concept, developed and programmed the numerical algorithms used to model the stochastic process considered, performed the data analysis, simplified the solution methodology, composed all figures and wrote and critically reviewed the manuscript both prior to and during the peer-review process.

- Baker, R. E. oversaw the drafting and redrafting of the manuscript prior to publication, critically reviewed and revised the manuscript during the peer-review process.

- Simpson, M. J. jointly developed the concept, prepared the cover and response letters, critically reviewed and revised the manuscript both prior to and during the peer-review process.

1.5.5   Chapter 10: An exact tool for disentangling the roles of adhesion and crowding for random walk models on a crowded lattice

The associated reference for this chapter is:

Ellery, Adam J and Baker, Ruth E and Simpson, Matthew J, An exact tool for disentangling the roles of adhesion and crowding for random walk models on a crowded lattice. *Physical Biology. Under Review*

This manuscript is was accepted for publication on the 24th of August, 2016.

Statement of joint authorship

The work is divided as follows:

- **Ellery, A. J. (Candidate)** jointly developed the concept, developed and programmed the numerical algorithms used to model the stochastic process considered, performed the data analysis, simplified the solution methodology, composed all figures and wrote and critically reviewed the manuscript both prior to and during the peer-review process.

- Baker, R. E. oversaw the drafting and redrafting of the manuscript prior to publication, critically reviewed and revised the manuscript during the peer-review process.

- Simpson, M. J. jointly developed the concept, prepared the cover letter, critically reviewed and revised the manuscript both prior to and during the peer-review process.

Chapter 2

Characterising transport through a crowded environment with different obstacle sizes

2.1 Abstract

Transport through crowded environments is often classified as anomalous, rather than normal (Fickian) diffusion. Several previous studies have sought to describe such transport processes using either a continuous time random walk model or fractional order differential equation model. For both these models the transport mechanism is characterised by a parameter α, where $\alpha = 1$ is associated with normal diffusion and $\alpha < 1$ is associated with anomalous subdiffusion. Here, we simulate a single agent migrating through a crowded environment that is populated by impenetrable immobile obstacles and estimate α from averaged mean squared displacement data. We also simulate the transport of a population of such agents through a similar crowded environment and match population density data to the solution of a related fractional order differential equation to obtain an alternative estimate of α. Our results allow us to examine the relationship between our estimate of α and the properties of the obstacle field for both a single agent and a population of agents; and we show that in both cases, α decreases as the obstacle density increases, and that the rate of decrease is greater for smaller obstacles than for larger

obstacles. Our work suggests that it may be inappropriate to model the transport of both a single agent and a population of agents through a crowded environment using standard approaches. In particular, despite the ubiquitous use of fractional differential equations to describe the transport of populations of agents through crowded environments, this modeling framework must be used with care.

2.2   Introduction

Many biological environments, both intracellular and extracellular, are densely crowded by large molecules and cells [4, 6, 9]. Experiments imply that transport through such crowded environments can be modelled as anomalous diffusion, not normal (Fickian) diffusion [4–6, 34, 35, 65]. Since crowding is a common feature of biological systems, it is important to understand how to characterise and quantify transport processes within these systems.

Several previous investigations have sought to quantitatively describe transport through crowded environments by studying the motion of a single agent through an environment that is populated by impenetrable immobile obstacles [11–14, 16, 17]. Theory indicates that for a diffusion process in two dimensions, the mean squared displacement (MSD) of a agent, averaged over a sufficiently large ensemble, obeys the power law

$$\langle r^2 \rangle = 4D\,t^\alpha, \tag{2.1}$$

where r is the displacement, t is time, D is a generalised diffusivity and $\langle \cdot \rangle$ is an ensemble average [7, 10, 37, 66, 67]. The exponent α indicates the type of transport, with $\alpha = 1$ for normal diffusion and $\alpha < 1$ for anomalous subdiffusion [7, 10, 37, 66]. As such, the averaged MSD of a single agent is often a key quantity of interest in experimental studies [33–35] since from it we can estimate α.

As an alternative to studying the motion of a single agent in a crowded environment, other experiments have studied the transport of a population of agents through crowded environments and described the density of agents using continuum models. Theory indicates that if the average MSD of an individual motile agent obeys the power law described by Equation (2.1), then the transport of a population of such agents obeys a fractional order differential equation

(FDE) [7, 10, 32, 37]

$$\frac{\partial^\alpha u}{\partial t^\alpha} = D\frac{\partial^2 u}{\partial x^2}, \quad 0 < x < L, \quad t > 0, \tag{2.2}$$

where $u(x,t)$ is the density of agents, $\partial^\alpha/\partial t^\alpha$ is a Caputo fractional derivative of order α taken with respect to time [31, 32] and L is the length of the spatial domain. The solution of Equation (2.2) requires the specification of appropriate initial conditions and boundary conditions relevant to the particular situation of interest. Equations (2.1) and (2.2) are two standard mathematical models that are used to represent transport through crowded environments. Both of these mathematical models are ubiquitous throughout the literature [7, 10, 32, 37].

In this chapter, we extend earlier work by investigating how obstacle size, shape and density influences the motion of both a single agent and a population of agents. In Section 2.3.1 we simulate the motion of a single agent through a crowded environment and estimate α from averaged MSD data. As illustrated in the work of Saxton [11, 12], the averaged MSD does not obey Equation (2.1) and certain challenges arise when we interpret such data using this power law. We also examine the relationship between our estimates of α and the size, shape and density of obstacles by repeating our simulations and systematically varying these properties of the obstacles. In Section 2.3.2 we study the transport of a population of agents and estimate α by matching the solution of Equation (2.2) with the observed agent density profiles obtained from our stochastic model. Again, we examine how the properties of the obstacle field influence our estimates of α by repeating our simulations and systematically varying the size, shape and density of obstacles. We also discuss the challenges which arise when comparing the solution of Equation (2.2) with the population density data. Finally, we summarise and discuss our results in Section 2.5, before concluding this work with some comments about how the present study could be extended.

2.3 Stochastic simulations

We consider a square lattice with lattice spacing Δ, of dimension $M \times N$, where we index sites (i, j), with $0 \le i \le M$ and $0 \le j \le N$, so that each site has location $(x, y) = (i\Delta, j\Delta)$. The dimensions of the lattice are $0 \le x \le L_x$ and $0 \le y \le L_y$, where $L_x = M\Delta$ and $L_y = N\Delta$. At the beginning of each simulation we randomly populate the lattice with impenetrable immobile

obstacles. We denote the probability that any individual site is occupied by an obstacle as $\phi \in [0, 0.5]$, where we have restricted ϕ to be less than the percolation threshold for a square lattice [68].

In this study we consider four types of impenetrable immobile obstacles: (i) obstacles which occupy a single lattice site; (ii) obstacles which occupy two adjacent lattice sites; (iii) obstacles which occupy four lattice sites in a two by two arrangement, and (iv) obstacles which occupy nine lattice sites in a three by three arrangement. We refer to these types of obstacles as 1×1, 1×2, 2×2 and 3×3 obstacles, respectively. We note that 1×1, 2×2 and 3×3 agents are symmetric with respect to the lattice whereas 1×2 obstacles are asymmetric. In all cases where we consider 1×2 obstacles, we always ensured that the lattice was populated with, on average, half the 1×2 obstacles aligned along the x axis and half aligned along the y axis.

Our stochastic transport model is an exclusion process [27]. Individual agents are allowed to undergo a usual nearest neighbour random walk [69] which incorporates crowding effects. The crowding effects are modelled by aborting potential motility events that would lead to an agent stepping to a site that is occupied by another agent or an obstacle. This means that an agent at location (x, y) will attempt to step to either $(x \pm \Delta, y)$ or $(x, y \pm \Delta)$, with the target site chosen with equal probability of $1/4$. If the target site is occupied by an agent or an obstacle then that potential motility event is aborted. We use a Gillespie algorithm to advance the simulation in time [63] and we terminate the algorithm once it reaches some predetermined inspection time $t = T$. Since we wish to generate averaged data from our stochastic algorithm, we always consider a large number of identically-prepared realisations of each kind of simulation. To minimise computational effort, we follow the previous work of Vilaseca and coworkers [13] and only regenerate the obstacle field after every R identically-prepared realisations.

2.3.1   Motion of a single agent

We first consider the transport of a single agent through a crowded environment. After populating the lattice with obstacles, a single agent is placed on a randomly chosen vacant site and allowed to undergo a random walk, as described previously, with periodic boundary conditions applied along all boundaries of the domain.

To minimise stochastic fluctuations in the MSD data, we average the data over an ensemble of K identically-prepared realisations. Since we initialise each realisation by placing the agent
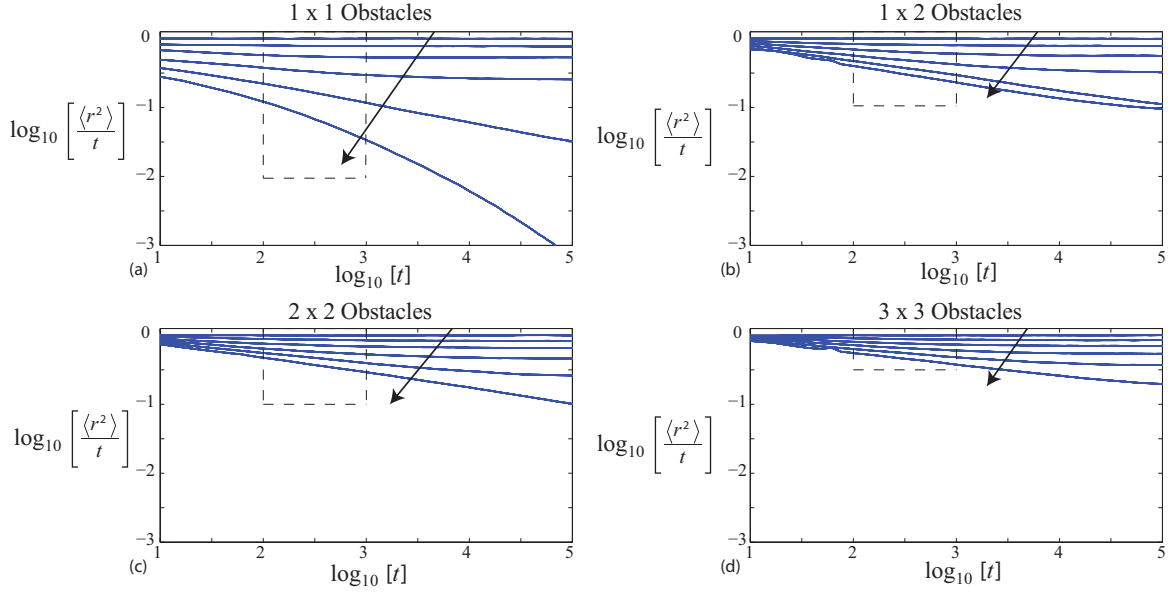
Figure 2.1: The averaged MSD (blue-solid) of a single agent migrating through a lattice populated by impenetrable immobile obstacles. Results in (a), (b), (c) and (d) were generated on a lattice occupied by 1×1, 1×2, 2×2 and 3×3 sized obstacles, respectively. Results are shown for $\phi = 0, 0.1, 0.2, 0.3, 0.4$ and 0.5, with the arrow indicating the direction of increasing ϕ. All results were generated on a 256×256 lattice and were averaged over an ensemble of $K = 50,000$ realisations. The obstacle field was regenerated every $R = 500$ realisations. The region enclosed by the dashed lines is shown in Figure 2.2.

at a randomly-located lattice site, the obstacle field is re-initialised every $R = 500$ realisations. For convenience, the MSD is recorded at geometrically-spaced temporal nodes which are related by $t_{n+1} = t_n + h$, where t_n is the nth node, $t_0 = 0$, $h = T(1 - g)/(1 - g^{P-1})$, P is the total number of nodes and g is a geometric growth factor, chosen to be $g = 1.1$. To analyse the averaged MSD data, we rewrite Equation (2.1) as

$$\log_{10}\left[\frac{\langle r^2 \rangle}{t}\right] = \log_{10}[4D] + (\alpha - 1)\log_{10}[t]. \tag{2.3}$$

Equation (2.3) implies that if our averaged MSD data follows the power law given by Equation (2.1), then plotting the data as $\log_{10}[\langle r^2 \rangle/t]$ as a function of $\log_{10}[t]$, the data will fall on a straight line with slope $\alpha - 1$. Our data is shown in Figure 2.1 for each obstacle type and for a selection of obstacle densities, $0 \leq \phi \leq 0.5$. This figure shows that, with the exception of the special (no crowding) case $\phi = 0$, the data does not lie on a straight line, which means that the averaged MSD does not obey the power law described in Equation (2.1). This observation is consistent with previous studies [11–14, 16, 17].

To provide an estimate of α we follow a similar strategy that has been implemented by

Table 2.1: The anomalous diffusion parameter α, calculated from averaged MSD data for 1×1, 1×2, 2×2 and 3×3 obstacles at concentrations $0 \leq \phi \leq 0.50$ on a 256×256 lattice. Data was averaged over $K = 50,000$ realisations and the obstacle field was regenerated every $R = 500$ realisations. The estimates of α were calculated using Equation (2.4). The reported variability is the maximum of E_L and E_R, which were calculated using Equation (2.6).

ϕ	0.00	0.05	0.10	0.15	0.20	0.25
1×1	$1.00 \pm 8.8 \times 10^{-4}$	$1.00 \pm 1.8 \times 10^{-4}$	$0.99 \pm 1.0 \times 10^{-3}$	$0.98 \pm 2.2 \times 10^{-3}$	$0.97 \pm 1.7 \times 10^{-3}$	$0.95 \pm 1.3 \times 10^{-3}$
1×2	$1.00 \pm 4.5 \times 10^{-4}$	$0.99 \pm 2.1 \times 10^{-3}$	$0.98 \pm 2.1 \times 10^{-3}$	$0.96 \pm 8.3 \times 10^{-4}$	$0.94 \pm 5.0 \times 10^{-3}$	$0.92 \pm 3.9 \times 10^{-3}$
2×2	$1.00 \pm 2.1 \times 10^{-3}$	$0.99 \pm 5.2 \times 10^{-4}$	$0.98 \pm 8.8 \times 10^{-4}$	$0.97 \pm 7.3 \times 10^{-4}$	$0.96 \pm 2.3 \times 10^{-3}$	$0.94 \pm 3.2 \times 10^{-3}$
3×3	$1.00 \pm 2.2 \times 10^{-3}$	$0.99 \pm 3.0 \times 10^{-3}$	$0.98 \pm 2.6 \times 10^{-4}$	$0.97 \pm 7.9 \times 10^{-4}$	$0.96 \pm 6.7 \times 10^{-4}$	$0.94 \pm 3.3 \times 10^{-3}$

ϕ	0.30	0.35	0.40	0.45	0.50
1×1	$0.90 \pm 4.1 \times 10^{-3}$	$0.81 \pm 3.6 \times 10^{-3}$	$0.72 \pm 4.3 \times 10^{-3}$	$0.56 \pm 8.0 \times 10^{-3}$	$0.44 \pm 1.6 \times 10^{-2}$
1×2	$0.87 \pm 2.9 \times 10^{-3}$	$0.84 \pm 8.0 \times 10^{-4}$	$0.80 \pm 1.3 \times 10^{-3}$	$0.77 \pm 3.0 \times 10^{-3}$	$0.76 \pm 2.8 \times 10^{-3}$
2×2	$0.92 \pm 1.5 \times 10^{-3}$	$0.88 \pm 3.0 \times 10^{-3}$	$0.85 \pm 3.3 \times 10^{-3}$	$0.81 \pm 2.1 \times 10^{-3}$	$0.79 \pm 1.7 \times 10^{-3}$
3×3	$0.92 \pm 4.0 \times 10^{-3}$	$0.90 \pm 9.1 \times 10^{-4}$	$0.88 \pm 6.8 \times 10^{-4}$	$0.86 \pm 3.9 \times 10^{-3}$	$0.83 \pm 2.3 \times 10^{-3}$
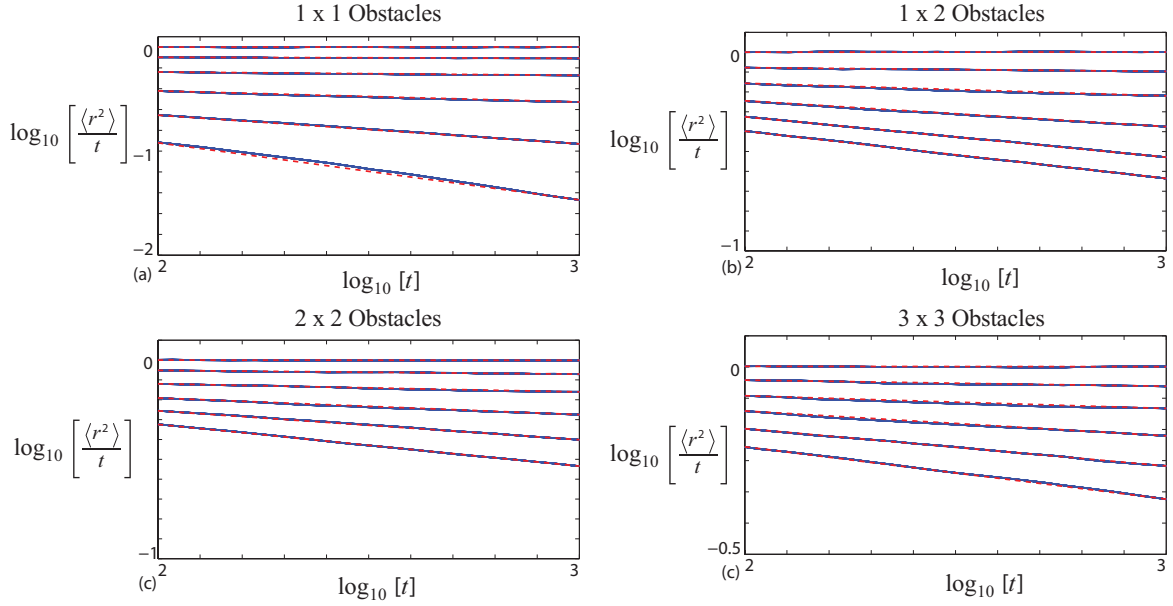
Figure 2.2: The averaged MSD (blue-solid) of a single agent migrating through a lattice populated by impenetrable immobile obstacles. All results are the same as those in Figure 2.1 except that here we only show the region bounded by $10^2 < t < 10^3$. A straight line (red-dotted) intersecting the ordinate of the averaged MSD data at $t = 10^2$ and $t = 10^3$ is superimposed. Equation (2.3) indicates that the slope of these lines should be equal to $\alpha - 1$. Corresponding values of α for each case are given in Table 2.1.

others [11–14, 16, 17]. We focus on small time data during the interval $10^2 \leq t \leq 10^3$, which we chose since the averaged MSD data forms an approximately straight line during this interval for each dataset in Figure 2.1. An estimate of α can be obtained by calculating the slope of the straight line that intersects the ordinate of the averaged MSD data at $t = 10^2$ and $t = 10^3$, as highlighted in Figure 2.2. This procedure allows us to estimate α using Equation (2.3). If we let q_i denote the ordinate of the averaged MSD curve at time 10^2 and q_j denote the ordinate of the averaged MSD data curve at time 10^3, our estimate of α is given by

$$\alpha \approx \frac{q_j - q_i}{10^3 - 10^2} + 1. \tag{2.4}$$

To quantify the variability in this estimate of α, we perform the same calculation after shifting the time interval one temporal node to the left, and then one node to the right. This provides us with two other estimates of α which are given by

$$\alpha_L \approx \frac{q_{j-1} - q_{i-1}}{10^3 - 10^2} + 1, \qquad \alpha_R \approx \frac{q_{j+1} - q_{i+1}}{10^3 - 10^2} + 1, \tag{2.5}$$

where α_L is our estimate of α obtained by shifting the time interval one temporal node to the
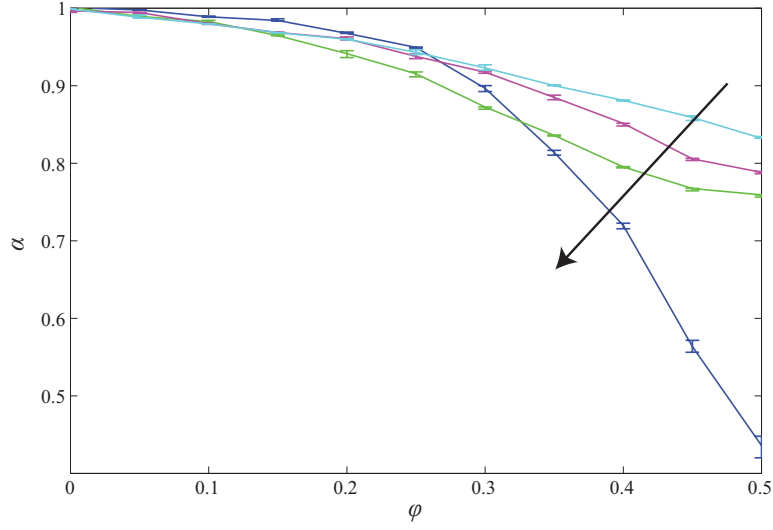
Figure 2.3: The dependence of α with obstacle concentration ϕ for each different obstacle type. Results correspond to 1×1 (dark blue), 1×2 (green), 2×2 (magenta) and 3×3 obstacles (light blue), respectively. The arrow indicates the direction of decreasing obstacle size. All results were generated on a 256×256 lattice and the associated MSD data was averaged over $K = 50,000$ identically-prepared realisations. The obstacle field was regenerated every $R = 500$ realisations. The estimates of α were calculated using Equation (2.4) and the error bars indicate the interval, $[\alpha - E_L, \alpha + E_R]$, which was calculated using Equation (2.6).

left and α_R is our estimate of α obtained by shifting the time interval one temporal node to the right. We estimate the uncertainty in our approximation of α using

$$E_L = \alpha_L - \alpha, \qquad E_R = \alpha - \alpha_R, \tag{2.6}$$

which allows us to identify an interval of $[\alpha - E_L, \alpha + E_R]$, as our estimate of the uncertainty in our estimate of α.

We show our estimates of α and the associated uncertainty interval for all obstacle types with $0 \leq \phi \leq 0.5$ in Table 2.1. The same data is presented graphically in Figure 2.3 with error bars indicating the magnitude of E_L and E_R below and above the data points respectively. For our data, $E_L \approx E_R$ so the error bars in Figure 2.3 are approximately symmetric. Our results confirm that when $\phi = 0$ the transport appears to be normal diffusion since we have $\alpha = 1$. For all the obstacle types considered, the transport process appears to become increasingly anomalous as ϕ increases since we observe $\alpha < 1$ in these cases and that our estimate of α decreases as the obstacle density increases. Furthermore, we note that the rate at which α decreases with ϕ is different for each obstacle type considered here. For a given value of ϕ, the greatest decrease in α is observed for 1×1 obstacles and the smallest decrease in α is observed

for 3×3 obstacles. One way of interpreting this trend is that populating the lattice with larger obstacles leaves larger spaces through which the agents can migrate than occurs for smaller obstacles at the same density. This result confirms that both the obstacle density and the obstacle size can have an important impact on the transport process. We note that the relationship we observe between α and ϕ is qualitatively similar to the results previously reported by Saxton [11, 12], as well as more recent work by Isvoran and coworkers [17]. In particular, Vilaseca and coworkers observed qualitatively similar trends for transport in three-dimensional crowded environments[13].

2.3.2 Population of agents

In practice, it is more common for experimentalists to report observations of the collective motion of a population of agents, such as molecules [70–72] or cells [73–77], rather than the motion of a single agent. This consideration motivates us to consider a second set of stochastic simulations where we consider the motion of a population of agents in a crowded environment.

To initiate our stochastic simulations we first randomly populate a lattice with impenetrable immobile obstacles, in exactly the same way that we did in Section 2.3.1. The simulations are initialised by populating all remaining vacant sites in the vertical strip where $x = 0$ with motile agents. These agents undergo the same random walk procedure as described in Section 2.3.1, except that in this case we have multiple agents on the lattice and potential motility events are aborted if an agent attempts to step to a lattice site that is occupied by either another agent or an obstacle. Once the Gillespie algorithm reaches a specified time, $t = T$, the algorithm is terminated. To generate averaged density data we perform many identically-prepared realisations of the same stochastic process. Since regenerating the obstacle field is computationally expensive, we again follow the work of Vilaseca and coworkers by regenerating the obstacle field every $R = 100$ realisations.

Simulations are performed by enforcing periodic boundary conditions along the horizontal boundaries where $y = 0$ and $y = L_y$. As the simulation proceeds, agents that were originally located along the vertical strip with $x = 0$ move from their original location and begin to migrate across the lattice. As soon as one of these agents steps off the vertical strip with $x = 0$ we replace that agent with a new agent. This ensures that the density of agents at $x = 0$ remains constant throughout the simulations and that new agents are constantly introduced onto the

lattice at $x = 0$. If, during the simulation, any agent reaches the vertical strip where $x = L_x$, we immediately remove those agents from the simulation which ensures that the density of agents along the boundary where $x = L_x$ remains zero for all time during the simulation.

Once the simulation reaches time T, we count the number of agents located within each vertical strip along the lattice and normalise this count by the number of agents located in the vertical strip with $x = 0$. We average this agent density data over a large ensemble of K identically prepared realisations and calculate the averaged agent density profile at time T in the following way: let $n_k(i, j)$ denote the occupancy of site (i, j) during the kth realisation such that $n_k(i, j) = 0$ corresponds to a vacant site and $n_k(i, j) = 1$ corresponds to an occupied site. Then, the average occupancy of sites in the ith vertical strip, estimated after performing K identically-prepared realisations, is

$$\tilde{u}(i\Delta, T) = \frac{1}{K} \sum_{k=1}^{K} \frac{1}{\bar{n}_k} \sum_{j=0}^{N} n_k(i, j), \tag{2.7}$$

where $\bar{n}_k = \sum_{j=0}^{N} n_k(0, j)$ denotes the number of agents within the vertical strip with $x = 0$ during the kth identically-prepared realisation. We note that Equation (2.7) is a double average such that our density profile is constructed by averaging first over the occupancy of each site in each vertical strip in the lattice, and second over an ensemble of K identically-prepared simulations [78].

An example of these simulations is shown in Figure 2.4 for each of the different obstacles considered in this study. In Figure 2.4 (a) we show a snapshot from a single realisation of the stochastic model and in Figure 2.4 (b) we show the averaged agent population density data obtained using an ensemble of $K = 50,000$ realisations for $\phi = 0$. Other results in Figure 2.4 (c)–(d), (e)–(f), (g)–(h) and (i)–(j) show a single realisation of the stochastic model together with the corresponding averaged agent density data for lattices populated with 1×1, 1×2, 2×2 and 3×3 obstacles, respectively. For all results in Figure 2.4 (c)–(d), (e)–(f), (g)–(h) and (i)–(j), the lattice is populated such that $\phi = 0.5$.

The results in Figure 2.4 illustrate how the obstacle size and shape affects the motion of a population of agents moving through the crowded environment. In Figure 2.4 (a), for $\phi = 0$, we observe that individual agents amongst the population almost reach the boundary at $x = L_x$ during the simulation. In contrast, the profiles in Figure 2.4 (c), (e), (g) and (i), in which
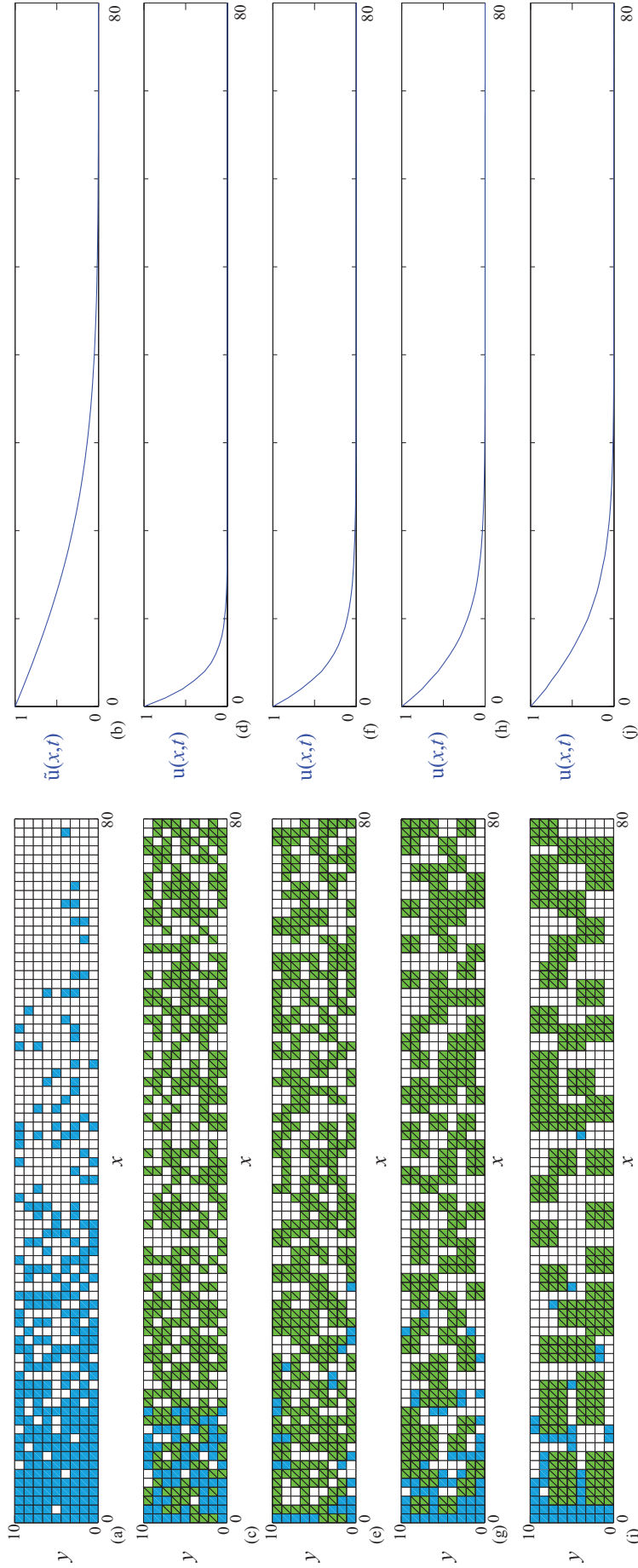
Figure 2.4: The transport of a population of agents (blue) through a lattice populated by impenetrable immobile obstacles (green-with diagonal). Results in (a)–(b) correspond to a lattice with no obstacles whilst results in (c)–(d), (e)–(f), (g)–(h) and (i)–(j) correspond to lattices populated by 1×1, 1×2, 2×2 and 3×3 obstacles with $\phi = 0.5$, respectively. Results in (a), (c), (e), (g) and (i) show a single simulation on a 80×10 lattice whilst results in (b), (d), (f), (h) and (j) show the average agent population density, $\tilde{u}(x, t)$, for an identically–prepared suite of simulations on a 100×1000 lattice, averaged over an ensemble of $K = 50,000$ realisations. All results are presented at time $T = 1000$.

$\phi = 0.5$, show that agents in a crowded environment are unable to move as far in the positive x direction owing to crowding effects. If we compare the snapshots in Figure 2.4 (c), (e), (g) and (i), we observe that the distance the agents move in the positive x direction varies with the size and shape of the obstacles even though the density of obstacles in Figure 2.4 (c), (e), (g) and (i) is the same. These results imply that 1×1 agents are more effective at retarding the collective motion of the agents than 3×3 obstacles at the same density. These trends observed in the individual snapshots from the stochastic model are consistent with the averaged density data in Figure 2.4 (b), (d), (f), (h) and (j).

To explore how the averaged density profiles from the stochastic simulations changes with time, we present $\tilde{u}(x, T)$ in Figure 2.6 for the different obstacle types at times $t = 100, 550, 1000$ for $\phi = 0.50$. In all cases the profiles in Figure 2.6 show that the distance the density profile propagates in the positive x direction increases with time; however, we observe very different behaviour depending on the shape and size of the obstacles. In particular, we observe that the smaller 1×1 obstacles have a greater impact on the propagation of the average density profile than the larger 3×3 obstacles at the same density. This trend is consistent with the averaged MSD data presented in Section 2.3.1 where we observed that the smaller 1×1 obstacles led to a slower increase in the averaged MSD data with time. We note that all results in Figure 2.6 are for $\phi = 0.5$ only. An equivalent set of density profiles for $\phi = 0$ and $\phi = 0.25$ illustrate the same trends and are presented in Chapter 3. We will make more specific comments on this agent density data in Section 2.4.

2.4   Fractional order differential equation model

We now attempt to model the transport process of Section 2.3.2 using Equation (2.2). Since the averaged MSD of a single agent migrating through a crowded lattice does not follow the power law described by Equation (2.1), the FDE given by Equation (2.2) may not be an appropriate representation of this transport process. Despite this possible weakness, we are interested in determining how well Eq. (2.2) describes this transport process, since modelling transport through crowded environments using a FDE framework is a standard approach that is ubiquitous throughout the literature[7, 10, 37, 66, 67]. To achieve this goal we will determine estimates of α and D such that the solution of the FDE matches our observed data. Furthermore we are interested in examining how these estimates of α and D vary with obstacle size, shape, density

and simulation time, T.

In our discrete simulations, described in Section 2.3.2, we ensured that lattice sites along the vertical strip with $x = 0$ were always occupied by agents whereas lattice sites along the vertical strip with $x = L_x$ were never occupied by agents. All simulations described in Section 2.3.2 were initialised without any agents on the lattice. These boundary conditions and initial conditions correspond to

$$u(0, t) = 1, \quad u(L_x, t) = 0, \quad u(x, 0) = 0, \tag{2.8}$$

where we have normalised the density at $x = 0$ to be unity. Equation (2.2), with the boundary conditions and initial condition described by Equation (2.8), can be solved using separation of variables [32, 79] to give

$$u(x, t) = \frac{L_x - x}{L_x} \\ - \sum_{n=1}^{\infty} \left(\frac{2}{n\pi} \right) \sin\left(\frac{n\pi x}{L_x} \right) \mathrm{E}_\alpha \left[-D \left(\frac{n\pi}{L_x} \right)^2 t^\alpha \right], \tag{2.9}$$

where $\mathrm{E}_\alpha[z]$ is the Mittag-Leffler function [32] with parameter α and argument z

$$\mathrm{E}_\alpha[z] = \sum_{k=0}^{\infty} \frac{z^k}{\Gamma(\alpha k + 1)}, \tag{2.10}$$

and $\Gamma(z)$ is the gamma function.

The parameters α and D in Equation (2.9) can be estimated by matching Equation (2.9) to our averaged agent density data, calculated in Section 2.3.2, using a nonlinear least-squares parameter estimation algorithm. For this study we use the Levenberg-Marquardt algorithm [80, 81]. To proceed, we first define a measure by which the solution of Equation (2.2) can be compared to our averaged density data from the stochastic model, which is given by

$$\epsilon_i = u(i\Delta, T) - \tilde{u}(i\Delta, T), \tag{2.11}$$

where $u(i\Delta, T)$ is the solution of Equation (2.9) and $\tilde{u}(i\Delta, T)$ is the averaged agent density data from the discrete simulations. The Levenberg-Marquardt algorithm seeks to minimize the sum of the squares of the residuals, $\mathcal{S}(\alpha, D) = \sum_{i=0}^{M} \epsilon_i^2$, where the sum is taken over each vertical

Table 2.2: The anomalous diffusion parameter, $\hat{\alpha}$, and the diffusion coefficient, $\hat{D}$, for averaged agent population data. Parameters were approximated by matching stochastic data generated using the algorithm described in Section 2.3.2 to Equation (2.9) using the Levenberg-Marquardt algorithm

	Time	1×1 Obstacles		1×2 Obstacles		2×2 Obstacles		3×3 Obstacles	
		$\hat{D}$	$\hat{\alpha}$	$\hat{D}$	$\hat{\alpha}$	$\hat{D}$	$\hat{\alpha}$	$\hat{D}$	$\hat{\alpha}$
	100	0.17	1.00	0.17	1.00	0.17	1.00	0.17	1.00
$\phi = 0.00$	550	0.21	1.00	0.21	1.00	0.21	1.00	0.21	1.00
	1000	0.22	1.00	0.22	1.00	0.22	1.00	0.22	1.00
	100	0.25	0.745	0.25	0.77	0.25	0.81	0.12	1.00
$\phi = 0.25$	550	0.09	1.00	0.1	1.00	0.125	1.00	0.145	1.00
	1000	0.09	1.00	0.105	1.00	0.13	1.00	0.150	1.00
	100	0.20	0.50	0.245	0.535	0.25	0.62	0.245	0.70
$\phi = 0.50$	550	0.115	0.64	0.25	0.6050	0.245	0.71	0.245	0.785
	1000	0.12	0.625	0.25	0.61	0.245	0.725	0.06	1.00

strip of the lattice. The Levenberg-Marquardt algorithm takes an initial guess of the parameters (α_0, D_0), and iteratively improves the parameter estimate by moving along the surface $\mathcal{S}(\alpha, D)$ to find the least-squares estimate of the parameters, $(\hat{\alpha}, \hat{D})$, such that $\mathcal{S}(\hat{\alpha}, \hat{D})$ is a minimum. To implement the Levenberg-Marquardt algorithm, we restrict our search to that region of the parameter space where $0.5 \leq \alpha \leq 1$ and $0 < D \leq 0.25$.

Results in Figure 2.5 show the error surfaces described by $\mathcal{S}(\alpha, D)$ for 3×3 obstacles with $\phi = 0, 0.25, 0.5$ and $T = 100, 550, 1000$. An equivalent set of results for 1×1, 1×2 and 2×2 obstacles are given in Chapter 3. On each error surface in Figure 2.5 we indicate the location of $(\hat{\alpha}, \hat{D})$ and we note that in each case the Levenberg-Marquardt algorithm converged to the same point $(\hat{\alpha}, \hat{D})$, regardless of the initial guess, (α_0, D_0). Our estimates of $(\hat{\alpha}, \hat{D})$ for each case are summarised in Table 2.2. For $\phi = 0$ the error surface is relatively shallow at $T = 100$, whereas by $T = 550$ the error surface has become steeper with a more clearly defined minimum with $(\hat{\alpha}, \hat{D}) \approx (1, 0.25)$ as we expect since this case corresponds to a standard exclusion process with no obstacles. For simulations with $\phi > 0$, however, the error surfaces are relatively shallow at $T = 100$ and remain relatively shallow at $T = 1000$, which means that there are large regions of the parameter space in which $\mathcal{S}(\alpha, D)$ is almost constant with no clear minimum. For a given simulation time, T, and obstacle density $\phi > 0$, there are a number of $(\hat{\alpha}, \hat{D})$ pairs for which $u(x, t)$ matches the data equally well. We also note that our estimates of $\hat{\alpha}$ and $\hat{D}$ appear to vary with the simulation time, T, and that the estimated best-fit value of $\hat{\alpha}$ tends to increase
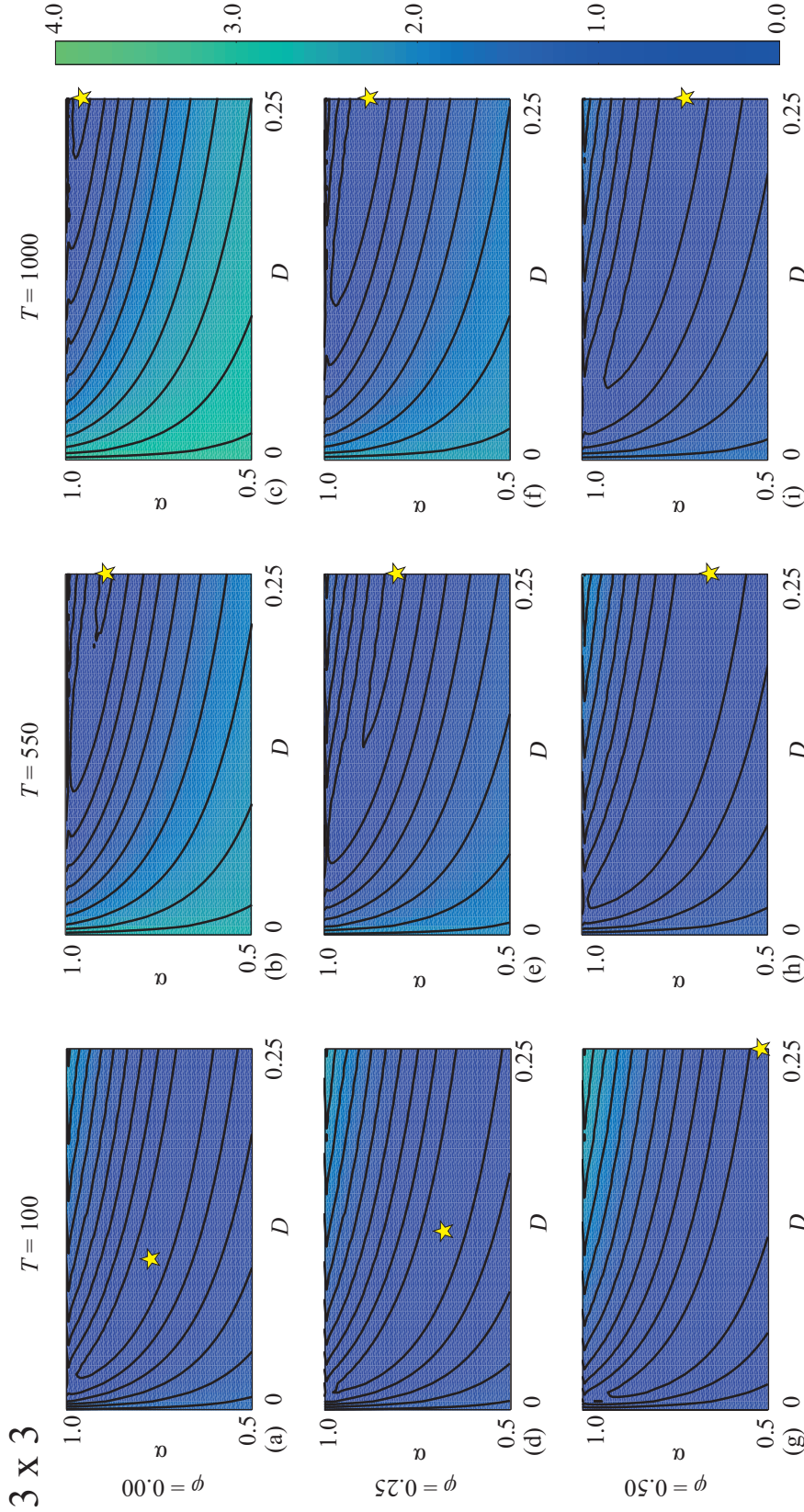
Figure 2.5: The magnitude of the sum of squared residuals, $\mathcal{S}(\alpha, D) = \sum_{i=0}^{M} \epsilon_i^2$, for $0 < D \leq 0.25$ and $0.5 \leq \alpha \leq 1$. All discrete results correspond to 3×3 obstacles. Results in (a),(d),(g): (b),(e),(h) and (c),(f),(i) are for $\phi = 0.0$, 0.25 and 0.50, respectively. Results in (a)–(c), (d)–(f) and (g)–(i) show results at $T = 100$, 550 and 1000 respectively. All results were generated on a 100×1000 lattice populated with 3×3 obstacles and were averaged over $K = 50,000$ realizations. All error surfaces were generated by considering 80 equally-spaced values of α and 40 equally-spaced values of D. Contour lines are given at increments of 0.25. The minimum of each error surface (yellow pentagon) was estimated by the Levenberg-Marquardt algorithm. The values of these minima, $(\hat{\alpha}, \hat{D})$, are given in Table 2.2.

as T increases. This means that associating an $(\hat{\alpha}, \hat{D})$ pair with our simulations is problematic since it is unclear which combination of parameters we should use at a given time, or at what simulation time, T, we should measure them.

To examine the sensitivity of the solution of Equation (2.2), $u(x,t)$, to variations in our estimate of $\hat{\alpha}$ we plot $u(x,t)$, with $\hat{\alpha} \pm 0.05$ and $\hat{D}$, in Figure 2.6. In generating these sensitivity results we have taken care to ensure that we only report results where $\alpha \leq 1$. For cases where $\hat{\alpha} + 0.05 > 1$ we do not plot any additional solution. Comparing the solutions with $\hat{\alpha} \pm 0.05$ to the original solution with $\hat{\alpha}$ in each subfigure of Figure 2.6 indicates that the results at $T = 100$ are relatively insensitive to our choice of α since the solutions with $\hat{\alpha} \pm 0.05$ are visually indistinguishable from the solution with $\hat{\alpha}$ at this scale. In contrast, the solution at $T = 1000$ indicates that we observe an increased sensitivity to the value of α since the solutions with $\hat{\alpha} \pm 0.05$ are clearly distinguishable from the solution with $\hat{\alpha}$ at this scale.

2.5 Discussion

In this work, we presented a discrete stochastic model of transport through a crowded environment that was randomly populated with impenetrable immobile obstacles. In particular, we focused on developing an understanding of how the obstacle shape, size and density affect the transport processes. To achieve this goal, we collected two different kinds of commonly-reported data from our stochastic simulations. We first considered the motion of a single agent through the crowded environment and we reported how the averaged MSD data varied as a function of time for this process. Our results showed that this data does not obey Equation (2.1). To make progress using this approach, we estimated α by assuming that the data could be approximated by the power law described by Equation (2.1) within a representative time interval, and fitted a straight line to the data within this time interval for each obstacle density and shape that we considered.

Our estimates of α from the averaged MSD data indicate that the degree to which the transport process could be interpreted as anomalous depends on the obstacle size, shape and density. In general, we found that as the obstacle density, ϕ, increased, our estimate of α decreased. Counter intuitively, we found that the decrease in α was most rapid for the smallest of our obstacle sizes, 1×1 obstacles. This implies that smaller obstacles give rise to a larger
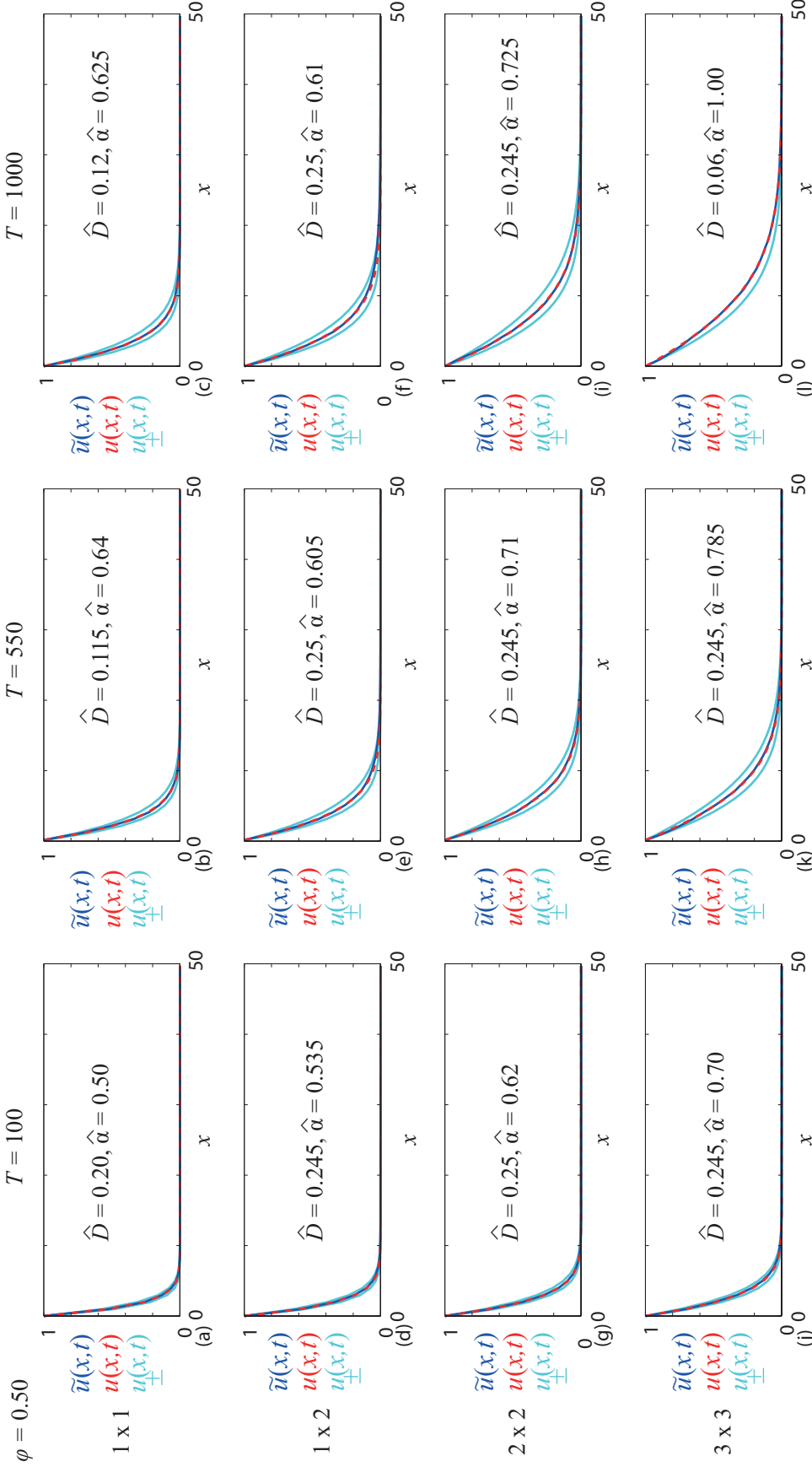
Figure 2.6: Averaged agent density data for $\phi = 0.5$. We show the normalised density of agents in each vertical strip, $\widetilde{u}(x,t)$ (dark blue), the analytical solution of Equation (2.2), $u(x,t)$, with $(\widehat{\alpha}, \widehat{D})$ (red-dashed) and the analytical solution of Equation (2.2), $u_{\pm}(x,t)$, with $\alpha = \widehat{\alpha} \pm 0.05$ and $D = \widehat{D}$ (light blue), where care was taken to only present results where $\alpha \leq 1$. Results in (a)–(c); (d)–(f); (g)–(i) and (j)–(l) correspond to lattices populated with 1×1, 1×2, 2×2 and 3×3 obstacles, respectively. Results in (a), (d), (g) and (j); (b), (e), (h) and (k) and (c), (f), (i) and (l) correspond to $T = 100$, $T = 550$ and $T = 1000$ respectively. The $\widetilde{u}(x,t)$ profiles were generated on a 100×1000 lattice and were averaged over $K = 50,000$ realisations. The obstacle field was regenerated every 100 simulations. Results for $u(x,t)$ used parameters $L = 1000$, T as indicated, and the least-squares estimates of $(\widehat{\alpha}, \widehat{D})$ as given in each subfigure and presented in Table 2.2. The analytical solution was truncated after $50,000$ terms in the series.

crowding effect than larger obstacles placed randomly at the same density. One way to interpret this trend is that populating a lattice with larger obstacles leads to larger vacant regions between the obstacles through which the smaller agents may migrate. Regardless of whether or not our averaged MSD data can be described using Equation (2.1), our simulation data implies that the shape, size and density of obstacles has a major impact on transport through a crowded environment.

To complement our averaged MSD data for the motion of a single agent through a crowded environment, we separately considered the transport of a population of agents through a crowded environment by using the same random walk framework, except that we considered simulations that contained many motile agents. In these simulations, the motion of a particular agent is affected by the presence of the obstacles as well as the presence of other agents on the lattice, since we only permitted those motility events that would place an agent on a vacant lattice site. For these simulations we chose initial conditions and boundary conditions so that averaged data describing this transport process was effectively one-dimensional. In particular, we averaged the number of agents over each strip in the y direction in order to track density profiles which propagated in the positive x-direction in time. To provide us with information about how the obstacle size, shape and density affected this averaged agent density profile, we performed many realizations of the same process and systematically varied properties of the obstacle field. Our suite of density profiles again shows that smaller obstacles were more effective at retarding the motion of the population of agents than larger agents placed at the same density.

In an attempt to describe the transport of a population of agents through a crowded environment using a continuum mathematical model, we applied a FDE to our averaged density data. To estimate how well the FDE model matched the data we calibrated the parameters α and D in the FDE model using a nonlinear least squares parameter estimation algorithm so that the solution of the FDE matched our averaged density data from the stochastic simulations. This procedure again confirmed that the transport process depends on obstacle size, shape and density. We observed a qualitatively similar trend to that which we observed in our earlier simulations of the transport of a single agent, namely, that as the obstacle density, ϕ, increased, α decreased. We also noted that smaller obstacles lead to a greater decrease in α than larger obstacles placed randomly at the same density and that, generally, our estimates of α increased as the simulation time increased.

Our studies indicate that it may be inappropriate to model the transport of an agent population through a crowded environment using a FDE, since the averaged data from our stochastic simulations do not match the solution of the standard FDE model. Our attempts to match the FDE to the population density data were problematic since we obtain different combinations of α and D at different simulation times. Furthermore, the nonlinear least-squares algorithm indicates that there are large regions in (α,D) parameter space in which the deviation between the solution of the FDE and the averaged simulation data is very small, suggesting that there are many different parameter combinations that match the observed transport process. For example, at any fixed value of time t, the averaged density profile associated with a high density of 1×1 obstacles can be matched to the solution of the FDE for any value of $0.5 \leq \alpha \leq 1.0$ provided that we make an appropriate choice of D.

In summary, our work has raised two key issues with respect to modelling transport through crowded environments. First, we have shown that obstacle shape, size and density play a key role in the transport process. This is an important point to make since many previous studies have dealt exclusively with one type of obstacle [11, 12]. Furthermore, those studies which did consider obstacles of different size examined averaged MSD data alone without any explicit consideration of averaged density information [13, 14]. One of the limitations of our present work is that we only considered transport through crowded environments where, in each simulation, only one obstacle type was considered. An important extension of the present work could be to consider the transport through a crowded environment where the obstacles size was described by a statistical distribution of different types of obstacles.

A second key issue raised in this work relates to the difficulties we have experienced when attempting to parameterise standard differential equation descriptions of the averaged density information using data from our discrete model. Despite the widespread use and analysis of FDE models, our attempt to fit the solution of Equation (2.2) to our density data has produced least-squares estimates of α that are strongly dependent on the inspection time. This result implies that Equation (2.2) does not describe the averaged properties of our discrete model, since any use of Equation (2.2) assumes the parameter α is a constant. Indeed, these observations are consistent with the fact that the averaged MSD data for the equivalent process for a single agent does not follow the widely-discussed power law given by Equation (2.1). We conclude that FDE models, such as Equation (2.2), should be used with care.

Chapter 3

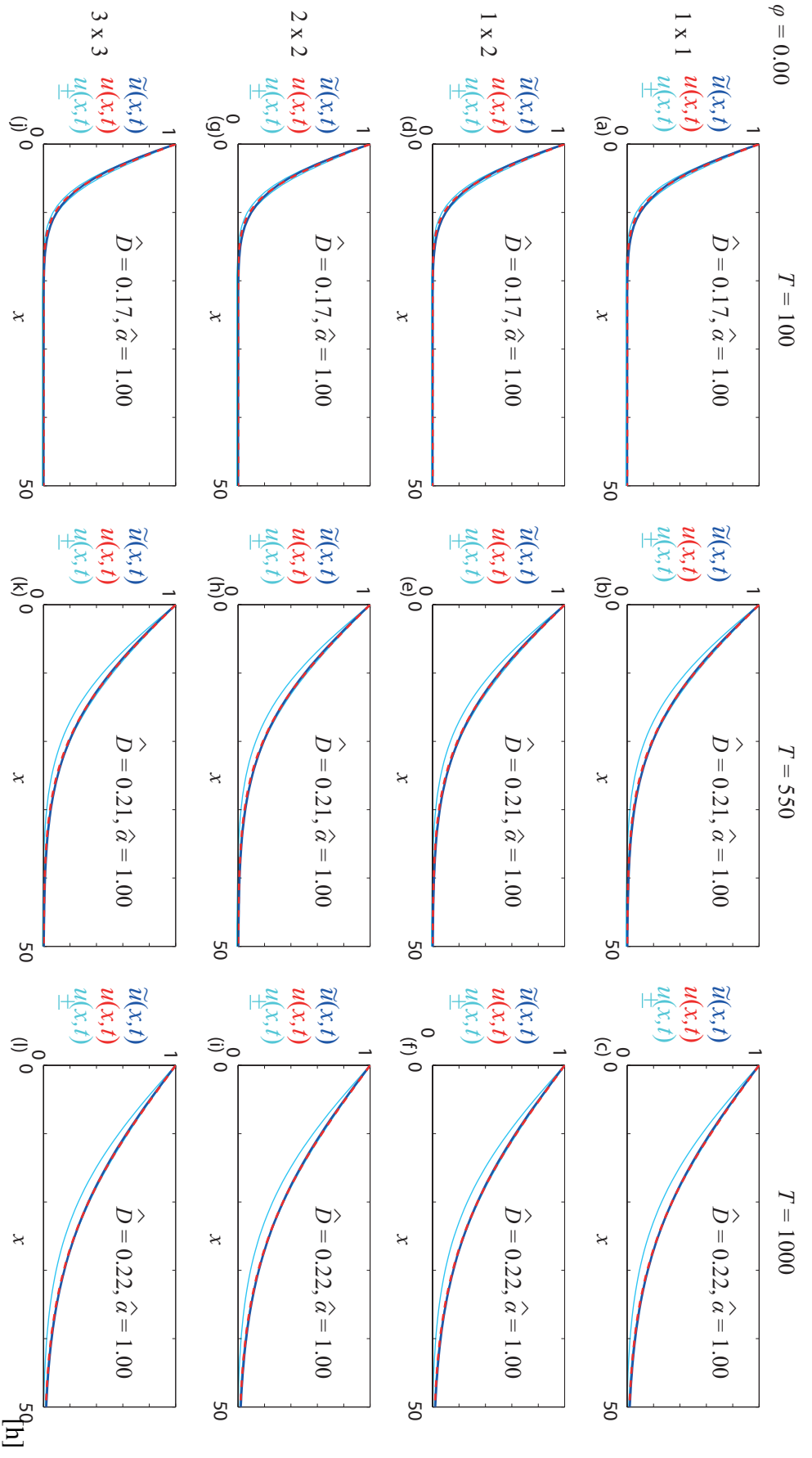# Additional results for Chapter 2

Results in Figures 3.1–3.2 are equivalent to the results in Figure 2.6 (Chap. 2) except that these results correspond to $\phi = 0$ and $\phi = 0.25$, respectively. Similarly, the results in Figures 3.3–3.5 are equivalent to the results in Figure 2.5 (Chap 2) except that these results correspond to 1×1, 1×2 and 2×2 obstacles, respectively.

Figure 3.1: Averaged agent density data for $\phi = 0$. The normalised density of agents in each vertical strip, $\tilde{u}(x,t)$ (dark blue), the analytical solution of Equation (2), $u(x,t)$, with $(\hat{\alpha}, \hat{D})$ (red-dashed) and the analytical solution of Equation (2), $u_\pm(x,t)$, with $\alpha = \hat{\alpha} \pm 0.05$ and $D = \hat{D}$ (light blue), where care was taken to only present results where $\alpha \leq 1$. Results in (a)-(c); (d)-(f); (g)-(i) and (j)-(l) correspond to lattices populated with 1×1, 1×2, 2×2 and 3×3 obstacles, respectively. Results in (a), (d), (g) and (j); (b), (e), (h) and (k) and (c), (f), (i) and (l) correspond to $T = 100$, $T = 550$ and $T = 1000$ respectively. The $\tilde{u}(x,t)$ profiles were generated on a 100×1000 lattice and were averaged over $K = 50,000$ realisations. The obstacle field was regenerated every 100 simulations. Results for $u(x,t)$ used parameters $L = 1000$, T as indicated, and the least-squares estimates of $(\hat{\alpha}, \hat{D})$ as given in each subfigure and presented in Table II. The analytical solution was truncated after $50,000$ terms in the series.

Figure 3.2: Averaged agent density data for $\phi = 0.25$. The normalised density of agents in each vertical strip, $\tilde{u}(x,t)$ (dark blue), the analytical solution of Equation (2), $u(x,t)$, with $(\hat{\alpha}, \hat{D})$ (red-dashed) and the analytical solution of Equation (2), $u_{\pm}(x,t)$, with $\alpha = \hat{\alpha} \pm 0.05$ and $D = \hat{D}$ (light blue), where care was taken to only present results where $\alpha \leq 1$. Results in (a)-(c); (d)-(f); (g)-(i) and (j)-(l) correspond to lattices populated with 1×1, 1×2, 2×2 and 3×3 obstacles, respectively. Results in (a), (d), (g) and (j); (b), (e), (h) and (k) and (c), (f), (i) and (l) correspond to $T = 100$, $T = 550$ and $T = 1000$ respectively. The $\tilde{u}(x,t)$ profiles were generated on a 100×1000 lattice and were averaged over $K = 50,000$ realisations. The obstacle field was regenerated every 100 simulations. Results for $u(x,t)$ used parameters $L = 1000$, T as indicated, and the least-squares estimates of $(\hat{\alpha}, \hat{D})$ as given in each subfigure and presented in Table II. The analytical solution was truncated after 50,000 terms in the series.
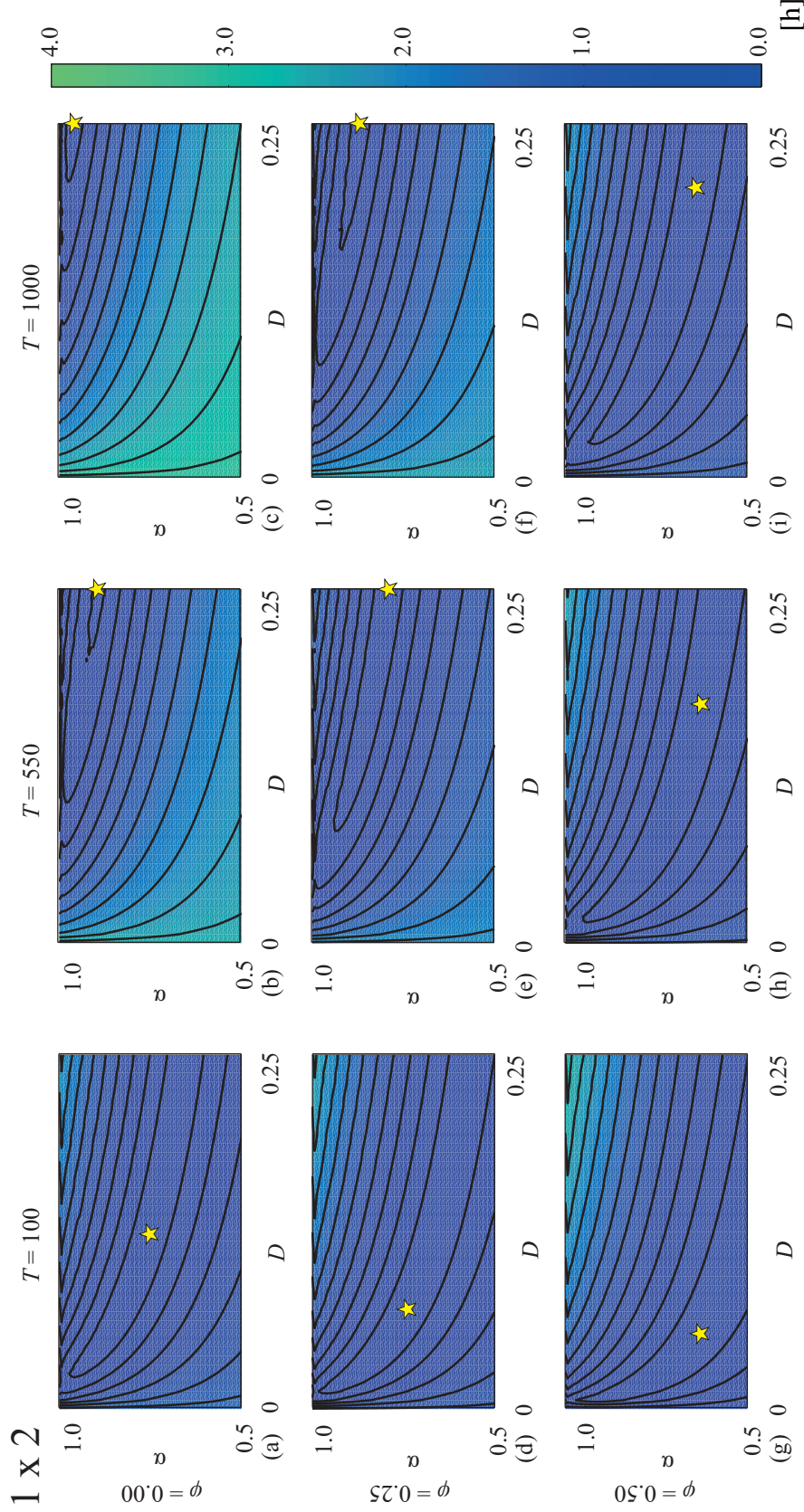
Figure 3.3: The magnitude of the sum of squared residuals, $S(\alpha, D) = \sum_{i=0}^{M} \epsilon_i^2$, for $0 < D \leq 0.25$ and $0.5 \leq \alpha \leq 1$. All discrete results correspond to 1×1 obstacles. Results in (a)-(c), (d)-(f) and (g)-(i) are for $\phi = 0.0, 0.25$ and 0.50, respectively. Results in (a),(d),(g); (b),(e),(h) and (c),(f),(i) show results at $T = 100, 550$ and 1000 respectively. All results were generated on a 100×1000 lattice populated with 3×3 obstacles and were averaged over $K = 50,000$ realisations. All error surfaces were generated by considering 80 equally-spaced values of D. Contour lines are given at increments of 0.25. The minimum of each error surface (yellow pentagon) was estimated by the Levenberg-Marquardt algorithm. The values of these minima, $(\hat{\alpha}, \hat{D})$, are given in Table II.

Figure 3.4: The magnitude of the sum of squared residuals, $\mathcal{S}(\alpha, D) = \sum_{i=0}^{M} \epsilon_i^2$, for $0 < D \leq 0.25$ and $0.5 \leq \alpha \leq 1$. All discrete results correspond to 1×2 obstacles. Results in (a)-(c), (d)-(f) and (g)-(i) are for $\phi = 0.0$, 0.25 and 0.50, respectively. Results in (a),(d),(g); (b),(e),(h) and (c),(f),(i) show results at $T = 100$, 550 and 1000 respectively. All results were generated on a 100×1000 lattice populated with 3×3 obstacles and were averaged over $K = 50,000$ realisations. All error surfaces were generated by considering 80 equally-spaced values of α and 40 equally-spaced values of D. Contour lines are given at increments of 0.25. The minimum of each error surface (yellow pentagon) was estimated by the Levenberg-Marquardt algorithm. The values of these minima, $(\hat{\alpha}, \hat{D})$, are given in Table II.
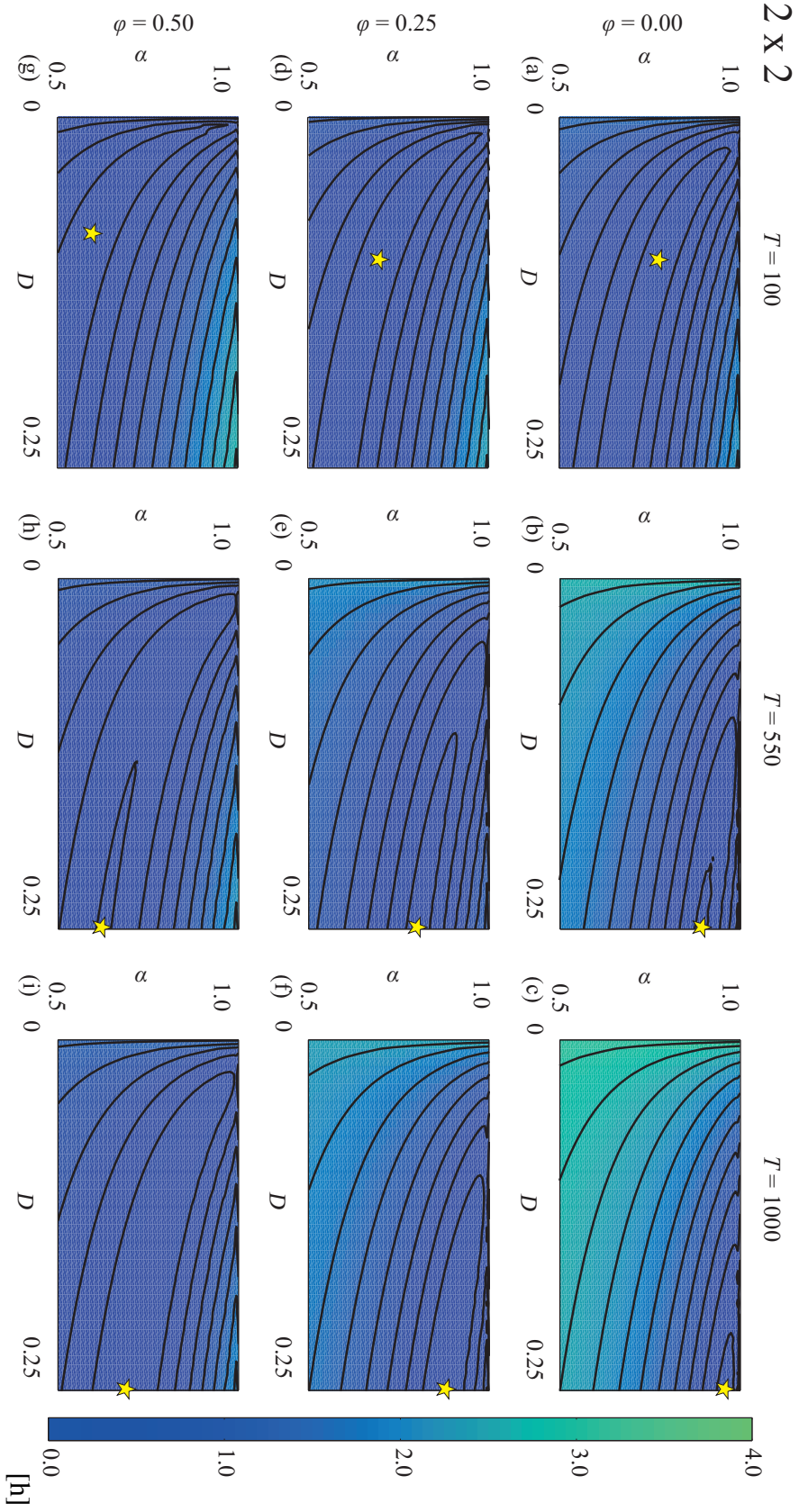
2 x 2

Figure 3.5: The magnitude of the sum of squared residuals, $\mathcal{S}(\alpha, D) = \sum_{i=0}^{M} \epsilon_i^2$, for $0 < D \leq 0.25$ and $0.5 \leq \alpha \leq 1$. All discrete results correspond to 2×2 obstacles. Results in (a)-(c), (d)-(f) and (g)-(i) are for $\phi = 0.0, 0.25$ and 0.50, respectively. Results in (a),(d),(g); (b),(e),(h) and (c),(f),(i) show results at $T = 100, 550$ and 1000 respectively. All results were generated on a 100×1000 lattice populated with 3×3 obstacles and were averaged over $K = 50,000$ realisations. All error surfaces were generated by considering 80 equally-spaced values of α and 40 equally-spaced values of D. Contour lines are given at increments of 0.25. The minimum of each error surface (yellow pentagon) was estimated by the Levenberg-Marquardt algorithm. The values of these minima, $(\hat{\alpha}, \hat{D})$, are given in Table II.

Chapter 4

Modelling transport through an environment crowded by a mixture of obstacles of different shapes and sizes

4.1   Abstract

Many biological environments are crowded by macromolecules, organelles and cells which can impede the transport of other cells and molecules. Previous studies have sought to describe these effects using either random walk models or fractional order differential equations. Here we examine the transport of both a single agent and a population of agents through an environment containing obstacles of varying size and shape, whose relative densities are drawn from a specified distribution. Our simulation results for a single agent indicate that smaller obstacles are more effective at retarding transport than larger obstacles, and these findings are consistent with our simulations of the collective motion of populations of agents. In an attempt to explore whether these kinds of stochastic random walk simulations can be described using a fractional order differential equation framework, we calibrate the solution of such a differential equation to our averaged agent density information. Our approach suggests that these kinds of commonly

(a)   (b)

Figure 4.1: (a) Intracellular image of mouse pancreatic acinar cells [41]. (b) Intracellular image of alpha cells from a diabetic mouse [41]. Images (a)-(b) are reproduced with kind permission from Springer.

used differential equation models ought to be used with care since we are unable to match the solution of a fractional order differential equation to provide a meaningful interpretation of our averaged discrete results.

4.2   Introduction

Many biological environments, such as those shown in Figure 4.1 (a)–(b), are crowded by macromolecules, organelles and cells of varying size and shape. Experimental and computational evidence suggests that crowding effects may impede the transport of macromolecules and cells in such environments [4, 6, 9, 82–85]. Therefore, the development of reliable mathematical models of this transport process is very important. Several previous studies have sought to describe crowded transport processes using either random walk simulation models [1, 11–13, 17, 23, 25, 55, 86–88] or fractional order differential equation (FDE) models [7, 10, 29, 30, 36–38, 89–91]. Although some previous studies have considered the effect of different obstacle shapes and sizes in detail [92–95], others have simply focused on studying transport through environments in which a single type of obstacle is present [13, 17]. Here, we focus on environments containing a mixture of different types of obstacles since experimental images (Figure 4.1 (a)–(b)) indicate that biological environments may contain multiple types of obstacles, whose sizes vary considerably.

In this work we examine the transport of both individual agents and populations of agents through crowded environments using a lattice-based unbiased nearest neighbour random walk model. We simulate crowding effects by randomly populating the lattice with immobile obstacles of different shapes and sizes, whose relative densities are specified by a particular

distribution. By holding the density of lattice sites occupied by obstacles, ϕ, constant, and varying the relative density of each individual obstacle type, we are able to create different crowding environments. Some of these environments are dominated by small obstacles, whilst others are dominated by large obstacles.

Although the idea of studying transport through a crowded environment using random walk simulations has become well established since Saxton's original studies over twenty years ago, this area of research remains active with many recent studies making valuable contributions. For example, recent theoretical advancements have extended Saxton's lattice–based results to lattice–free frameworks [92, 96, 97], including studying the role of obstacle orientation [98]. Progress has also been made by combining experimental and theoretical approaches, for example, studying overlapping circular and elliptical obstacles [99] and studying more complicated environments containing up to 15 different types of obstacles [93]. Other more experimentally–oriented studies have sought to interpret trajectory data describing the motion of individual cells or molecules using various mathematical frameworks [94, 95, 100]. In addition to this collection of studies which explicitly focus on motion through crowded environments, other researchers have made progress towards the development, application and solution of FDE models that are thought to implicitly represent crowded transport. Such FDE models have been analysed in various biological settings including chemical reactions [29], reaction fronts [30, 36] and reaction–diffusion mechanisms [37]. We would like to emphasise that the group of studies described here, focussing explicitly on motion through crowded environments using experimental and simulation data [92–100], have not attempted to interpret their results using any kind of FDE framework. Conversely, the group of studies described here focussing on FDE models [29, 30, 36, 37, 91] have not attempted to connect the solution of any FDE model to measurements from any simulation or experiment which explicitly represents transport through a crowded environment. Therefore, given the discrepancy between these two active areas of the literature, one of the aims of the present study is to consider a stochastic model of transport through a crowded environment containing a mixture of different obstacle shapes and sizes and to use averaged data from the stochastic model to examine whether it is possible to represent the transport process using a simpler FDE framework. Although there is a current debate in the literature about how to discriminate between obstructed diffusion, CTRWs and FDEs, and fractional Brownian motion [8], we concentrate on CTRWs and FDEs in this work.

4.3   Stochastic simulations

We consider a two–dimensional square lattice, with lattice spacing Δ, where we index sites (i,j), with $0 \leq i \leq M$ and $0 \leq j \leq N$, so that each site has location $(x,y) = (i\Delta, j\Delta)$. The dimension of the lattice is $0 \leq x \leq L_x$ and $0 \leq y \leq L_y$, where $L_x = (M+1)\Delta$ and $L_y = (N+1)\Delta$. At the start of a simulation we randomly populate the lattice with immobile obstacles to a specified, spatially uniform density, ϕ. We then place either a single motile agent (Section 4.4) or a population of motile agents (Section 4.5) on vacant sites. These agents undergo an unbiased nearest neighbour random walk in which we enforce a simple exclusion condition [27]. Potential motility events that would lead to an agent occupying the same site as another agent or an obstacle are aborted. We use the Gillespie algorithm [63] to advance the simulation until we reach some time T. We always average our results over K identically prepared realisations. The initial location of the motile agent is randomly chosen in each realisation. To minimise the computational expense, we regenerate the obstacle field every R realisations [1, 13]. Provided that R is sufficiently small, this has no observable effect on the averaged results [1, 13]. For all results presented we always checked that the results were insensitive to the size of the lattice.

In this study, we consider four types of obstacles which occupy: (i) a single lattice site (1×1); (ii) two adjacent lattice sites (1×2); (iii) four lattice sites in a square arrangement (2×2); and (iv) nine lattice sites in a square arrangement (3×3). We note that 1×1, 2×2 and 3×3 obstacles are symmetric with respect to the lattice whilst 1×2 obstacles are not. When placing the asymmetric 1×2 obstacles on the lattice we always take care to randomly orient the obstacles so that, on average, there is no preferred direction of alignment.

For any distribution of obstacles placed on the lattice at random, the total number of obstacles is approximately given by $\sum_m A_m n_m = \lfloor NM\phi \rfloor$, where A_m and n_m denote the area and number of the mth obstacle type, respectively, $\lfloor \cdot \rfloor$ denotes the floor function and the sum is taken over all obstacle types. Although this relationship is an approximation, we find that $\sum_m A_m n_m - \lfloor NM\phi \rfloor$ is extremely small provided that we consider a sufficiently large lattice, which means that the approximation is very accurate and does not impact our results. For example, for all choices of M, N and ϕ used in this work, we find that $\sum_m A_m n_m - \lfloor NM\phi \rfloor < 3 \times 10^{-5}$. Here we use the floor function because in any stochastic realisation of the model the summation is always an integer whereas $NM\phi$ is not always an integer.

In all cases that we consider, with four types of obstacles, we have

$$n_{(i)} + 2n_{(ii)} + 4n_{(iii)} + 9n_{(iv)} = \lfloor NM\phi \rfloor, \tag{4.1}$$

where we have expanded the sum and substituted the size of each obstacle into the equation. Since Equation (4.1) is Diophantine [101] with four unknowns, it is necessary to enforce some additional relationships between the different types of obstacles to ensure that the solution is unique. In particular, we consider three different situations:

I. *Decreasing distribution:* A distribution in which the number of lattice sites occupied by each type of obstacle forms a decreasing geometric series, in which smaller obstacles are more abundant than larger obstacles. In this case, the ratio of the number of sites occupied by each successive type of obstacle is a positive constant, r. Mathematically, we can write this as $(A_{(i)}n_{(i)})/(A_{(ii)}n_{(ii)}) = (A_{(ii)}n_{(ii)})/(A_{(iii)}n_{(iii)}) = (A_{(iii)}n_{(iii)})/(A_{(iv)}n_{(iv)}) = r$. To solve explicitly for the number of each obstacle type, we note that

$$A_{(i)}n_{(i)} = r^3 A_{(iv)}n_{(iv)},$$
$$A_{(ii)}n_{(ii)} = r^2 A_{(iv)}n_{(iv)},$$
$$A_{(iii)}n_{(iii)} = r A_{(iv)}n_{(iv)}. \tag{4.2}$$

Substituting Eqs. (4.2) into Equation (4.1) gives

$$A_{(iv)}n_{(iv)} \left(1 + r + r^2 + r^3\right) = \lfloor NM\phi \rfloor. \tag{4.3}$$

Finally, combining the solution of Equation (4.3) with Eqs. (4.2) gives

$$n_{(i)} = \frac{r^3 \lfloor NM\phi \rfloor}{A_{(i)}\beta}, \; n_{(ii)} = \frac{r^2 \lfloor NM\phi \rfloor}{A_{(ii)}\beta},$$
$$n_{(iii)} = \frac{r \lfloor NM\phi \rfloor}{A_{(iii)}\beta}, \; n_{(iv)} = \frac{\lfloor NM\phi \rfloor}{A_{(iv)}\beta}, \tag{4.4}$$

where $\beta = 1 + r + r^2 + r^3$. When the coefficients in Eqs. (4.4) are non-integers we apply the

floor function. Choosing $r = 4$, and substituting the values for $A_{(m)}$ for each case, we obtain

$$n_{(i)} = \frac{576}{765} \lfloor NM\phi \rfloor, \; n_{(ii)} = \frac{72}{765} \lfloor NM\phi \rfloor,$$
$$n_{(iii)} = \frac{9}{765} \lfloor NM\phi \rfloor, \; n_{(iv)} = \frac{1}{765} \lfloor NM\phi \rfloor. \tag{4.5}$$

The coefficients in Eqs. (4.5) determine the number of occupied lattice sites for each obstacle type. As expected, the number of lattice sites occupied by smaller 1×1 obstacles is much greater than the number occupied by larger 3×3 obstacles.

II. *Increasing distribution:* A distribution in which larger obstacles are more abundant than smaller obstacles. In this case we assume that the number of 1×1, 1×2, 2×2 and 3×3 obstacles form the first, second, fourth and ninth terms in an increasing geometric series in which the ratio between successive terms is r. These terms are chosen to coincide with the area of each obstacle type. It follows that

$$n_{(ii)} = r \, n_{(i)},$$
$$n_{(iii)} = r^3 \, n_{(i)},$$
$$n_{(iv)} = r^8 \, n_{(i)}. \tag{4.6}$$

The solution of Equation (4.1) with Eqs. (4.6) is

$$n_{(i)} = \frac{\lfloor NM\phi \rfloor}{\gamma}, \; n_{(ii)} = \frac{r \lfloor NM\phi \rfloor}{\gamma},$$
$$n_{(iii)} = \frac{r^3 \lfloor NM\phi \rfloor}{\gamma}, \; n_{(iv)} = \frac{r^8 \lfloor NM\phi \rfloor}{\gamma}, \tag{4.7}$$

where $\gamma = 1 + 2r + 4r^3 + 9r^8$. In our case, choosing $r = 5/4$, we have

$$n_{(i)} = \frac{65536}{4257001} \lfloor NM\phi \rfloor, \; n_{(ii)} = \frac{81920}{4257001} \lfloor NM\phi \rfloor,$$
$$n_{(iii)} = \frac{128000}{4257001} \lfloor NM\phi \rfloor, \; n_{(iv)} = \frac{390625}{4257001} \lfloor NM\phi \rfloor. \tag{4.8}$$

As expected, the number of larger 3×3 obstacles is much greater than the number of smaller 1×1 obstacles.
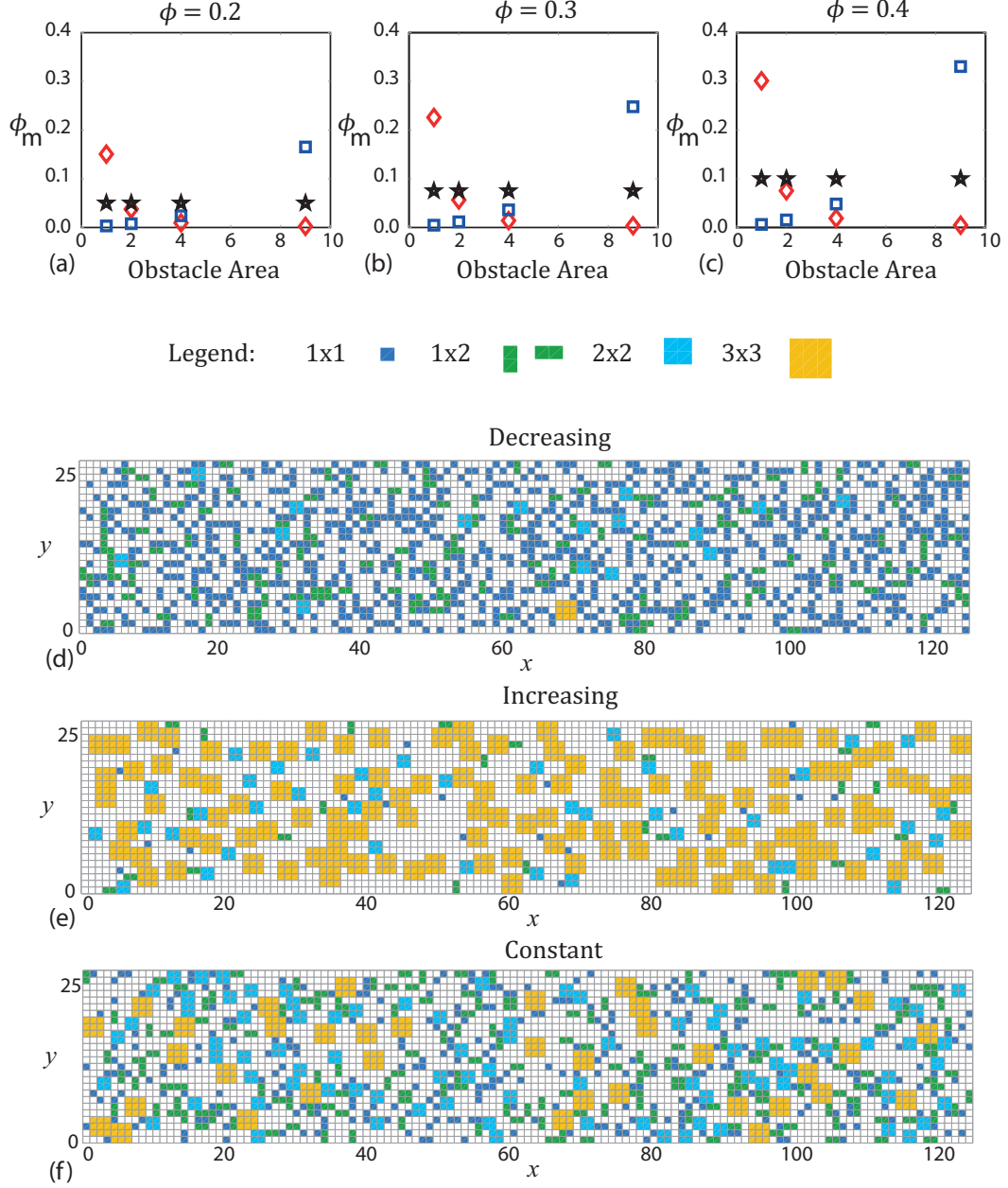
III. *Constant distribution:* A distribution in which the number of lattice sites occupied by each type of obstacle is equal: $n_{(i)} = 2n_{(ii)} = 4n_{(iii)} = 9n_{(iv)}$. The solution of Equation (4.1) with this condition is given by

$$n_{(i)} = \frac{36}{144} \lfloor NM\phi \rfloor, \ n_{(ii)} = \frac{8}{144} \lfloor NM\phi \rfloor,$$
$$n_{(iii)} = \frac{9}{144} \lfloor NM\phi \rfloor, \ n_{(iv)} = \frac{4}{144} \lfloor NM\phi \rfloor. \tag{4.9}$$

In this case, no obstacle type occupies a larger proportion of lattice sites than any other. Distribution III is an intermediate case relative to distributions I and II, and we refer to distributions I, II and III as decreasing, increasing and constant distributions, respectively.

In Figure 4.2 (a), (b) and (c) we show the proportion of lattice sites occupied by each obstacle type for $\phi = 0.2, 0.3, 0.4$, respectively. Specifically, in each subfigure, we show the relative density of occupied lattice sites, $\phi_m = A_{(m)} n_{(m)} / (\lfloor NM\phi \rfloor)$, for each obstacle type. For each value of ϕ shown, the decreasing distribution has a relative abundance of small obstacles, the increasing distribution has a relative abundance of large obstacles, and the constant distribution lies between. Figure 4.2 (d), (e) and (f) show lattices occupied by obstacles from the decreasing, increasing and constant distributions, respectively. Visually, in Figure 4.2 (e), which shows a lattice occupied by obstacles drawn from an increasing distribution, we see that the crowded environment contains many vacant, interconnected and spacious corridors. Conversely, Figure 4.2 (d), which shows a lattice occupied by obstacles drawn from the decreasing distribution, appears to contain far less of these vacant interconnected corridors. Figure 4.2 (f), which corresponds to the constant distribution, lies between these two cases. Therefore, in summary, visual inspection of the different crowding environments indicate that a lattice crowded using the increasing distribution appears to contain the highest degree of interconnected free space which we anticipate will facilitate transport more readily than the decreasing or constant lattice environments. We note that while it might be straightforward to anticipate this qualitative trend, it is not, by any means, obvious what the quantitative differences between transport through these different environments might be. In Sections 4.4 and 4.5 we attempt to apply mathematical models to describe motion through these different environments in order to provide such quantitative information.

To be consistent with previous simulation studies we take care to ensure that ϕ is always less than the site percolation threshold [13, 23, 25] which, for a square lattice occupied by 1×1

Figure 4.2: (a)-(c) Density of lattice sites, ϕ_m, occupied by each type of obstacle as a function of obstacle size, for $N = 100$, $M = 100$ and $\phi = 0.2, 0.3, 0.4$, respectively. The decreasing, increasing and constant distributions are shown as red-diamond, blue-square and black-pentagrams, respectively. Images in (d)-(f) show lattice environments occupied by decreasing, increasing and constant distributions, respectively, each with $\phi = 0.4$. Each type of obstacle is uniquely coloured, as described in the legend.

obstacles, is approximately 0.5927 [27]. We also note that visual inspection of the crowding environments in Figure 4.2 confirms the presence of closed regions of free space.

4.4 Transport of a single agent

We first consider the transport of a single agent through a crowded environment randomly populated with obstacles, to density ϕ, whose relative numbers are drawn from one of the distributions described in Secs. 4.3. After placing the obstacles on the lattice, we then place a single agent at a randomly chosen vacant site and allow it to undergo a random walk with periodic boundary conditions applied along all boundaries. To assess the effect of the different crowding environments on the transport process, we record the squared displacement of the agent, $r(t)^2 = (x(t) - x(0))^2 + (y(t) - y(0))^2$, at geometrically spaced time intervals which are related by $t_{n+1} = t_n + hg^n$, where $t_0 = 0$, $h = T(1-g)/(1-g^{P-1})$, P is the total number of time points and $g = 1.1$ is a geometric factor. Repeating this process for many identically prepared simulations allows us to calculate an ensemble average of $r(t)^2$. Many previous studies have analysed this kind of data by assuming that the MSD follows a power law [1, 11–13]

$$\langle r^2 \rangle = 4Dt^\alpha, \tag{4.10}$$

where $D\ [L^2T^{-\alpha}]$ is a generalised diffusion coefficient, $0 < \alpha < 2$ indicates the type of transport process taking place, with $\alpha = 1$ corresponding to Fickian diffusion, $\alpha < 1$ corresponding to subdiffusion, $\alpha > 1$ corresponding to superdiffusion [7, 10] and $\langle \cdot \rangle$ denotes an average over a large ensemble of simulations. In this work we focus on $0 < \alpha \leq 1$ because transport through a crowded environment is thought to be subdiffusive ($\alpha < 1$) [7, 10], whereas transport through an uncrowded environment is known to be Fickian ($\alpha = 1$). We rewrite Equation (4.10) as $\log_{10}(\langle r^2 \rangle /t) = \log_{10}(4D) + (\alpha - 1)\log_{10}(t)$, which suggests that, if the MSD follows Equation (4.10), plotting $\log_{10}(\langle r^2 \rangle /t)$ as a function of $\log_{10}(t)$ will lead to a straight line with slope $\alpha - 1$.
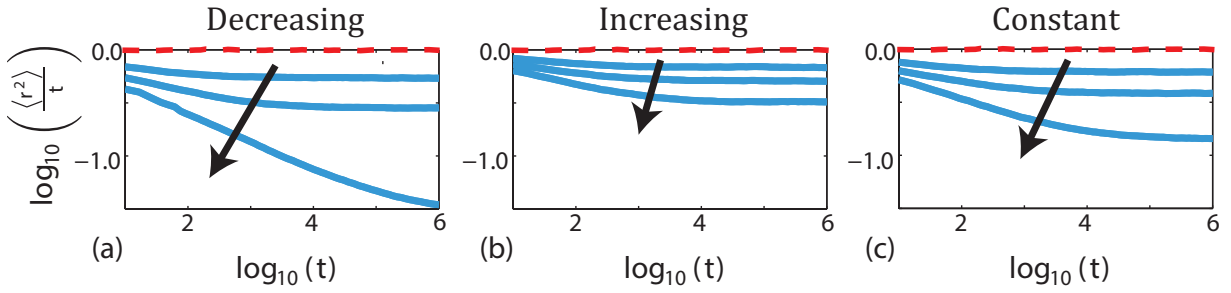
Figure 4.3: (a)-(c) MSD for a single agent moving through a lattice randomly populated with obstacles whose relative densities are drawn from the decreasing, increasing, and constant distributions, respectively (solid blue). Results are also shown for the control case with no obstacles present (dashed red). In each case we have $N = M = 256$ and $\phi = 0.0, 0.2, 0.3, 0.4$. Averaged simulation data was constructed with $R = 200$ and $K = 50,000$. The arrow points in the direction of increasing ϕ.

MSD data associated with a crowded environment populated by obstacles drawn from decreasing, increasing and constant distributions is shown in Figure 4.3 (a), (b) and (c), respectively. In each plot we include results from a control case, with no obstacles present and $\phi = 0$. For the control case we see that the MSD data forms a perfectly straight line, lying on the horizontal axis, for all t considered. This confirms that without any obstacles present we have Fickian diffusion with $\alpha = 1$, as expected.

Results for the MSD data in Figure 4.3 with $\phi > 0$ are more interesting. A visual, qualitative comparison of these results confirms that the details of the crowding environment has an important impact on the transport process since the curves describing the MSD are different for each obstacle distribution. To demonstrate these differences quantitatively we calculate the slope of each MSD curve in Figure 4.3, for $\phi = 0.4$, at $t = 10^4$. To do this, we perform a linear regression through the five temporal intervals closest to $t = 10^4$ in each data set. The linear regression analysis provides us with an estimate of the slope from which we estimate α. This procedure gives $\alpha = 0.73$ for the decreasing distribution, $\alpha = 0.98$ for the increasing distribution and $\alpha = 0.92$ for the constant distribution, suggesting that the decreasing distribution is most effective at retarding the transport process, that the increasing distribution is least effective at retarding the transport process, and that the constant distribution is between these two extremes.

Our results for the MSD data in Figure 4.3 indicate that the data does not follow the power law given by Equation (4.10) when $\phi > 0$. If the MSD data were to obey this power law, the plots in Figure 4.3 would be straight lines for all t. However, this is not the case, since the MSD data with $\phi > 0$ forms a family of curves. Each of these curves eventually asymptotes to a horizontal line as $t \to \infty$. This result has been observed previous by us [1] and many others [11–13]. We note that there are other discrete random walk process which genuinely obey power laws, such as Equation (4.10). For example, the previous stochastic model analysed by Kehr and Kutner [102] is associated with MSD data that follows a power law with $\alpha = 1/2$. However, for the biologically motivated random walk models like we consider here, this is not the case.

4.5 Transport of a population of agents

The development of mathematical models that can be used to describe and predict the transport of a population of agents through a crowded environment is very important as this kind of situation is often observed and measured during biological experiments For example, Kicheva [39] considered the motion of a population of initially confined molecules within the developing wing disc, and the motion of these molecules is hindered by the presence of other biomolecules and obstacles within the wing disc. Similarly, Simpson [75] considered the motion of a population of initially confined neural crest cells along the tissues of the developing gut tissues in a chick embryo, and the motion of these cells is hindered by the presence of other cells and obstacles in the gut tissues. To mimic this kind of biological experiment we now consider a transport process in which an initially confined population of agents moves through a crowded environment. As in Section 4.4, we initially populate the lattice with obstacles drawn from an increasing, decreasing or constant distribution to density ϕ. To initialise the simulation, we populate all vacant lattice sites in the vertical columns for which $(L_x - w) \le 2x \le (L_x + w)$ with agents. This corresponds to a population of agents initially confined to a vertical strip, of width w, located at the centre of the domain. We then allow the agents to undergo an unbiased nearest neighbour random walk in which we enforce a straightforward exclusion mechanism by aborting potential motility events which would lead to an agent occupying the same lattice site as another agent or an obstacle. Absorbing boundary conditions at $x = 0$ and $x = L_x$ are enforced.
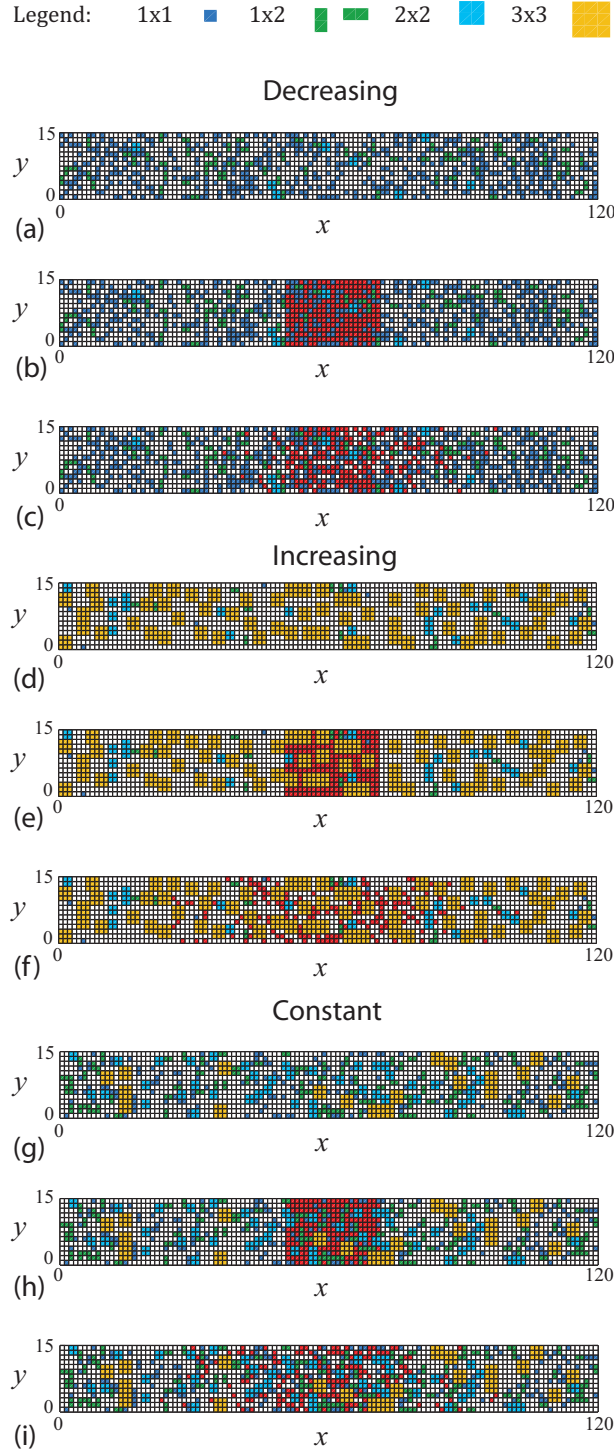
Figure 4.4: Results in (a)-(c); (d)-(f) and (g)-(i) show a lattice occupied by a decreasing, increasing and constant distribution of obstacles, respectively. Each type of obstacle is uniquely coloured, as described in the legend. Results in (a), (d) and (g) show the lattice occupied by the obstacles without any agents present, each with $\phi = 0.40$. Results in (b), (e) and (h) show the same lattice and obstacle distribution where the vacant sites within the central 21 columns of the lattice have been initialised with motile agents. Results in (c), (f) and (i) show the distribution of agents after performing a random walk simulation until $T = 1000$. All results correspond to $M = 120$, $N = 15$ and $w = 21$.

Figure 4.4 (a), (d) and (g) shows a lattice which has been stochastically populated with obstacles from the decreasing, increasing and constant distributions, respectively, with $\phi = 0.4$. In Figure 4.4 (b), (e) and (h) we show the same lattices as in Figure 4.4 (a), (d) and (g), except that now we have placed a population of agents onto all vacant sites in the central 21 columns. We treat the system shown in Figure 4.4 (b), (e) and (h) as the initial condition for our simulations describing the transport of a population of agents through a crowded environment. We apply periodic boundary conditions along the horizontal boundaries and reflecting boundary conditions along the vertical boundaries. In Figure 4.4 (c), (f) and (i), we show the resulting distribution of agents from a single realisation at $T = 1000$. One way of comparing the distribution of agents in Figure 4.4 (c), (f) and (i) is to measure the width of the spreading population of agents. Recalling that the width of the initial distribution of agents was 21 lattice sites at $t = 0$, by $t = 1000$ the widths of the spreading population are 61, 77 and 75 lattice sites for the decreasing, increasing and constant distributions, respectively. These differences suggest that the rate at which the initially confined population of agents is able to spread through the crowded environment is greatest for the environment populated by obstacles from the increasing distribution, and smallest when the obstacles are drawn from the decreasing distribution. This trend is consistent with the results described in Section 4.4 describing the motion of a single agent. Since we have only dealt with a single realisation of the stochastic model to arrive at these preliminary observations, we now consider performing many identically prepared realisations to investigate whether similar differences occur when we describe the process using averaged data. To ensure that we do not encounter the Fickian regime we consider two observation times, $T = 1000$ and $T = 3000$, as our MSD simulations suggest that the transition from non–Fickian to Fickian behaviour occurs after $T = 10^4$ for all situations that we consider.

Since our initial distribution of agents in Figure 4.4 is, on average, independent of vertical position, we can characterise the averaged transport process as a function of the horizontal coordinate, x, and time, t [78, 103]. We construct averaged agent population density data in the following way: once the simulation reaches time T we calculate the density of agents in each vertical column of the lattice. Let $n_k(i, j)$ denote the occupancy of site (i, j) during the kth identically prepared realisation such that $n_k(i, j) = 0$ corresponds to a vacant site and $n_k(i, j) = 1$ corresponds to a site which is occupied by an agent. The density of agents in each vertical column is $[\sum_{j=1}^{M} n_k(i, j)]/\bar{n}_k$, where we have normalised the density by dividing by the number of agents which initially occupy the central column at $x = L_x/2$, $\bar{n}_k = \sum_{j=1}^{M} n_k(L_x/2, j)$.

The average density of agents in each column, at time T, further averaged using data from K identically prepared realisations, is given by [78, 103]

$$\bar{u}(x, T) = \frac{1}{K} \sum_{k=1}^{K} \left(\frac{1}{\bar{n}_k} \sum_{j=1}^{M} n_k(i, j) \right). \tag{4.11}$$

It has become increasingly common for researchers to implicitly represent transport through crowded environments using FDE models [7, 10, 29, 30, 36, 37, 89–91], and we note that many of these previous applications neglect to consider the relationship between the FDE description and the underlying stochastic mechanism. To improve our understanding of whether averaged density data from our relatively straightforward stochastic model can be accurately represented by an FDE framework, we now attempt to match our averaged agent density information with the solution of

$$\frac{\partial^{\alpha} u}{\partial t^{\alpha}} = D \frac{\partial^2 u}{\partial x^2}, \qquad 0 < x < L_x, \tag{4.12}$$

where $\partial^{\alpha}/\partial t^{\alpha}$ denotes a Caputo fractional derivative [32] of order α and L_x is the length of the spatial domain. Appropriate boundary and initial conditions that match our stochastic simulations are $u(0, t) = 0$, $u(L_x, t) = 0$ and $u(x, 0) = \mathrm{H}\left(x - [L_x - w]/2\right) - \mathrm{H}\left(x - [L_x + w]/2\right)$, where $\mathrm{H}(\cdot)$ is the Heaviside function. For these conditions the solution of Equation (4.12) is

$$u(x, t) = \sum_{k=1}^{\infty} A_k \sin\left(\frac{k\pi x}{L_x}\right) \mathrm{E}_{\alpha}\left[-D\left(\frac{k\pi}{L_x}\right)^2 t^{\alpha}\right], \tag{4.13}$$

where $\mathrm{E}_{\alpha}[\cdot]$ denotes a Mittag–Leffler function [32], and $A_k = 4\{\sin\left[k\pi/2\right]\sin\left[k\pi w/(2L_x)\right]\}/(k\pi)$.

To investigate whether Equation (4.12) provides an accurate framework to describe our averaged density data we must determine appropriate values of D and α. We estimate D and α by matching $u(x, t)$ to the averaged agent population density, $\bar{u}(x, t)$, using the Levenberg–Marquardt algorithm [80]. To apply this algorithm we first define $\epsilon_i = \bar{u}(x, T) - u(x, T)$, which measures the difference between the observed averaged data and the solution of Equation (4.12) at $t = T$. The Levenberg–Marquardt algorithm minimises $\mathcal{S}(\alpha, D) = \sum_{i=0}^{M} \epsilon_i^2$, where the sum is taken over all vertical columns of the lattice, by iteratively stepping from an initial guess, (α_0, D_0), down the gradient of $\mathcal{S}(\alpha, D)$ to the least squares estimate, $(\hat{\alpha}, \hat{D})$. As the algorithm proceeds we always ensure that $0 < D \leq 1/4$ and $0 < \alpha \leq 1$, as solutions outside of this
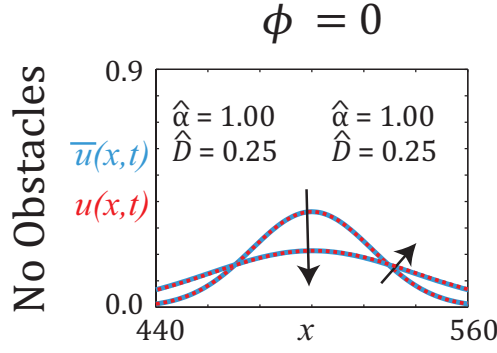
Figure 4.5: Evolution of the average population density, $\bar{u}(x,t)$ (blue), and the least squares solution of Equation (4.12), $u(x,t)$ (red-dashed). Results show density profiles for $\phi = 0$ and correspond to two different simulation times, $T = 1000$ and $T = 3000$, with the arrows indicating the direction of increasing time. The least squares estimates $\hat{\alpha}$ and $\hat{D}$ are given in the top left of each subfigure for $T = 1000$, and in the top right of each figure for $T = 3000$. Simulation parameters correspond to $N = 100$, $M = 1000$ and $w = 21$, with $R = 100$ and $K = 100,000$. The Fourier series solution for $u(x,t)$ was obtained by truncating the infinite series, Equation (4.13), after $30,000$ terms.

parameter range are physically unrealistic. Furthermore, we always test that our estimates of $(\hat{\alpha}, \hat{D})$ are independent of the initial guess, (α_0, D_0).

We first consider a control case with no obstacles and $\phi = 0$. Results are shown in Figure 4.5, confirming that the match between the density profiles from the averaged stochastic data and the solution of the Equation (4.12) with the least squares parameter estimates, $(\hat{\alpha}, \hat{D})$, is excellent. Furthermore, the Levenberg-Marquardt algorithm shows that we have $\hat{\alpha} = 1.00$ and $\hat{D} = 0.25$ at both $T = 1000$ and $T = 3000$. This is an expected result since there are no obstacles on the lattice and previous research has shown, from a theoretical point of view, that averaged density data associated with this random walk model without any obstacles is governed by Equation (4.12) with $\alpha = 1$ and $D = 1/4$ [78, 103]. In this case Equation (4.12) reduces to the linear diffusion equation. For this study it is relevant for us to make note of the fact that we obtain the same estimates of $\hat{\alpha} = 1.00$ and $\hat{D} = 0.25$ at two different inspection times, $T = 1000$ and $T = 3000$.

Results in Figure 4.6 show the averaged agent population density, $\bar{u}(x,t)$, superimposed on the solution of Equation (4.12), $u(x,t)$, obtained using the least squares parameter estimates, $(\hat{\alpha}, \hat{D})$, for $\phi > 0$. Several observations can be made from the results in Figure 4.6. Firstly, the match between the averaged agent density data and the solution of Equation (4.12) with $(\hat{\alpha}, \hat{D})$ is excellent. However, our estimates of $\hat{D}$ and $\hat{\alpha}$ are very sensitive to the different types
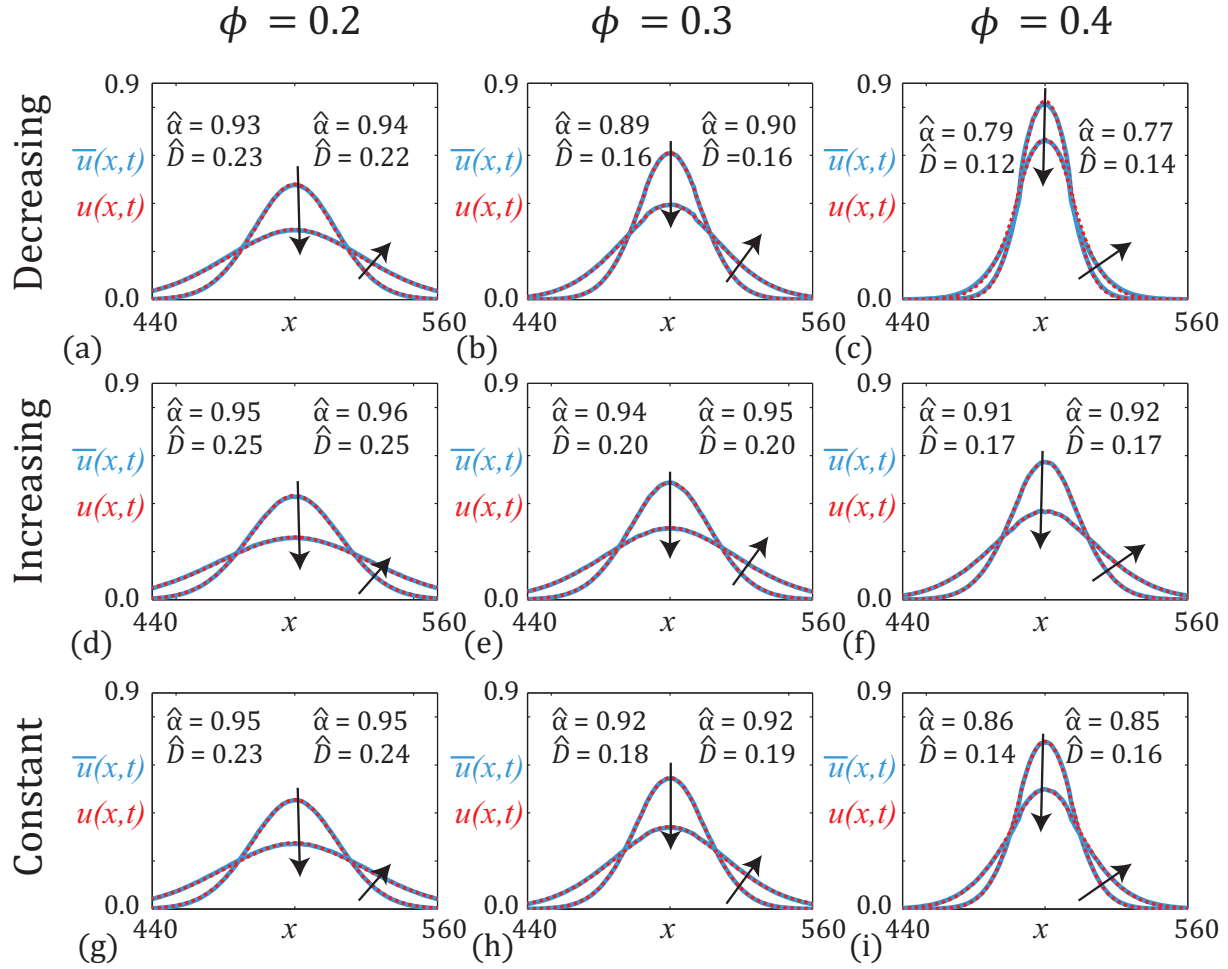
Figure 4.6: Evolution of the average population density, $\bar{u}(x,t)$ (blue), and the least squares solution of Equation (4.12), $u(x,t)$ (red-dashed). Results in (a)-(c); (d)-(f) and (g)-(i) correspond to decreasing, increasing and constant obstacle distributions, respectively. Results in (a), (d), (g); (b), (e), (h) and (c), (f), (i) show density profiles for $\phi = 0.2, 0.3, 0.4$, respectively. Results in each subfigure correspond to two different simulation times, $T = 1000$ and $T = 3000$, with the arrows indicating the direction of increasing time. The least squares estimates $\hat{\alpha}$ and $\hat{D}$ are given in the top left of each subfigure for $T = 1000$, and in the top right of each figure for $T = 3000$. Simulation parameters correspond to $N = 100$, $M = 1000$ and $w = 21$, with $R = 100$ and $K = 100,000$. The Fourier series solution for $u(x,t)$ was obtained by truncating the infinite series, Equation (4.13), after $30,000$ terms.

of obstacle distributions. For example, at $T = 1000$ with $\phi = 0.4$, we have $\hat{\alpha} = 0.79, 0.91$ and 0.86 for the decreasing, increasing and constant obstacle distributions, respectively. This suggests that the decreasing distribution is very effective at retarding the transport process, that the increasing distribution is least effective at retarding the transport process, and that the constant distribution lies between these two cases. Secondly, unlike the control case with $\phi = 0$, the calibration procedure for the data with $\phi > 0$ indicates that our estimates of $\hat{D}$ and $\hat{\alpha}$ depend upon the inspection time, T. This observation is contrary to the assumptions underpinning Equation (4.12), where D and α are supposed to be constant.

4.6 Discussion

In this work, we consider a transport process through a crowded environment that is populated by immobile obstacles of varying size and shape. In particular, we focus on three distributions of obstacle size and shape which represent an environment crowded by a relative abundance of small obstacles, an environment crowded by a relative abundance of large obstacles and an intermediate case. This framework allows us to create qualitatively different crowded environments whilst holding the density of occupied lattice sites constant, and to explore how the details of the distribution of agent shape and size impacts the transport properties.

We first consider the motion of a single motile agent and record the MSD as a function of time. To analyse these data, we use a standard method [1, 11–13, 17] and plot $\log_{10}(\langle r^2 \rangle / t)$ as a function of $\log_{10}(t)$. If the MSD followed a power law, these data would fall on a straight line. Instead, we observe that these data do not fall on a straight line, indicating that the transport process does not follow Equation (4.10). This kind of observation is consistent with several previous studies [11–13, 17]. To quantify how the transport process is affected by different distributions of obstacle shapes and sizes, we follow a standard approach and estimate the slope of the plot of $\log_{10}(\langle r^2 \rangle / t)$ as a function of $\log_{10}(t)$. These results confirm that the details of the distribution of the obstacles can play an important role since different distributions with constant ϕ lead to different MSD data.

To extend our analysis to apply to biological experiments that involve the motion of populations of cells or molecules, we also consider the motion of a population of motile agents through various crowded environments. To simplify our analysis, we choose an initial condition that is,

on average, symmetric in the vertical direction and recorded average density of agents in each column of the lattice. This framework allows us to describe the transport of a population of agents as a function of the horizontal coordinate, x, and time, t. Extracting averaged density data from our stochastic model confirms that the details of the distribution of obstacle size and shape has an important impact on the transport process since we observe that otherwise identical populations of agents are able to move through some environments far more easily than others, even though the density of obstacles, ϕ, is the same.

To provide quantitative insight into our results describing the transport of a population of agents, we match our averaged density data with the solution of a standard FDE model, Equation (4.12), to provide a least squares estimate of D and α for the various crowding environments. Our results confirm that α decreases with ϕ, as expected, with the additional result that α also decreases when we consider distributions of obstacles in which small obstacles dominate. This trend is consistent with the MSD data, and together our observations confirm that obstacle distributions in which smaller obstacles dominate are more effective at retarding the transport process [104]. These outcomes imply that if we are to reliably predict and model transport through a crowded environment, we must characterise both the total density of obstacles, ϕ, as well as additional details of the distribution of obstacle shapes and sizes.

We conclude with some cautionary remarks. Since our least squares estimates of D and α in Equation (4.12) appear to depend on the inspection time T, our results suggest that FDE models ought to be used with care since a fundamental assumption underlying the use of these models is that D and α are constants that do not depend on the inspection time. Despite the widespread use of FDE models like Equation (4.12), our model calibration procedure implies that even a relatively straightforward random walk model, such as the model we consider here, cannot be properly described using this kind of FDE model. Our observation that the averaged density profiles are not described by Equation (4.12) is consistent with our analysis of MSD data which do not follow the commonly invoked power law, Equation (4.10).

Chapter 5

Calculating the Fickian diffusivity for a lattice–based random walk with agents and obstacles of different shapes and sizes

---

A paper published in *Physical Biology*.

Ellery, Adam J and Baker, Ruth E and Simpson, Matthew J, Calculating the Fickian diffusivity for a lattice-based random walk with agents and obstacles of different shapes and sizes. *Physical Biology* **12** 066010 (2015).

5.1   Abstract

Random walk models are often used to interpret experimental observations of the motion of biological cells and molecules. A key aim in applying a random walk model to mimic an in vitro experiment is to estimate the Fickian diffusivity (or Fickian diffusion coefficient), D. However, many in vivo experiments are complicated by the fact that the motion of cells and molecules is hindered by the presence of obstacles. Crowded transport processes have been modelled using repeated stochastic simulations in which a motile agent undergoes a random walk on a lattice that is populated by immobile obstacles. Early studies considered the most straightforward case in which the motile agent and the obstacles are the same size. More recent studies considered stochastic random walk simulations describing the motion of an agent through an environment populated by obstacles of different shapes and sizes. Here, we build on previous simulation studies by analysing a general class of lattice based random walk models

with agents and obstacles of various shapes and sizes. Our analysis provides exact calculations of the Fickian diffusivity, allowing us to draw conclusions about the role of the size, shape and density of the obstacles, as well as examining the role of the size and shape of the motile agent. Since our analysis is exact, we calculate D directly without the need for random walk simulations. In summary, we find that the shape, size and density of obstacles has a major influence on the exact Fickian diffusivity. Furthermore, our results indicate that the difference in diffusivity for symmetric and asymmetric obstacles is significant.

5.2   Introduction

Random walk models are routinely used to model both *in vitro* and *in vivo* experimental observations describing the motion of cells and biomolecules [67, 69, 105–107]. Often the aim of applying a random walk model to mimic *in vitro* observations is to provide an estimate of the diffusivity, D [108–110]. Unlike simpler *in vitro* experiments, *in vivo* experiments are complicated by the fact that the cells and biomolecules move through an environment populated by various types of obstacles that, owing to crowding effects, hinder their motion [93, 100, 111, 112].

Early analysis of random walk models describing motion through crowded environments involved repeated stochastic simulations of the random walk of an agent on a lattice, where the lattice is populated by immobile obstacles [11, 12]. In these early models both the size of the agent and the obstacles are equal to the lattice spacing [11, 12]. Analysing the temporal evolution of the mean squared displacement (MSD) of the motile agent indicates that, after a sufficient period of time, the MSD grows in proportion to time. Measuring the constant of proportionality from repeated computer simulations provides a means of estimating the long–time Fickian diffusivity, D [11, 12, 23, 25]. Using this approach, it is possible to demonstrate that D decreases as the density of obstacles increases, as we might anticipate [11, 12, 23, 25]. Other avenues of investigation involved the use of perturbation theory [113], percolation theory [114–116] and the eigenvalue spectrum [117]. More recent studies attempt to provide more realistic descriptions of cell and biomolecule motion by considering the motion of agents through environments that are populated by obstacles of varying shapes and sizes [1, 13, 94]. Similar to earlier models, these more detailed simulation studies show that, after a sufficient period of time, the MSD increases in proportion to time, and this observation can also be used

to estimate the long–time Fickian diffusivity, D [1, 13]. In addition to showing that D depends on the density of obstacles, these studies suggest that D also depends on the size and shape of the obstacles [1, 13].

Instead of relying on repeated stochastic random walk simulations, here we present a method that enables us to exactly calculate the long–time Fickian diffusivity, D, for a lattice–based random walk in which we vary the shape and size of both the motile agent and the immobile obstacles. We achieve this by generalising an approach previously described by Mercier and Slater [42–44]. The algorithm is described in Section 5.3, where we also confirm the accuracy of the approach by comparing exact calculations of D with estimates obtained using standard simulation methods. In Section 5.4.1 we systematically vary the size of the agent, the size of the obstacles and the density of the obstacles to examine how these details affect D for a two–dimensional random walk in which both the agents and obstacles are symmetric in shape. In Section 5.4.2 we consider a suite of two–dimensional scenarios in which either the agent or the obstacles are asymmetric. We also demonstrate how our approach can be implemented for three–dimensional problems in Section 5.4.3 where we systematically vary the size, shape and density of symmetric obstacles in three–dimensions. In Section 5.4.4 we calculate D for obstacle densities up to 50%. Finally, in Section 5.5, we discuss the implications of our results.

For symmetric agents and obstacles of the same size, we show that D decreases with the density of obstacles. This is an expected result that has been observed previously in simulation studies, however we also make further observations that have not been identified previously. For a given obstacle density, we find that D is most reduced for larger motile agents, relative to smaller motile agents, provided that the obstacles are symmetric. However, the opposite can be true when we consider the motion of agents in an environment populated by asymmetric obstacles. Furthermore, we find that D is sensitive to the size of the agents and obstacles relative to the size of the lattice spacing. In summary, our results indicate that the value of D is strongly linked to the details of the shape, size, symmetry and density of the obstacles. Therefore, caution ought to be exercised when D is estimated without a detailed characterisation of the obstacle shape, size and density.
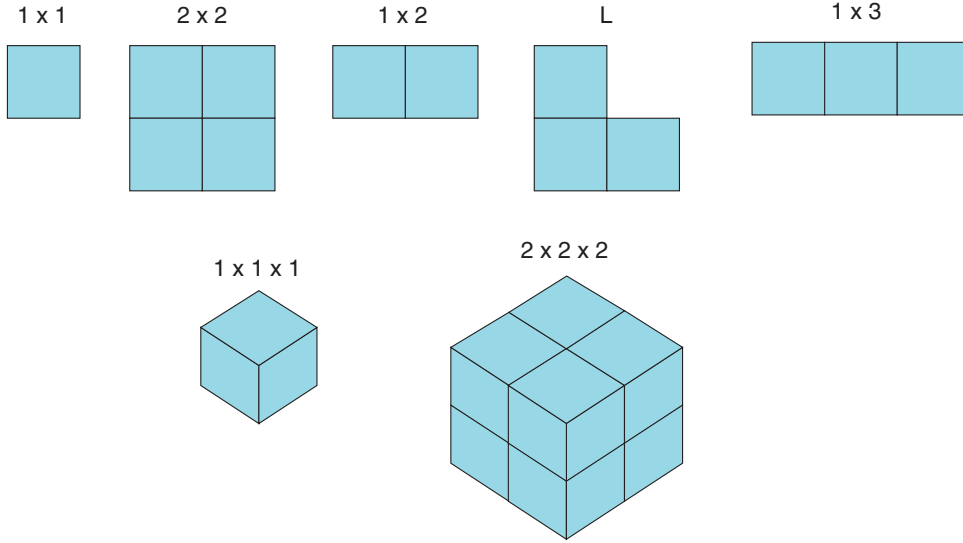
Figure 5.1: Various sizes and shapes of the two– and three–dimensional agents and obstacles used in this study. The dimensions relative to the lattice spacing are indicated next to each object.

5.3   Theory

We now consider a two–dimensional square lattice of dimension $X \times Y$, with unit lattice spacing $\Delta = 1$. Sites are indexed (i, j) so that each site has location $(x, y) = (i, j)$, with $0 \leq x \leq (X - 1)$ and $0 \leq y \leq (Y - 1)$. We also consider a three–dimensional square lattice of dimension $X \times Y \times Z$, with unit lattice spacing $\Delta = 1$. Sites are indexed (i, j, k) so that each site has location $(x, y, z) = (i, j, k)$, with $0 \leq x \leq (X - 1)$, $0 \leq y \leq (Y - 1)$ and $0 \leq z \leq (Z - 1)$. Since we always work with unit lattice spacing and unit rate constants, all calculations of diffusivity are dimensionless. These calculations can be redimensioned by rescaling with an appropriate dimensional lattice spacing, Δ, if required.

We represent various crowding environments by randomly populating a lattice with immobile obstacles to a specified spatially uniform density, $\phi = m_0 \nu / m$, where m_0 is the number of obstacles, ν is the number of sites per obstacle, and m is the total number of lattice sites. For the two–dimensional lattice we consider the five different types of agents and obstacles depicted in Figure 5.1, namely: (i) a square obstacle of area 1 (1×1, $\nu = 1$); (ii) a square obstacle of area 4 (2×2, $\nu = 4$); (iii) an asymmetric obstacle of area 2, consisting of two adjacent lattice sites (1×2, $\nu = 2$); (iv) an asymmetric obstacle of area 3 in an L–shaped arrangement ($\nu = 3$); and (v) an asymmetric obstacle of area 3 consisting of three lattice sites in a row (1×3, $V = 3$). When placing asymmetric obstacles on the lattice we always take care to randomly

orient the obstacles so that, on average, there is no preferred direction of alignment. For the three–dimensional lattice we consider two types of obstacles that are also depicted in Figure 5.1, namely: (vi) a cubic obstacle of volume 1 ($1 \times 1 \times 1$, $\nu = 1$); and (vii) a cubic obstacle of volume 8 ($2 \times 2 \times 2$, $\nu = 8$). Although our results focus on these seven specific obstacle and agent shapes, the exact procedure for calculating D can be applied to other obstacle and agent shapes by extending our analysis in an obvious way. Throughout this study we always ensure that ϕ is well below the relevant percolation threshold [68]. In the first part of the study we focus on modest obstacle densities, $0 < \phi \leq 0.15$. In the second part of the study we provide additional results for higher obstacle densities, $\phi \leq 0.50$.

To provide a check on the accuracy of our exact calculations of D we perform stochastic random walk simulations with the aim of showing that the exact calculations match estimates of D from a simulation approach. To initiate the random walk simulations we place a single motile agent at a randomly chosen location on the lattice, being careful to ensure that the agent does not overlap with any obstacles. The shape of the agent is chosen from one of the types depicted in Figure 5.1. The agent undergoes an unbiased nearest neighbour random walk with unit step length ($\Delta = 1$), periodic boundary conditions and an exclusion condition [27]. The exclusion condition means that any potential motility event that would lead to part of the agent occupying any site that is already occupied by an obstacle is aborted [27]. Our discrete model is similar to a blind-ant random walk [114]. We use the Gillespie1977 algorithm [63] to advance the simulation through time until we reach a pre–specified termination time, T. In all situations the rate at which the motile agent attempts to undergo a motility event is set to unity. Since the random walk simulations are stochastic, we always average our results over a large ensemble of identically prepared realisations. As each random walk simulation proceeds, we track the position of the agent and record the agent trajectory, from which we can calculate the MSD.

After performing a large number of identically prepared realisations of each random walk, we make the standard assumption that the average MSD data follows a power law [11, 12, 23, 25]

$$\langle r^2 \rangle = (2dD)t^\alpha, \tag{5.1}$$

where $r^2 = x^2 + y^2 + z^2$ is the dimensionless displacement squared, t is dimensionless time, d is the dimension of the system, α is an exponent, $0 < D \leq 1/(2d)$ denotes the dimensionless diffusivity and $\langle \cdot \rangle$ denotes an average over a large ensemble. Fickian diffusion is associated

with $\alpha = 1$ [69]. To estimate D from this data we rewrite Equation (5.1) as

$$\log_{10}\left(\frac{\langle r^2 \rangle}{t}\right) = \log_{10}\left(2dD\right) + (\alpha - 1)\log_{10}(t). \qquad (5.2)$$

Equation (5.2) suggests that if the data follows this power law, when we plot $\log_{10}\left(\langle r^2 \rangle / t\right)$ as a function of $\log_{10}(t)$ we should observe a straight line with slope $\alpha - 1$. It is well–known that for MSD data generated in this way, a plot of $\log_{10}\left(\langle r^2 \rangle / t\right)$ as a function of $\log_{10}(t)$ asymptotes to a horizontal line [11, 12, 23, 25]. This indicates that, after a sufficient amount of time we have $\alpha = 1$ and we can estimate the Fickian diffusion coefficient by estimating the intercept of the horizontal asymptote of the plot of $\log_{10}\left(\langle r^2 \rangle / t\right)$ as a function of $\log_{10}(t)$ [11, 12, 23, 25].

Instead of recording the square of the total displacement, $r^2 = x^2 + y^2 + z^2$, an alternative approach is to record the temporal evolution of the square of the displacement in each component direction and apply a similar technique. This approach would allow us to estimate the diffusion coefficient in each direction. For example, treating the x, y and z components of the MSD data in this way can be used to provide estimates of D_x, D_y and D_z, respectively, allowing us to explore whether there are any differences in the diffusivity in each direction. Here, $0 < D_x \leq 1/d$, $0 < D_y \leq 1/d$ and $0 < D_z \leq 1/d$, where d is the dimension of the problem. To implement this approach we plot $\log_{10}\left(\langle x^2 \rangle / t\right)$, $\log_{10}\left(\langle y^2 \rangle / t\right)$ or $\log_{10}\left(\langle z^2 \rangle / t\right)$ as a function of $\log_{10}(t)$, and we estimate D_x, D_y and D_z from measuring the long time intercept of these curves, which asymptote to $\log_{10}\left(2D_x\right)$, $\log_{10}\left(2D_y\right)$ and $\log_{10}\left(2D_z\right)$, respectively.

Using this approach we plot the MSD data, focusing at first on the x–component of the trajectory data, for several different combinations of different sized agents and obstacles, in both two and three dimensions, in Figure 5.2. Results in Figure 5.2(a) show plots of $\log_{10}\left(\langle x^2 \rangle / t\right)$ as a function of $\log_{10}(t)$ for both 1×1 and 2×2 shaped agents undergoing a random walk on a two–dimensional lattice that is randomly populated by either 1×1 obstacles or 2×2 obstacles. Results in Figure 5.2(b) show plots of $\log_{10}\left(\langle x^2 \rangle / t\right)$ as a function of $\log_{10}(t)$ for both 1×2 and 1×1 agents and obstacles as well as results for both 1×1 and L–shaped agents and obstacles. Similar plots for three–dimensional random walk simulations are shown in Figure 5.2(c) for both a $1 \times 1 \times 1$ and $2 \times 2 \times 2$ agent moving on a three–dimensional lattice populated with either $1 \times 1 \times 1$ or $2 \times 2 \times 2$ obstacles. Regardless of the dimension of the problem, or the combination of agent and obstacle shape and size, each plot in Figure 5.2 shows that the MSD curve eventually asymptotes to a horizontal line confirming that we eventually observe Fickian
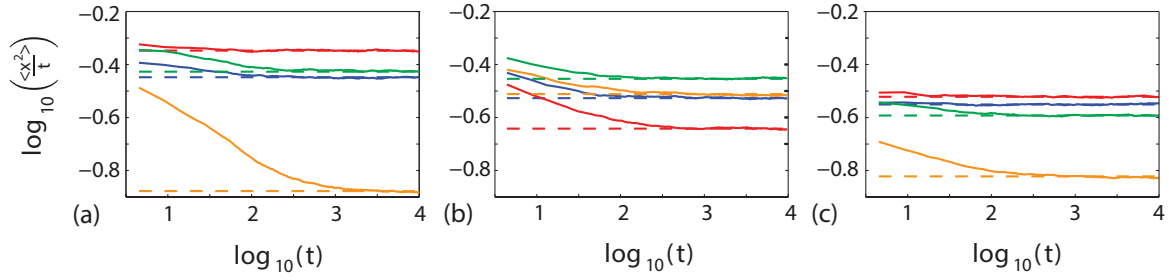
Figure 5.2: Results in (a) show averaged MSD data, $\log_{10}(\langle x^2\rangle/t)$, for a 1×1 agent moving on a lattice populated with 1×1 (blue) and 2×2 obstacles (red), and similar data for a 2×2 agent moving on a lattice populated with 1×1 (orange) and 2×2 obstacles (green). Results in (b) show $\log_{10}(\langle x^2\rangle/t)$ for a 1×2 agent moving on a lattice populated with 1×1 obstacles (blue), a 1×1 agent moving on a lattice populated with 1×2 obstacles (red), an L–shaped agent moving on a lattice populated with 1×1 obstacles (orange) and a 1×1 agent moving on a lattice populated with L–shaped obstacles (green). Results in (c) show $\log_{10}(\langle x^2\rangle/t)$ for a $1 \times 1 \times 1$ agent moving on a three–dimensional lattice populated with $1 \times 1 \times 1$ obstacles (blue) and $2 \times 2 \times 2$ obstacles (red), and similar data for a $2 \times 2 \times 2$ agent moving on a lattice populated with $1 \times 1 \times 1$ obstacles (orange) and $2 \times 2 \times 2$ obstacles (green). The size of the lattice and density of obstacles are $M = N = 10$, $P = Q = R = 10$ and $\phi = 0.1$, respectively. All random walk simulations are averaged over $50,000$ identically prepared realisations. We also superimpose, for each case, in each subfigure, a dashed horizontal line, $\log_{10}(2D_x)$, where D_x is the long time Fickian diffusivity in the x–direction. Exact values of D_x are calculated using the Mercier–Slater algorithm using GMRES with a strict error tolerance of 10^{-8}.

diffusion. Since these curves asymptote to $\log_{10}(2D_x)$, as indicated by Equation (5.2), we can estimate D_x from these data by measuring the intercept of the horizontal asymptote. This is a standard approach that has been used in many previous studies [11, 12, 23, 25].

Results in Figure 5.2 suggest that, in both two and three dimensions, smaller obstacles are more effective at reducing the diffusivity than larger obstacles at the same density. For a two–dimensional random walk with symmetric agents and obstacles, as shown in Figure 5.2(a), we find that a lattice populated with small obstacles is most effective at reducing the diffusivity, and that this effect is more pronounced for larger agents. Results for a two–dimensional random walk with asymmetric agents and obstacles, as shown in Figure 5.2(b), also suggest that small obstacles are more effective at reducing the diffusivity and that this reduction is more pronounced if the agent is asymmetric than if it is symmetric. Comparing the data in Figure 5.2(a)–(b) suggests that the reduction in diffusivity is greater for a 2×2 agent than for an asymmetric 1×2 agent. Data in Figure 5.2(c) indicate that similar trends apply in three dimensions.

In practice, trajectory data from stochastic random walk simulations is very noisy [118]

and to make sense of these data it is necessary to average over a very large ensemble of identically prepared realizations to obtain accurate estimates of the long time diffusivity. In some cases, calculating the diffusivity directly from stochastic random walk simulations can be overwhelmingly computationally expensive. This observation motivates us to apply an alternative, exact approach.

5.3.1   Algorithm and worked example

We now calculate the diffusivity using the method proposed by Mercier and Slater [42–44]. This algorithm provides an exact solution for a given obstacle configuration of interest. The Mercier–Slater method involves applying a vanishingly small bias, $\epsilon > 0$, to the random walk making it more probable for the agent to attempt to move in a particular direction. The bias can be applied separately in either the x, y or z directions, and is therefore applicable to random walks in both two and three dimensions. If the bias is applied in the x–direction, we calculate the exact diffusivity in that direction using the Nernst–Einstein relationship (a special case of the fluctuation-dissipation theorem [64]),

$$\mathcal{D}_x = \frac{D_x}{D_{0_x}} = \lim_{\epsilon \to 0} \frac{\mu(\epsilon)}{\mu_0},$$

(5.3)

where $0 < D_x \leq 1/d$ is the dimensionless diffusivity in the x–direction, $D_{0_x} = 1/d$ is the dimensionless diffusivity in the x–direction when there are no obstacles present, $\mu(\epsilon)$ is the motility of the agent moving in the x–direction under the action of the bias and μ_0 is the motility of the agent moving in the x–direction without the influence of the bias. $\mathcal{D}_x$ denotes the ratio of D_x to D_{0_x} so that $0 < \mathcal{D}_x \leq 1$. Applying the bias in the y or z–directions can be used to calculate $\mathcal{D}_y$ or $\mathcal{D}_z$, respectively.

Throughout this work we always apply the Mercier–Slater method by applying the bias in the positive x, y or z directions. We note that applying the bias in the negative x, y or z direction does not change our results since the sign of ϵ does not affect the value of the limit in Equation (5.3). Since $\mu(\epsilon)$ and μ_0 do not vary with time, we can calculate them by considering properties of the long time expected motion of the agent on the lattice. Equation (5.3) thus permits an exact calculation of the long time Fickian diffusivity, and it can be applied to each combination of agent and obstacle shapes and sizes in Figure 5.2.

We calculate $\mu(\epsilon)$ from the mean agent velocity at each lattice site. Let $\mathbf{v}$ be a vector whose q^{th} element, $v(q)$, denotes the mean agent velocity at site q. If we consider the x direction, the mean agent velocity is given by

$$v(q) = p_+ L_+ - p_- L_-, \tag{5.4}$$

where $p_\pm$ are the probabilities of movement in the positive and negative x–directions, respectively, and $L_\pm = 1$ if the relevant target site is vacant and zero if it is occupied.

The probability of finding the agent at any particular lattice site in the long time limit is given by solving the eigenvalue problem

$$\mathbf{T}\,\mathbf{n} = \mathbf{n},$$

where $\mathbf{T}$ represents a transition matrix in which the element of the ath row and b^{th} column, T_{ab}, is the probability that an agent located at site b will step to site a in the next time step, and $\mathbf{n}$ is a vector whose q^{th} element, $n(q)$, denotes the probability that an agent is located at site q in the long time limit. Generally, we normalise $\mathbf{n}$ to ensure that $\sum_q n(q) = 1$, and we do this by calculating the unit vector, $\hat{\mathbf{n}}$. The mean (global) velocity is given by $\mathbf{v} \cdot \hat{\mathbf{n}}$, and from these quantities we can derive

$$\mu(\epsilon) = \frac{\mathbf{v} \cdot \hat{\mathbf{n}}}{\epsilon}, \tag{5.5}$$

from which we can recover the diffusivity using Equation (5.3).

In summary, applying the Mercier–Slater algorithm involves the following steps:

1. for a given obstacle configuration, construct the transition matrix, $\mathbf{T}$;
2. solve $\mathbf{T}\,\mathbf{n} = \mathbf{n}$;
3. calculate $\hat{\mathbf{n}}$;
4. calculate the mean velocity, $\mathbf{v}$, at each lattice site;
5. calculate $\mu(\epsilon)$ using Equation (5.5);
6. calculate $\mathcal{D}_x$ using Equation (5.3).

To save a mathematical step we take advantage of the fact that the row rank of $(\mathbf{T} - \mathbf{I})$ is less than or equal to the number of rows of $\mathbf{T}$, and is only equal in the special case in which $\mathbf{T} = \mathbf{I}$. Accordingly, we introduce the normalisation condition by rewriting $\mathbf{T}\,\mathbf{n} = \mathbf{n}$ as $(\mathbf{T} - \mathbf{I})\,\mathbf{n} = \mathbf{0}$,
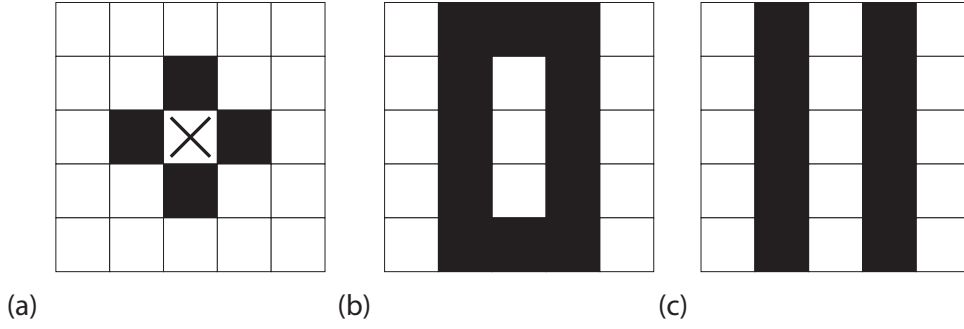
Figure 5.3:   (a) Special case (i), a lattice in which the obstacles (solid black) are laid down in a configuration so that the agent (represented by X) cannot move. (b)–(c) Special case (ii), two examples of lattices in which the obstacles (solid black) are laid down so that the lattice contains two or more independent closed regions.

where $\mathbf{I}$ is an identity matrix of appropriate size, and we replace a row of the new coefficient matrix, $(\mathbf{T} - \mathbf{I})$, with ones. This gives $\mathbf{A}\,\mathbf{n} = \mathbf{b}$ where $\mathbf{A}$ is the modified coefficient matrix and $\mathbf{b} = [0, 0, ..., 1]^{\mathrm{T}}$, which enforces the normalisation condition.

A further simplification can also be implemented. If $\mathbf{v}_\epsilon$ and $\mathbf{v}_I$ denote the ϵ dependent and ϵ independent components of $\mathbf{v}$, respectively, and $\mathbf{n}_\epsilon$ and $\mathbf{n}_I$ denote the ϵ dependent and ϵ independent components of $\hat{\mathbf{n}}$, respectively, and neglect terms of order ϵ^2 and higher, then Equation (5.3) and Equation (5.5) can be re–expressed in the simpler form [42]

$$\mathcal{D} = \mathbf{v}_\epsilon \cdot \mathbf{n}_I + \mathbf{v}_I \cdot \mathbf{n}_\epsilon. \tag{5.6}$$

To solve for $\mathbf{n}_\epsilon$ and $\mathbf{n}_I$ we separate $\mathbf{A}$ into its ϵ dependent and ϵ independent components (so that $\mathbf{A} = \mathbf{A}_I + \epsilon\,\mathbf{A}_\epsilon$), and note that $\mathbf{n}_I$ and $\mathbf{n}_\epsilon$ satisfy [42]

$$\mathbf{A}_I\,\mathbf{n}_I = \mathbf{b}, \tag{5.7}$$

$$\mathbf{A}_I\,\mathbf{n}_\epsilon = -\mathbf{A}_\epsilon\,\mathbf{n}_I. \tag{5.8}$$

There are a number of special cases in which the algorithm leads to interesting results. Here we will explicitly discuss two of these special cases:

(i) It is possible that the obstacles may be placed in a way that prevents the agent from moving. In Figure 5.3 (a) we show an example of this special case. Here, we have $\mathbf{T} = \mathbf{I}$ and

the algorithm gives

$$\mathbf{n} = \left(\frac{1}{N}, \frac{1}{N}, ..., \frac{1}{N} \right)^{\mathrm{T}},$$

$$\mathbf{v} = \mathbf{0},$$

where N is the total number of vacant lattice sites. For this system, Equation (5.6) gives $\mathcal{D} = 0$, as expected.

(ii) In the special case in which the lattice contains closed and independent regions, the agent will remain trapped in the starting region for all time. We show two example lattices, in Figure (5.3)(b)–(c), in which obstacles are laid down in a manner that separates the available lattice sites into two independent regions, each of which has an independent set of probability equations. For scenarios in which the agent has been placed into a closed region, there are two possible ways to proceed. Firstly, if we take the usual approach and consider the entire lattice we find that $\mathbf{T}$ is block diagonal and $\mathcal{D} = 0$. Secondly, if we treat each independent region separately we find that $\mathcal{D} > 0$ in each region.

For all of the results presented in this work, we always consider a random arrangement of obstacles. We do not consider these two scenarios any further in this Chapter.

To demonstrate the application of the algorithm we present a worked example for the lattice and obstacle configuration shown in Figure 5.4(a). This is a two–dimensional lattice, of size 4×2, containing a 1×2 obstacle in the lower left portion of the lattice. If we bias the motion in the positive x–direction and consider the case where the agent is initially located at site 1, the probability that the agent will step to site 2 is $(1 + \epsilon)/4$ and the probability that the agent will step to site 4 is $(1 - \epsilon)/4$. The agent will attempt to step in the negative y–direction with probability $1/4$, however this attempted motility event will be aborted because of the obstacle. Similarly, the agent will attempt to step in the positive y direction with probability $1/4$ and this attempted motility event will also be aborted due to the periodic boundary conditions and the location of the obstacle. Therefore, there is a probability of $1/4 + 1/4 = 1/2$ that the agent will remain at site 1. Following a similar process of reasoning for the remaining lattice sites,
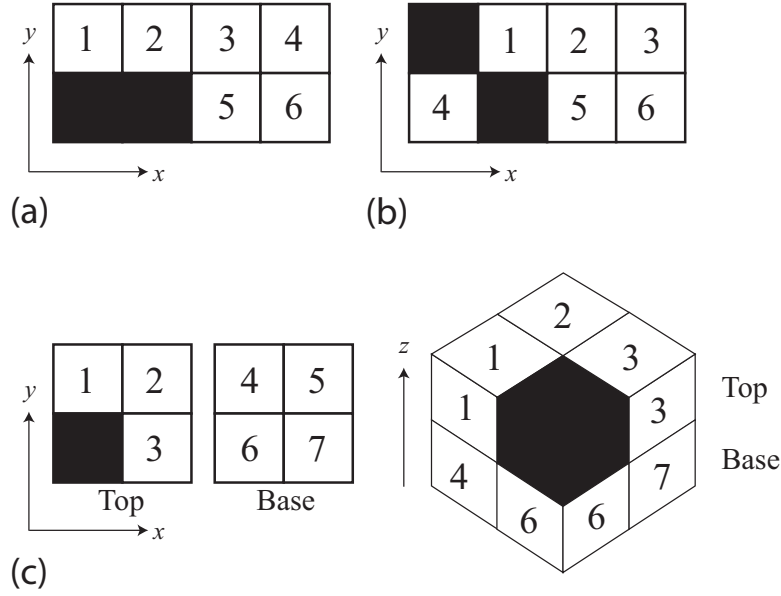
Figure 5.4: (a) and (b) show two examples of two–dimensional lattices, used for the worked calculations. In each case the site numbering and obstacle locations (black) are given. (c) shows an example of a three–dimensional lattice, used for the worked calculations. The site numbering and obstacle location (black) is given. For the three–dimensional lattice we show both the entire lattice (lower right) as well as the two layers of the lattice (lower left).

the transition matrix for this lattice, with a bias in the positive x direction, is given by

$$\mathbf{T} = \begin{pmatrix}
\frac{1}{2} & \frac{1+\epsilon}{4} & 0 & \frac{1-\epsilon}{4} & 0 & 0 \\
\frac{1-\epsilon}{4} & \frac{1}{2} & \frac{1+\epsilon}{4} & 0 & 0 & 0 \\
0 & \frac{1-\epsilon}{4} & 0 & \frac{1+\epsilon}{4} & \frac{1}{2} & 0 \\
\frac{1+\epsilon}{4} & 0 & \frac{1-\epsilon}{4} & 0 & 0 & \frac{1}{2} \\
0 & 0 & \frac{1}{2} & 0 & \frac{1+\epsilon}{4} & \frac{1+\epsilon}{4} \\
0 & 0 & 0 & \frac{1}{2} & \frac{1-\epsilon}{4} & \frac{1-\epsilon}{4}
\end{pmatrix}.$$

The mean velocity vectors, whose elements are given by Equation (5.4), are

$$\mathbf{v}_I = \left(0, 0, 0, 0, -\tfrac{1}{4}, \tfrac{1}{4} \right)^{\mathrm{T}}, \tag{5.9}$$

$$\mathbf{v}_\epsilon = \left(\tfrac{1}{2}, \tfrac{1}{2}, \tfrac{1}{2}, \tfrac{1}{2}, \tfrac{1}{4}, \tfrac{1}{4} \right)^{\mathrm{T}}. \tag{5.10}$$

From Eqs. (5.7)–(5.8) it follows that

$$\mathbf{n}_I = \left(\frac{1}{6}, \frac{1}{6}, \frac{1}{6}, \frac{1}{6}, \frac{1}{6}, \frac{1}{6} \right)^{\mathrm{T}}, \tag{5.11}$$

$$\mathbf{n}_\epsilon = \left(-\frac{1}{792}, \frac{23}{792}, \frac{47}{792}, -\frac{25}{792}, \frac{95}{792}, -\frac{73}{792} \right)^{\mathrm{T}}. \tag{5.12}$$

Combining Eqs. (5.9)–(5.12) with Equation (5.6) gives $\mathcal{D}_x = 4/11$.

If we bias motion in the positive y–direction, following a similar procedure, the transition matrix for this lattice is

$$\mathbf{T} = \begin{pmatrix} \frac{1}{2} & \frac{1}{4} & 0 & \frac{1}{4} & 0 & 0 \\[2mm] \frac{1}{4} & \frac{1}{2} & \frac{1}{4} & 0 & 0 & 0 \\[2mm] 0 & \frac{1}{4} & 0 & \frac{1}{4} & \frac{1}{2} & 0 \\[2mm] \frac{1}{4} & 0 & \frac{1}{4} & 0 & 0 & \frac{1}{2} \\[2mm] 0 & 0 & \frac{1}{2} & 0 & \frac{1}{4} & \frac{1}{4} \\[2mm] 0 & 0 & 0 & \frac{1}{2} & \frac{1}{4} & \frac{1}{4} \end{pmatrix}.$$

Note that the coefficients appear to be independent of ϵ owing to a number of algebraic cancellations. For example, the probability of stepping in the positive y direction, from site 3 to site 5, is $(1 + \epsilon)/4$. The probability of stepping in the negative y direction, from site 3 to site 5, is $(1 - \epsilon)/4$. This means that the net probability of stepping from site 3 to site 5 is $(1 + \epsilon)/4 + (1 - \epsilon)/4 = 1/2$, which is independent of ϵ. The mean velocity vectors are

$$\mathbf{v}_I = \left(0, 0, 0, 0, 0, 0 \right)^{\mathrm{T}}, \tag{5.13}$$

$$\mathbf{v}_\epsilon = \left(0, 0, \frac{1}{2}, \frac{1}{2}, \frac{1}{2}, \frac{1}{2}, \right)^{\mathrm{T}}. \tag{5.14}$$

From Eqs. (5.7)–(5.8) it follows that

$$\mathbf{n}_I = \left(\frac{1}{6}, \frac{1}{6}, \frac{1}{6}, \frac{1}{6}, \frac{1}{6}, \frac{1}{6} \right)^{\mathrm{T}}, \tag{5.15}$$

$$\mathbf{n}_\epsilon = \left(0, 0, 0, 0, 0, 0 \right)^{\mathrm{T}}. \tag{5.16}$$

Combining Eqs. (5.13)–(5.16) with Equation (5.6) gives $\mathcal{D}_y = 1/3$. Additional worked examples in both two and three dimensions are given in Chapter 6.

The systems of linear equations that we derive are exact, however we always solve these equations numerically. In general, the transition matrix is large and sparse. Under these conditions Eqs. (5.7)–(5.8) can be solved efficiently using the generalised minimal residual method (GMRES) [119]. GMRES is an iterative method which efficiently solves for the solution to the matrix equation $\mathbf{A}\mathbf{x} = \mathbf{b}$ in the Krylov subspace $K_n = \mathrm{span}\,\{\mathbf{b}, \mathbf{A}\mathbf{b}, \mathbf{A}^2\mathbf{b}, ..., \mathbf{A}^{n-1}\mathbf{b}\}$ by finding the vector $\mathbf{x}_n$ which minimises the Euclidean norm of the residual $\mathbf{A}\mathbf{x}_n - \mathbf{b}$ to within any given error tolerance [119]. To demonstrate our implementation of this approach we apply it to calculate the diffusivity in the x–direction for each combination of agent and obstacle depicted in Figure 5.2. Using our estimate of $\mathcal{D}_x$, we plot horizontal lines at $\log_{10}(2D_x)$ on each subfigure in Figure 5.2. Comparing the averaged MSD data in Figure 5.2 with the relevant horizontal lines at $\log_{10}(2D_x)$ confirms that there is very good agreement between the exact calculations of D_x and the results from the averaged MSD data since the averaged MSD data asymptotes to the same horizontal line indicated by the exact calculations. Note that all MSD data in Figure 5.2 corresponds to the x-component of the trajectory data which is why the estimates of diffusivity correspond to the x-component.

5.4   Results

Now that we have described and verified the algorithm for calculating the diffusivity on a range of small lattices, we apply the algorithm to calculate the diffusivity on larger, more practically sized lattices. We interpret our results by applying the algorithm to a large number of identically-prepared lattices with the same value of ϕ but with randomly arranged obstacles. Since the obstacles are always randomly oriented we always find that $\langle \mathcal{D}_x \rangle = \langle \mathcal{D}_y \rangle = \langle \mathcal{D}_z \rangle$ (results not shown), confirming that there is, on average, no anisotropy. Therefore, for the
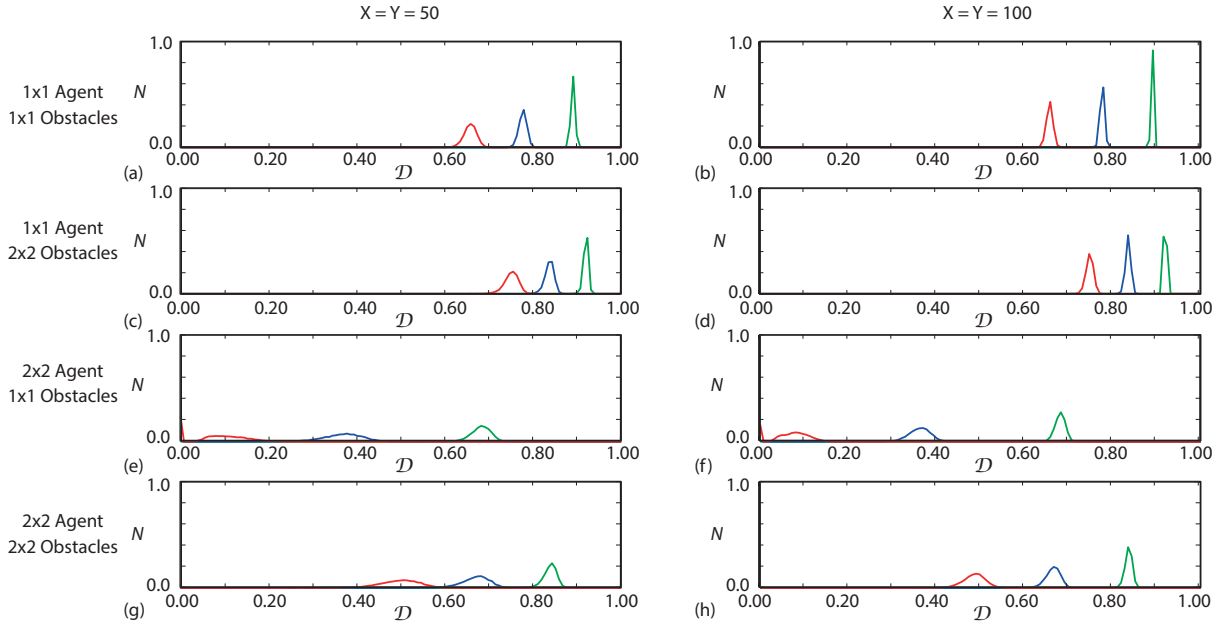
Figure 5.5: Results in (a)–(h) show a normalised histogram of $\mathcal{D}$ values for $10,000$ lattices which are randomly populated with obstacles to densities $\phi = 0.15$ (red), $\phi = 0.10$ (blue) and $\phi = 0.05$ (green). N is the normalised number of counts in each histogram box. Results in (a)–(d) and (e)–(h) correspond to 1×1 and 2×2 agents, respectively. Results in (a)–(b); (e)–(f) and (c)–(d); (g)–(h) correspond to 1×1 and 2×2 obstacles, respectively. Results in (a), (c), (e), (g) and (b), (d), (f), (h) correspond to $M = 50$ and $M = 100$, respectively. All histograms are constructed with 250 equally spaced intervals between 0.00 to 1.00. The solution of all systems of linear equations use GMRES with a strict error tolerance of 10^{-8}.

remainder of this study we only present results for $\langle \mathcal{D}_x \rangle$, and for simplicity we drop the subscript x and the triangular brackets.

For a small number of simulations the agent is placed in a closed region and $\mathcal{D} = 0$. We have included these simulations in Figures 5.5–5.8.

5.4.1 Two–dimensional random walk with symmetric agents and obstacles

We first consider two–dimensional lattices involving either 1×1 or 2×2 agents moving on a lattice which has been randomly populated with either 1×1 or 2×2 obstacles at density ϕ. We use the Mercier–Slater algorithm to calculate $\mathcal{D}$ for each lattice, and we consider an ensemble of $10,000$ identically prepared lattices. Results are shown as a histogram of $\mathcal{D}$ in Figure 5.5. The mean estimates of $\mathcal{D}$ are given in Table 5.1.

For each system we consider, our results indicate that $\mathcal{D}$ decreases with increasing obstacle density and that smaller obstacles are more effective at reducing $\mathcal{D}$ than larger obstacles at the

same density. For all densities considered, $\mathcal{D}$ is smaller for 1×1 obstacles than for 2×2 obstacles for both 1×1 and 2×2 agents at the same density. We also note that these effects are more pronounced for larger agents than for smaller agents. On average, the diffusivity of a 2×2 agent on a given lattice is smaller than the diffusivity of a 1×1 agents on the same lattice.

We find that, in situations where the agent and obstacles are the same size, the absolute size of the agent and obstacles relative to the size of the lattice spacing has an impact on $\mathcal{D}$. For example, for $\phi = 0.15$, with 1×1 agents and 1×1 obstacles we have $\mathcal{D} = 0.6564$, whereas for a similar situation with 2×2 agents and 2×2 obstacles we have $\mathcal{D} = 0.4849$, corresponding to a reduction in $\mathcal{D}$ by approximately 26%.

A histogram of calculated diffusivities is given in Figure 5.5. Results in the left column correspond to lattices with $X = Y = 50$ while results in the right column correspond to a larger lattice with $X = Y = 100$. Our results indicate that the mean diffusivity for each combination of agent and obstacle sizes is approximately independent of the size of the lattice. However, the standard deviation of each distribution decreases as the lattice size increases. For example, for a system in which 2×2 agents move through a lattice populated with 2×2 obstacles to density $\phi = 0.15$, we have $\mathcal{D} = 0.4841 \pm 0.0491$ and $\mathcal{D} = 0.4849 \pm 0.0279$ for $X = Y = 50$ and $X = Y = 100$, respectively. This reduction in variability suggests that for a larger lattice fewer realisations are required to estimate $\mathcal{D}$ reliably.

5.4.2   Two–dimensional random walk with asymmetric agents and obstacles

We now consider a two–dimensional system in which either the agent or the obstacles are asymmetric. Specifically, we consider the situation where we have: (i) either a 1×1 agent moving on a lattice populated with 1×2 obstacles or we have a 1×2 agent moving on a lattice populated with 1×1 obstacles; (ii) the situation where we have either a 1×1 agent moving on a lattice populated with L–shaped obstacles or we have a L–shaped agent moving on a lattice populated with 1×1 obstacles; (iii) the situation where we have either a 1×1 agent moving on a lattice populated with 1×3 obstacles or we have a 1×3 agent moving on a lattice populated with 1×1 obstacles. A histogram of the ensemble of the diffusivity results is shown in Figure 5.6 and the sample mean and variability, given by the sample standard deviation, for each system are shown in Table 5.2.

Our results for the asymmetric agents and obstacles are interesting because some of the

	1 × 1 Agent		2 × 2 Agent	
ϕ	1 × 1 Obstacles	2 × 2 Obstacles	1 × 1 Obstacles	2 × 2 Obstacles
0.05	0.8907 ± 0.0021	0.9192 ± 0.0026	0.6807 ± 0.0133	0.8364 ± 0.0079
0.10	0.7765 ± 0.0045	0.8352 ± 0.0054	0.3573 ± 0.0452	0.6646 ± 0.0176
0.15	0.6564 ± 0.0210	0.7479 ± 0.0081	0.0683 ± 0.0400	0.4849 ± 0.0279

Table 5.1: Average diffusivity, $\mathcal{D}$, with the variability indicated by the sample standard deviation, for a system in which a 1×1 agent moves on a lattice randomly populated with 1×1 obstacles. All results correspond to a 100×100 lattice and are calculated from an ensemble of $10,000$ identically prepared realisations.
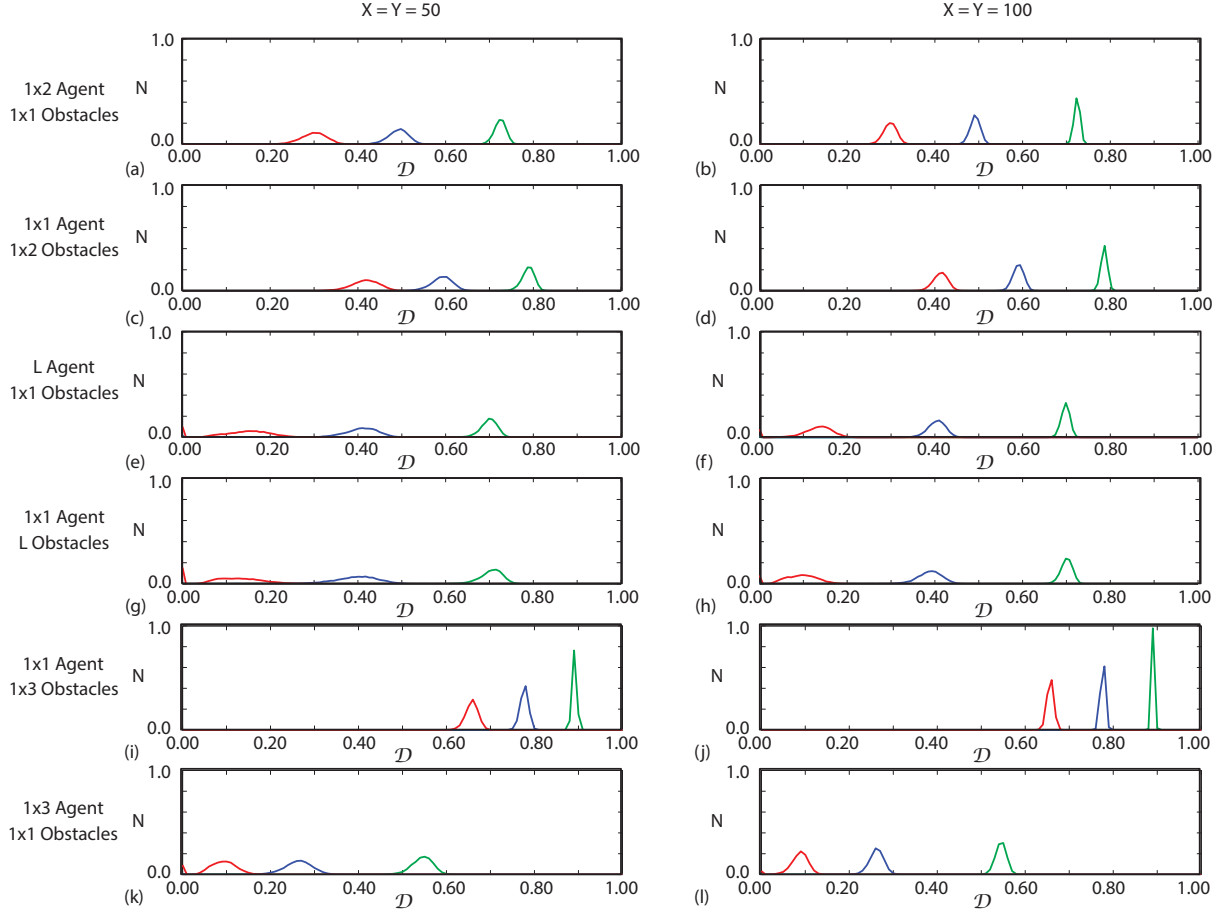
Figure 5.6:   Results in (a)–(l) show a normalised histogram of $\mathcal{D}$ values for $10,000$ lattices which are randomly populated with obstacles to densities $\phi = 0.15$ (red), $\phi = 0.10$ (blue) and $\phi = 0.05$ (green). N is the normalised number of counts in each histogram box. Results in (a)–(b), (c)–(d), (e)–(f), (g)–(h), (i)–(j), (k)–(l) correspond to a 1×2 agent with 1×1 obstacles, a 1×1 agent with 1×2 obstacles, an L–shaped agent with 1×1 obstacles, a 1×1 agent with L–shaped obstacles, a 1×1 agent with 1×3 obstacles, and a 1×3 agent with 1×1 obstacles, respectively. Results in (a), (c), (e), (g), (i), (k) and (b), (d), (f), (h), (j), (l) correspond to $X = Y = 50$ and $X = Y = 100$, respectively. All histograms are constructed with 250 equally spaced intervals between 0.00 to 1.00. The solution of all systems of linear equations use GMRES with a strict error of tolerance 10^{-8}.

trends we observed in Section 5.4.1 for symmetric agents and obstacles do not apply. Specifically, while the data in Table 5.2 suggest that the smaller 1×1 obstacles are more effective are reducing $\mathcal{D}$ than larger 1×2 obstacles for each density considered. However, we see that larger L–shaped obstacles are more effective at reducing the diffusivity than the smaller 1×1 obstacles for higher densities. 1×3 obstacles are less effective at reducing the diffusivity compared to L–shaped obstacles. This particular result is interesting because it shows that obstacles of the same size can have a different impact on the diffusivity, and we attribute this to the difference in obstacle shape. However, 1×3 agents have a lower diffusivity, on average, than L–shaped agents when they are placed on a lattice populated with 1×1 obstacles. We also observe other differences when we compare the symmetric and asymmetric cases. For example, a 1×1 agent moving on a lattice occupied with L–shaped obstacles to a density of $\phi = 0.15$ is associated with $\mathcal{D} = 0.0898$ whilst an L–shaped agent moving on a lattice occupied with 1×1 obstacles has $\mathcal{D} = 0.1247$, an increase of approximately 40%. Similarly, a 1×1 agent moving on a lattice occupied with 1×3 obstacles has $\mathcal{D} = 0.6560$ whilst a 1×3 agent moving on a lattice occupied with 1×1 obstacles has $\mathcal{D} = 0.0846$, a decrease of approximately 87%. Therefore, unlike the symmetric cases considered in Section 5.4.1, increasing the size of asymmetric agents does not necessarily decrease the diffusivity.

5.4.3 Three–dimensional random walk with symmetric obstacles

We now demonstrate how to apply the algorithm to three–dimensional problems in which either $1 \times 1 \times 1$ or $2 \times 2 \times 2$ agents move on a lattice that is randomly populated with either $1 \times 1 \times 1$ or $2 \times 2 \times 2$ obstacles. To manage the computational expense of dealing with three–dimensional calculations we consider three–dimensional lattices that contain approximately the same number of lattice sites as those considered in the two–dimensional simulations in Sections 5.4.1 and 5.4.2. We show a histogram of the ensemble calculations of $\mathcal{D}$ in Figure 5.6. The sample mean and variability, indicated by the sample standard deviation, are reported in Table 5.3.

Similar to the results in two dimensions, we find that $\mathcal{D}$ decreases with ϕ for all combinations of agents and obstacles in three dimensions. Our calculations indicate that smaller $1 \times 1 \times 1$ obstacles are more effective at reducing $\mathcal{D}$ than larger $2 \times 2 \times 2$ obstacles, for both types of agents and for all obstacle densities considered. Furthermore, for all obstacle types and densities

ϕ	1 × 2 Agent 1 × 1 Obstacles	1 × 1 Agent 1 × 2 Obstacles	L–shaped Agent 1 × 1 Obstacles	1 × 1 Agent L–shaped Obstacles	1 × 3 Agent 1 × 1 Obstacles	1 × 1 Agent 1 × 3 Obstacles
0.05	0.7240 ± 0.0067	0.7858 ± 0.0073	0.6971 ± 0.0220	0.6999 ± 0.0165	0.5443 ± 0.0077	0.8907 ± 0.0011
0.10	0.4910 ± 0.0216	0.5900 ± 0.0124	0.3985 ± 0.0501	0.3861 ± 0.0391	0.2608 ± 0.0114	0.7763 ± 0.0045
0.15	0.2951 ± 0.0310	0.4122 ± 0.0183	0.1247 ± 0.0459	0.0898 ± 0.0409	0.0846 ± 0.0118	0.6560 ± 0.0124

Table 5.2: Average diffusivity, $\mathcal{D}$, with the variability indicated by the sample standard deviation, for each two–dimensional combination of asymmetric agents and obstacles considered. All results correspond to a 100×100 lattice and are calculated from an ensemble of $10,000$ identically prepared realisations.
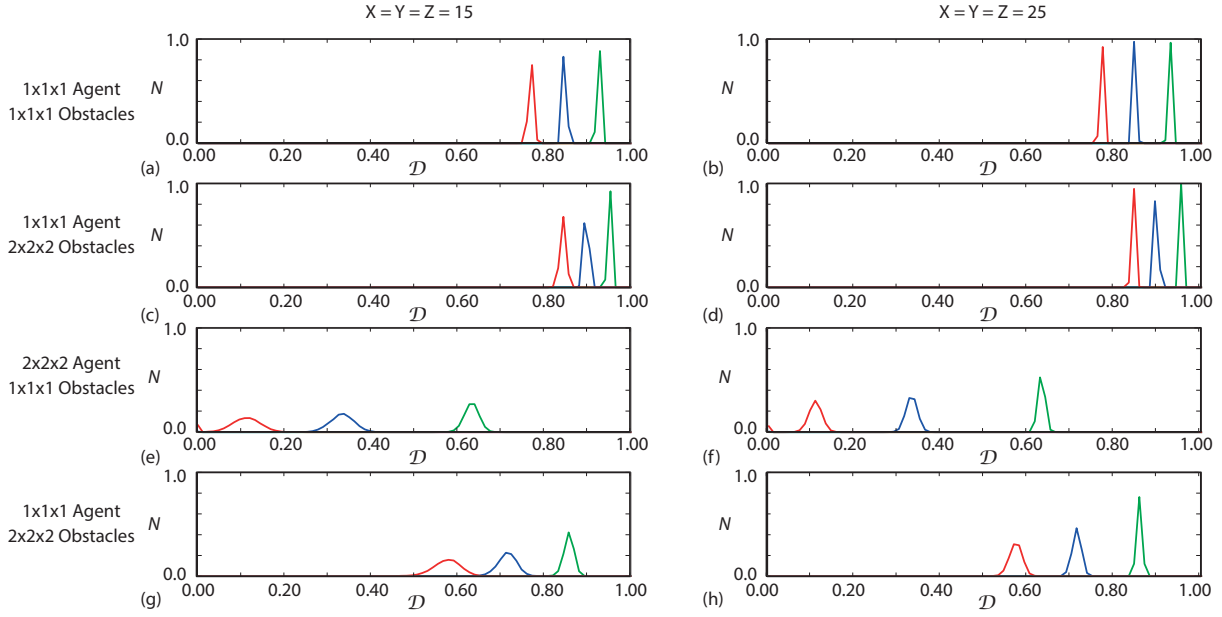
Figure 5.7: Results in (a)–(h) show a normalised histogram of $\mathcal{D}$ values for $10,000$ lattices which are randomly populated with obstacles to densities $\phi = 0.15$ (red), $\phi = 0.10$ (blue) and $\phi = 0.05$ (green). N is the normalised number of counts in each histogram box. Results in (a)–(b), (c)–(d), (e)–(f) and (g)–(h) correspond to simulations involving a $1 \times 1 \times 1$ agent with $1 \times 1 \times 1$ obstacles, a $1 \times 1 \times 1$ agent with $2 \times 2 \times 2$ obstacles, a $2 \times 2 \times 2$ agent with $1 \times 1 \times 1$ obstacles, and a $2 \times 2 \times 2$ agent with $2 \times 2 \times 2$ shaped obstacles, respectively. Results in (a), (c), (e), (g), and (b), (d), (f), (h) correspond to $P = Q = R = 15$ and $P = Q = R = 25$, respectively. All histograms are constructed with 250 equally spaced intervals between 0.00 to 1.00. The solution of all systems of linear equations use GMRES with a strict error tolerance of 10^{-8}.

considered, these effects are most pronounced for larger $2 \times 2 \times 2$ agents than they are for smaller $1 \times 1 \times 1$ agents. These results are consistent with the general conclusions we reached for a two–dimensional systems in Section 5.4.1.

Similar to the two–dimensional results, we find that situations in which the agent and obstacle are the same size, the absolute size of the agent and obstacles relative to the lattice spacing affects $\mathcal{D}$. Generally, increasing the size of the agents and obstacles relative to the lattice spacing decreases $\mathcal{D}$. For example, for $\phi = 0.10$, we have $\mathcal{D} = 0.8463$ and $\mathcal{D} = 0.7136$ for systems involving $1 \times 1 \times 1$ and $2 \times 2 \times 2$ agents and obstacles, respectively.

Two sets of histograms of each ensemble of $\mathcal{D}$ are given in Figure 5.7, corresponding to two differently sized three–dimensional square lattices: $P = Q = R = 15$ and $P = Q = R = 25$. Our results indicate that increasing the size of the lattice does not alter the mean $\mathcal{D}$ for any combination of agents and obstacles considered. However, increasing the size of the lattice reduces the sample standard deviation, which is consistent with our exact calculations of $\mathcal{D}$ in
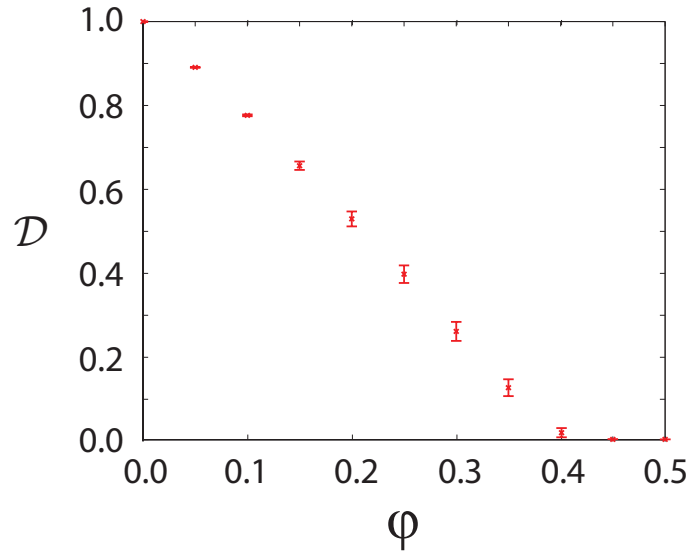
Figure 5.8: $\mathcal{D}$ for a 1×1 agent moving on a 100×100 two–dimensional lattice randomly populated with 1×1 obstacles to density ϕ. Results are given for $0 \le \phi \le 0.5$. Here the data points correspond to $\langle \mathcal{D} \rangle$, constructed using 10,000 identically prepared lattices. The error bars denote the sample standard deviation.

two dimensions.

5.4.4   Higher values of obstacle density

We now consider a wider range of values of ϕ, $0 \le \phi \le 0.5$, for a situation in which 1×1 agents move on a lattice that is randomly populated with 1×1 obstacles. Without any obstacles, we have $\phi = 0$ and $\mathcal{D} = 1$. Additional results in Table 5.4 and Figure 5.8 report values of $\mathcal{D}$ for $0 \le \phi \le 0.5$. As ϕ increases, $\mathcal{D}$ decreases, as expected. For $\phi = 0.45$ and $\phi = 0.50$ we find that $\mathcal{D} = 4.46 \times 10^{-5}$ and $\mathcal{D} = 5.37 \times 10^{-8}$ which both round to zero at four decimal places. We find that the standard deviation of the distribution increases with ϕ, and decreases as the size of the lattice increases, as shown in Figure 5.9.

5.5   Discussion and conclusion

A routine aim of applying a random walk model to replicate observations made from cellular and molecular experiments is to provide an estimate of the Fickian diffusivity [108–110]. While these concepts are relatively straightforward in an *in vitro* experimental setting, applying a random walk model to an *in vivo* situation is complicated by the fact that the motion of cells and molecules is hindered by the presence of obstacles of varying shapes and sizes [93, 100,

ϕ	$1 \times 1 \times 1$ Agent		$2 \times 2 \times 2$ Agent	
	$1 \times 1 \times 1$ Obstacles	$2 \times 2 \times 2$ Obstacles	$1 \times 1 \times 1$ Obstacles	$2 \times 2 \times 2$ Obstacles
0.05	0.9236 ± 0.0016	0.9487 ± 0.0021	0.6313 ± 0.0209	0.8558 ± 0.0111
0.10	0.8463 ± 0.0031	0.8962 ± 0.0042	0.3305 ± 0.0380	0.7136 ± 0.0215
0.15	0.7686 ± 0.0090	0.8426 ± 0.0061	0.1044 ± 0.0421	0.5742 ± 0.0308

Table 5.3: Average diffusivity, $\mathcal{D}$, with the variability indicated by the sample standard deviation, for each three–dimensional combination of agents and obstacles considered. All results correspond to a $25 \times 25 \times 25$ lattice and are calculated from an ensemble of $10,000$ identically prepared realisations.
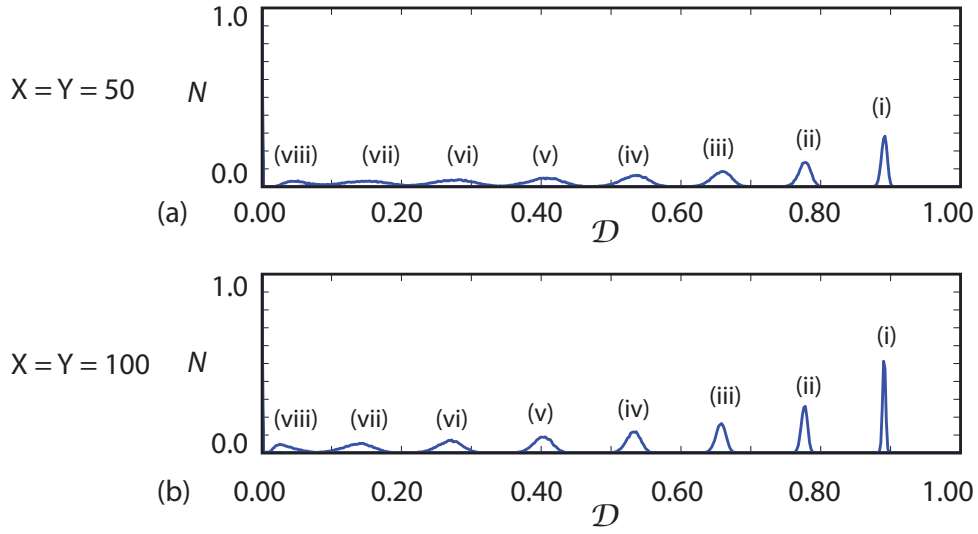
Figure 5.9: Results in (a)–(b) show a normalised histogram of $\mathcal{D}$ values for $10,000$ lattices which are randomly populated with obstacles to densities $\phi = 0.05, 0.10, 0.15, 0.20, 0.25, 0.30,$ 0.35 and 0.40, which are labelled in sequential order (i)–(viii), respectively. N is the normalised number of counts in each histogram box. Results in (a)–(b) correspond to $X = Y = 50$ and $X = Y = 100$, respectively. All histograms are constructed with 250 equally spaced intervals between 0.00 to 1.00. The solution of all systems of linear equations use GMRES with a strict error tolerance of 10^{-8}.

ϕ	1×1 Agents with 1×1 obstacles
0.05	0.8907 ± 0.0011
0.10	0.7765 ± 0.0022
0.15	0.6564 ± 0.0100
0.20	0.5297 ± 0.0178
0.25	0.3980 ± 0.0210
0.30	0.2617 ± 0.0226
0.35	0.1275 ± 0.0201
0.40	0.0203 ± 0.0110
0.45	0.0000 ± 0.0007
0.50	0.0000 ± 0.0000

Table 5.4: Average diffusivity, $\mathcal{D}$, with the variability indicated by the sample standard deviation, for each two–dimensional combination of symmetrical agents and symmetrical obstacles considered. All results correspond to a 100×100 lattice and are calculated from an ensemble of $10,000$ identically prepared realisations.

111, 112]. Previous approaches for estimating the diffusivity from a random walk model in a crowded environment involve performing repeated stochastic random walk simulations and collecting MSD data [11, 12, 23, 25]. Since agent trajectory data can be very noisy and estimates of diffusivity require long time MSD data, it can be computationally demanding to estimate the Fickian diffusivity from repeated simulations of such models.

In this work we calculate D using a different approach that provides an exact result without the need for performing repeated stochastic simulations [42–44]. Our results provide insight into the details of how varying the shape and size of the obstacles affects the Fickian diffusivity. Furthermore, we are also able to explore how varying the shape and size of the motile agent affects the diffusivity. In summary, our results show that the diffusivity is strongly dependent on the details of the obstacle field and is sensitive to the density of obstacles, the size of obstacles, the shape of obstacles and the size of the obstacles relative to the agent.

Although our approach for calculating $\mathcal{D}$ overcomes certain limitations of relying solely upon stochastic simulation data, our approach is subject to other limitations. For example, the approach used to calculate $\mathcal{D}$ in this study is only relevant to the situation where the obstacles are stationary. This is relevant for certain problems, whereas other previous studies have considered mobile obstacles for which the exact calculations are not relevant. While the results presented in this study are limited to four different types of two–dimensional obstacles and agents, and two different types of three–dimensional obstacles and agents, the approach outlined here can also be applied to other lattices, such as a triangular lattice, and other types of agents and obstacles of varying shapes and size.

Chapter 6

Additional results for Chapter 5

We now calculate the long time diffusivity in each direction for the lattices shown in Figure 5.4(b)–(c). For the lattice in Figure 5.4(b), when we bias motion in the positive x–direction, the transition matrix is given by

$$
\mathbf{T} = \begin{pmatrix}
\frac{3+\epsilon}{4} & \frac{1+\epsilon}{4} & 0 & 0 & 0 & 0 \\
\frac{1-\epsilon}{4} & 0 & \frac{1+\epsilon}{4} & 0 & \frac{1}{2} & 0 \\
0 & \frac{1-\epsilon}{4} & \frac{1-\epsilon}{4} & 0 & 0 & \frac{1}{2} \\
0 & 0 & 0 & \frac{3-\epsilon}{4} & 0 & \frac{1-\epsilon}{4} \\
0 & \frac{1}{2} & 0 & 0 & \frac{1+\epsilon}{4} & \frac{1+\epsilon}{4} \\
0 & 0 & \frac{1}{2} & \frac{1+\epsilon}{4} & \frac{1-\epsilon}{4} & 0
\end{pmatrix},
$$

and the mean velocity vectors are given by

$$
\mathbf{v}_I = \left(-\frac{1}{4}, 0, \frac{1}{4}, \frac{1}{4}, -\frac{1}{4}, 0 \right)^{\mathrm{T}},
$$

$$
\mathbf{v}_\epsilon = \left(\frac{1}{4}, \frac{1}{2}, \frac{1}{4}, \frac{1}{4}, \frac{1}{4}, \frac{1}{2} \right)^{\mathrm{T}}.
$$

Equations (5.7)–(5.8) gives

$$\mathbf{n}_I = \left(\tfrac{1}{6}, \tfrac{1}{6}, \tfrac{1}{6}, \tfrac{1}{6}, \tfrac{1}{6}, \tfrac{1}{6} \right)^{\mathrm{T}},$$

$$\mathbf{n}_\epsilon = \left(\tfrac{1}{2}, \tfrac{1}{6}, -\tfrac{1}{6}, -\tfrac{1}{2}, \tfrac{1}{6}, -\tfrac{1}{6} \right)^{\mathrm{T}},$$

from which we arrive at the diffusivity

$$\mathcal{D}_x = \mathbf{v}_\epsilon \cdot \mathbf{n}_I + \mathbf{v}_I \cdot \mathbf{n}_\epsilon = 0.$$

This result is expected as the location of the two 1×1 obstacles on this lattice mean that the displacement of the x–component of the trajectory is always confined by the obstacles and cannot increase indefinitely. When we bias the motion in the positive y–direction, the transition matrix is given by

$$\mathbf{T} = \begin{pmatrix} \tfrac{3}{4} & \tfrac{1}{4} & 0 & 0 & 0 & 0 \\ \tfrac{1}{4} & 0 & \tfrac{1}{4} & 0 & \tfrac{1}{2} & 0 \\ 0 & \tfrac{1}{4} & \tfrac{1}{4} & 0 & 0 & \tfrac{1}{2} \\ 0 & 0 & 0 & \tfrac{3}{4} & 0 & \tfrac{1}{4} \\ 0 & \tfrac{1}{2} & 0 & 0 & \tfrac{1}{4} & \tfrac{1}{4} \\ 0 & 0 & \tfrac{1}{2} & \tfrac{1}{4} & \tfrac{1}{4} & 0 \end{pmatrix},$$

and the mean velocity vectors are

$$\mathbf{v}_I = \left(0, 0, 0, 0, 0, 0 \right)^{\mathrm{T}},$$

$$\mathbf{v}_\epsilon = \left(0, 0, \tfrac{1}{2}, \tfrac{1}{2}, \tfrac{1}{2}, \tfrac{1}{2} \right)^{\mathrm{T}}.$$

Using Eqs. (5.7)–(5.8), we have

$$\mathbf{n}_I = \left(\frac{1}{6}, \frac{1}{6}, \frac{1}{6}, \frac{1}{6}, \frac{1}{6}, \frac{1}{6} \right)^{\mathrm{T}},$$

$$\mathbf{n}_\epsilon = \left(0, 0, 0, 0, 0, 0 \right)^{\mathrm{T}},$$

giving a diffusivity of

$$\mathcal{D}_y = \mathbf{v}_\epsilon \cdot \mathbf{n}_I + \mathbf{v}_I \cdot \mathbf{n}_\epsilon = \frac{1}{3}.$$

We now consider the three–dimensional lattice depicted in Figure 5.4(c). The algorithm is identical to the algorithm for a two–dimensional lattice except that each lattice site has a maximum of six nearest neighbors instead of four. Introducing a bias in the positive x–direction, the transition matrix for this lattice is given by

$$\mathbf{T} = \begin{pmatrix} \frac{1}{3} & \frac{1}{3} & 0 & \frac{1}{3} & 0 & 0 & 0 \\ \frac{1}{3} & 0 & \frac{1}{3} & 0 & \frac{1}{3} & 0 & 0 \\ 0 & \frac{1}{3} & \frac{1}{3} & 0 & 0 & 0 & \frac{1}{3} \\ \frac{1}{3} & 0 & 0 & 0 & \frac{1}{3} & \frac{1}{3} & 0 \\ 0 & \frac{1}{3} & 0 & \frac{1}{3} & 0 & 0 & \frac{1}{3} \\ 0 & 0 & 0 & \frac{1}{3} & 0 & \frac{1}{3} & \frac{1}{3} \\ 0 & 0 & \frac{1}{3} & 0 & \frac{1}{3} & \frac{1}{3} & 0 \end{pmatrix},$$

and the mean velocity vector is given by

$$\mathbf{v}_I = \left(0, 0, 0, 0, 0, 0, 0 \right)^{\mathrm{T}},$$

$$\mathbf{v}_\epsilon = \left(0, \frac{1}{3}, \frac{1}{3}, \frac{1}{3}, \frac{1}{3}, \frac{1}{3}, \frac{1}{3} \right)^{\mathrm{T}}.$$

Equations (5.7)–(5.8) give

$$\mathbf{n}_I = \left(-\tfrac{1}{7}, \tfrac{1}{7}, \tfrac{1}{7}, \tfrac{1}{7}, \tfrac{1}{7}, \tfrac{1}{7}, \tfrac{1}{7} \right)^{\mathrm{T}},$$

$$\mathbf{n}_\epsilon = \left(0, 0, 0, 0, 0, 0, 0 \right)^{\mathrm{T}},$$

and the diffusivity is

$$\mathcal{D}_x = \mathbf{v}_\epsilon \cdot \mathbf{n}_I + \mathbf{v}_I \cdot \mathbf{n}_\epsilon = \frac{2}{7}.$$

Because the lattice in Figure 5.4(c) is symmetric in each direction, it follows that $\mathcal{D}_x = \mathcal{D}_y = \mathcal{D}_z = 2/7$, and this can be confirmed by repeating the calculations by biasing the motion in the positive or negative y and z directions, respectively.

Chapter 7

Distinguishing between short-time non-Fickian diffusion, and long-time Fickian diffusion for a random walk on a crowded lattice

7.1   Abstract

The motion of cells and molecules through biological environments is often hindered by the presence of other cells and molecules. A common approach to modelling this kind of hindered transport is to examine the mean squared displacement (MSD) of a motile tracer particle in a lattice-based stochastic random walk in which some lattice sites are occupied by obstacles. Unfortunately, stochastic models can be computationally expensive to analyse because we must average over a large ensemble of identically-prepared realisations to obtain meaningful results. To overcome this limitation we describe an exact method for analysing a lattice-based model of the motion of an agent moving through a crowded environment. Using our approach we calculate the exact MSD of the motile agent. Our analysis confirms the existence of a transition period where, at first, the MSD does not follow a power law with time. However, after a sufficiently long period of time, the MSD increases in proportion to time. This latter

phase corresponds to Fickian diffusion with a reduced diffusivity owing to the presence of the obstacles. Our main result is to provide a mathematically motivated, reproducible and objective estimate of the amount of time required for the transport to become Fickian. Our new method to calculate this crossover time does not rely on stochastic simulations.

7.2   Introduction

Modelling the transport of cells and molecules can be complicated because many biological environments are crowded with structures that can obstruct cellular and molecular motion. In the literature, this kind of hindered transport is often modelled using a lattice-based nearest neighbour random walk in which a proportion of lattice sites are populated with immobile obstacles [1–3, 11–14, 25, 40, 55, 56, 120]. In these simulations, crowding effects are modeled explicitly by enforcing an exclusion principle that prevents the motile agent from stepping onto any site that is occupied by obstacles [27]. Mean squared displacement (MSD) data from simulations indicate the existence of a transition period where, at first, the MSD does not follow a power law in time [1–3, 11–14, 25]. However, after a sufficiently long period of time, the MSD increases in proportion with time, and the transport process eventually becomes Fickian [67, 69, 121]. Since it is common to quantify biological transport in terms of a Fickian diffusivity, it is of interest to predict the amount of time required for the transport process to effectively reach the Fickian regime. We refer to this amount of time as the crossover time.

Here, we propose a new, exact method for calculating the transient MSD and crossover time for a lattice-based random walk in which the lattice is partially occupied by immobile obstacles. Our results do not depend on performing stochastic simulations. We apply existing results from Markov chain theory to show that the transient phase approaches the Fickian phase exponentially fast. Using this information we present an objective, mathematically based estimate of the crossover time using the concept of mean action time [45, 48, 49].

7.3   Stochastic simulations

We consider a two-dimensional square lattice, of dimension $X \times Y$, with unit lattice spacing. Sites are indexed (i, j) so that each site has location $(x, y) = (i, j)$. The lattice is randomly

populated with obstacles, with density ϕ. A motile agent is placed on an unoccupied site and allowed to undergo a discrete time nearest neighbour random walk [122] with time steps of unit duration. Periodic boundary conditions are enforced on all boundaries. Crowding effects are modelled explicitly by aborting all potential motility events that would lead to the motile agent stepping to a site that is occupied by an obstacle [27].

As the simulation proceeds we record the displacement of the agent, $r(t)$, and we use this information to calculate the MSD, $\langle r^2(t) \rangle$, where $\langle \cdot \rangle$ denotes an average over a large ensemble of identically prepared realisations in which the motile agent has the same starting position in each realisation. Several earlier studies [11–14, 25] suggest that $\langle r^2(t) \rangle$ may evolve as a power law, $\langle r^2(t) \rangle = 4Dt^{\alpha}$, where $0 < \alpha < 2$ is a constant that indicates the type of transport taking place [69]. Subdiffusion is associated with $\alpha < 1$, superdiffusion is associated with $\alpha > 1$, and classical Fickian diffusion is associated with $\alpha = 1$. To explore this power law behaviour, we follow a standard approach by plotting $\log_{10}\left(\langle r^2(t) \rangle / t\right)$ as a function of $\log_{10}(t)$ [11, 12]. If the MSD follows this power law, the data in this plot should fall on a straight line. If the power law holds, the straight line will have a negative slope if $\alpha < 1$, a positive slope if $\alpha > 1$, or it will be a horizontal line if the transport is Fickian and $\alpha = 1$.

Results in Figure 7.1 (a)–(c) show stochastic MSD data for $\phi = 0.05, 0.15, 0.25$, respectively. In each subfigure we show plots of $\log_{10}\left(\langle r^2(t) \rangle / t\right)$ as a function of $\log_{10}(t)$ for five randomly-chosen starting locations. After a sufficiently large amount of time, each MSD curve, for each value of ϕ, appears to approach to the same, approximately horizontal, straight line. This is consistent with previous analysis since the MSD is proportional to t, giving $\langle r^2(t) \rangle = 4Dt$, in the long time limit [42, 43], as $t \to \infty$. In this case, the crowded Fickian diffusivity, D, is reduced relative to the standard obstacle-free diffusivity, $D_0 = 1/4$ in two dimensions on a unit lattice, and the value of D depends on ϕ. For each value of ϕ considered in Figure 7.1, we observe a different horizontal asymptote, and we see that D decreases with ϕ.

All stochastic simulation results in Figure 7.1 are obtained by performing many identically prepared realisations of a random walk in which the initial location of the motile agent is held constant. Additional results, given in Figure 7.2, are obtained by performing many identically prepared realisations of a random walk in which the initial location of the motile agent is chosen randomly in each realisation. Since the MSD data in Figure 7.2 (a)–(c) are further averaged over different starting locations, we denote the MSD data in Figure 7.2 as $\langle \bar{r}^2(t) \rangle$. For each value
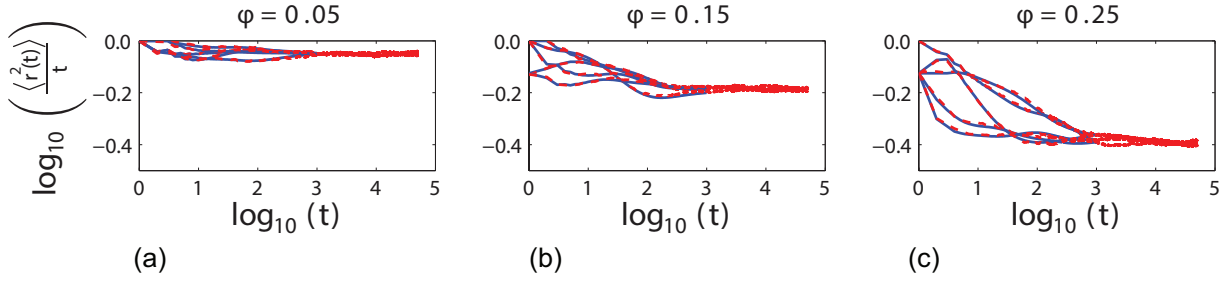
Figure 7.1: (a)–(c) show $\log_{10}\left(\langle r^2(t)\rangle / t\right)$ as a function of $\log_{10}(t)$ for five randomly chosen starting positions on lattices with $\phi = 0.05, 0.15, 0.25$, respectively. Exact results, calculated using the Markov chain approach (solid blue), are superimposed on results from stochastic simulations (dashed red). All results correspond to $X = Y = 10^3$, and simulation data is averaged over 10^4 identically prepared realisations. The exact solution is calculated until $t = 10^3$, whereas the stochastic simulations are calculated until $t = 5 \times 10^4$.
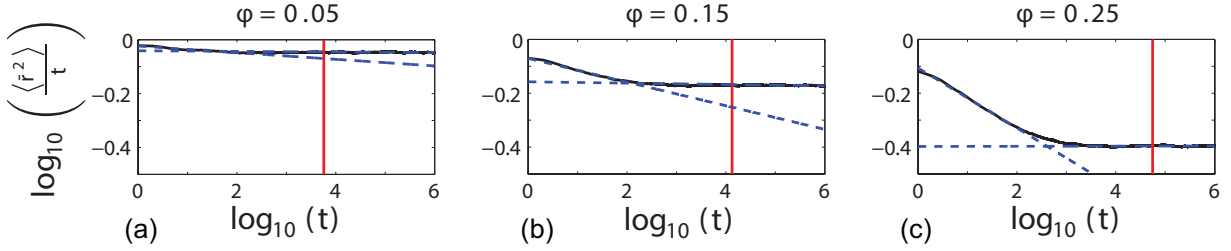
Figure 7.2:   (a)–(c) show plots of $\log_{10}\left(\langle \bar{r}^2(t)\rangle / t\right)$ as a function of $\log_{10}(t)$ for $\phi = 0.05, 0.15, 0.25$, respectively (solid black). In each case the logarithm of the crossover time, $\log_{10}(C)$, is superimposed (vertical red). The least–squares best fit straight lines for *early* time data $(0 \leq t \leq 10^2)$ and *late* time data $(10^4 \leq t \leq 10^6)$ are also given (blue–dashed). The ordinate of the intersection of these fitted straight lines is Saxton's crossover time [11, 12]. All simulations use $X = Y = 25$, and averaged MSD data is generated using 5×10^4 identically prepared realisations. The MSD data is generated until $t = 10^6$.

of ϕ, the MSD data in Figure 7.2 forms a curve which, like the data in Figure 7.1, eventually asymptotes to a horizontal line after a sufficient amount of time [11–14, 25].

Now that we have presented standard MSD data from a stochastic random walk algorithm in Figures 7.1-7.2, we aim to present some analysis allowing us to predict key features of the simulated data without the need for performing stochastic simulations.

7.4 Analysis

Let $\mathbf{p}(t)$ be a vector whose k^{th} element denotes the probability of finding the motile agent at the kth lattice site at time t. The evolution of $\mathbf{p}(t)$ is given by the Markov chain

$$\mathbf{p}(t) = \mathbf{p}(0)\,\mathbf{T}^t, \tag{7.1}$$

where $\mathbf{T}$ is the transition matrix [122, 123] and the superscript t indicates exponentiation to the value of time, t. The elements of $\mathbf{T}$, $T_{a,b}$, denote the probability that the agent will step from site a to site b per time step. Evaluating Equation (7.1) in a computationally efficient manner is challenging. Although $\mathbf{T}$ is sparse, $\mathbf{T}^t$ is not, and even a modestly sized lattice may require several petabytes to store and manipulate. To manage computational limitations, we evaluate Equation (7.1) iteratively at discrete time steps, $t_m = m$, for $m = 0, 1, 2, 3, \ldots$. This allows us to take advantage of the relation $\mathbf{p}(t) = \left(\mathbf{p}(0)\mathbf{T}^{t-1}\right)\mathbf{T}$, from which it follows that

$$\mathbf{p}(t_m) = \mathbf{p}(t_{m-1})\,\mathbf{T}, \quad \forall\, m = 1, 2, 3, \ldots \tag{7.2}$$

This approach allows us to calculate $\mathbf{p}(t)$ by storing just $\mathbf{p}(t_m)$ and the sparse transition matrix, $\mathbf{T}$.

Simulation data in Figures 7.1-7.2 is obtained by imposing periodic boundary conditions. To evaluate the MSD in the simulations we record the number of times that the motile agent crosses the boundaries of the lattice to arrive at a particular site. However, in our analysis, the vector $\mathbf{p}(t)$ does not contain any information about the number of times that the agent crosses the lattice boundaries. To deal with this analytically, we consider a large lattice that is composed of a periodic tiling of the smaller lattice used in the simulations. The tiling is chosen to be sufficiently large to ensure that the probability that the agent reaches the boundaries of the larger tiled lattice during the time interval considered is zero. Because $\mathbf{p}(t)$ is the exact probability of locating the agent at any site at time t, we calculate the MSD exactly, without considering an ensemble

$$r^2(t) = \sum_{i,j} x_{i,j}^2(t)\,p_{ij}(t), \tag{7.3}$$

where $x_{i,j}^2(t) = [i(t) - i(0)]^2 + [j(t) - j(0)]^2$ and $p_{ij}(t)$ denotes the probability of finding the agent at site (i, j), on the tiled lattice, at time t. At each discrete value of time, we use

Equation (7.3) to calculate the exact value of $r^2(t)$. We apply Equations (7.2)–(7.3) to mimic the stochastic simulation data in Figure 7.1. Exact results are superimposed on averaged simulation results in Figure 7.1 (a)–(c). For each of ϕ, and for each of the five starting positions we find that the Markov chain calculation compares very well with the averaged stochastic simulation data. Exact and simulation data in Figure 7.1 are compared for $t < 10^3$ since it becomes increasingly expensive to evaluate the exact results for larger t.

7.5   Crossover time

Transport of single cells or molecules is often quantified in terms of a Fickian diffusivity. Therefore, we are interested in predicting the amount of time required for the transport process to effectively reach the Fickian regime. Previous estimates of the crossover time have been obtained using simulation data. For example, Saxton [11, 12] obtained averaged stochastic MSD data and fitted two straight lines to that data. The first straight line is fitted to the small time, early portion of the MSD data. The second straight line is fitted to the large time, late portion of the MSD data. Using this approach, Saxton estimated the crossover time by finding the time at which these two straight lines intersect. This method suffers from the limitation that it requires the generation of stochastic simulation data. Furthermore, the choice of fitting straight lines to *early* and *late* time data involves making subjective choices. In particular, without an objective definition of *early* time and *late* time, this definition of crossover time is not reproducible. In contrast, we provide a mathematically motivated and reproducible estimate of the crossover time that avoids performing stochastic simulations.

The rate at which $\mathbf{p}(0)\mathbf{T}^t$ approaches $\mathbf{p}(0)\mathbf{\Pi}$ is bounded by an exponential (Chapter 8), with rate $\lambda_2^t = \mathrm{e}^{\log_e(\lambda_2)\,t}$, where λ_2 is the real eigenvalue of $\mathbf{T}$ that has the second-largest magnitude.. Using this bound we use the theory of mean action time (Chapter 9) to provide a finite estimate of the crossover time,

$$C = -\frac{2}{\log_e \lambda_2}. \tag{7.4}$$

This definition of crossover time is simpler to implement than Saxton's [11, 12] approach because we do not need to perform stochastic simulations, nor do we need to make subjective choices about fitting straight lines to *early* time and *late* time simulation data.

In practice, it is straightforward to calculate λ_2 using the following algorithm: (i) Calculate the eigenvector, $\mathbf{u}$, corresponding to the leading eigenvalue of $\mathbf{T}$ using the power–iteration method [124]; (ii) Calculate Hotelling's deflated matrix [124], $\mathbf{A} = \mathbf{T} - \lambda_1 \mathbf{v}\mathbf{v}^{\mathrm{T}}$, where $\mathbf{v} = \mathbf{u}/|\mathbf{u}|$ and the superscript $^{\mathrm{T}}$ denotes a transpose; and (iii) Apply the power–iteration method a second time to the matrix $\mathbf{A}$ and use the Rayleigh coefficient $\lambda_2 = \mathbf{w}^{\mathrm{T}}\mathbf{A}\mathbf{w}/\mathbf{w}^{\mathrm{T}}\mathbf{w}$, where $\mathbf{w}$ is the eigenvector of the leading eigenpair of $\mathbf{A}$, to recover λ_2.

Results in Figure 7.2 (a)–(c) shows $\log_{10}(C)$ superimposed on the simulated MSD curves. Visually, the values of C appear to act as a useful estimate of the crossover time because the simulated MSD curves appear to be effectively horizontal for $t > C$. In particular, we have $C = 0.57 \times 10^4$, 1.3×10^4 and 5.6×10^4 for $\phi = 0.05, 0.15$ and 0.25, respectively. These results show that the crossover time increases with ϕ, as we might anticipate. In Figure 7.2(a)–(c) we also show the least–squares best fit straight lines for both *early* and *late* time. The intersection of these straight lines gives Saxton's crossover time. In these cases we have $C_{\text{Saxton}} = 0.37 \times 10^2$, 1.2×10^2 and 4.1×10^2 for $\phi = 0.05, 0.15$ and 0.25, respectively. These estimates are two orders of magnitude smaller than the estimates given by our new definition. We note that, unlike Saxton's method, our approach is based on an objective mathematical definition, is reproducible, and does not require any stochastic simulations.

7.6 Discussion

We present an exact method for modelling the motion of a tracer particle on a crowded lattice. The Markov chain method leads to exact calculations of the probability of finding an agent at a site at any time, and from this information we can calculate the MSD exactly. These exact results compare very well with simulation data.

Our analysis shows that λ_2^t is an upper bound for the difference between a vector describing the time dependent probabilities of finding an agent at any site, and the long time limit. Here, λ_2 is the real eigenvalue of $\mathbf{T}$ that has the second largest magnitude. Since we have exponential decay, we use the theory of mean action time to define an objective, mathematically motivated estimate of the amount of time required to effectively reach the long time limit. Therefore, our mathematically motivated definition of crossover time is less subjective than previous approaches that rely on generating stochastic data and fitting straight lines to that data [11, 12].

Our analysis of the crossover time is useful if we wish to implement the previous analysis of Mercier and Slater [42, 43]. Mercier and Slater describe a method for calculating the long time Fickian diffusivity, D, for a lattice-based random walk in which a proportion of the sites are occupied by obstacles. An implicit assumption in applying Mercier and Slater's algorithm is that the transport process has been taking place for a sufficiently long period of time because this analysis is relevant only in the long time limit, $t \to \infty$. To implement Mercier and Slater's approach, one must first decide whether a sufficient amount of time has passed so that the long time limit is relevant. Our approach for calculating C provides this information without performing simulations.

Although this Chapter focuses on two–dimensional examples, our definition of C, and the approach for calculating C applies directly to three-dimensional lattices without any modification.

Chapter 8

Additional results for Chapter 7: Part I

Let the ith element of the vector $\mathbf{p}(t)$ denote the probability of locating the agent at site i at time t. In this appendix we prove that the vector $\mathbf{p}(t)$ satisfies the identity

$$||\mathbf{p}(0)\mathbf{T}^t - \mathbf{p}(0)\mathbf{\Pi}||_2 \le \lambda_2^t,$$

where T is a transition matrix and λ is the second eigenvalue of T.

We begin by considering the long time limit of $\mathbf{p}(t)$ satisfies,

$$\lim_{t\to\infty} \mathbf{p}(t) = \lim_{t\to\infty} \mathbf{p}(t-1)\mathbf{T},$$
$$= \mathbf{p}(0)\,\mathbf{\Pi},$$

where $\mathbf{\Pi} = \lim_{t\to\infty} \mathbf{T}^t$. The spectral norm of any square matrix, $\mathbf{A}$, is given by [125]

$$||\mathbf{A}||_2 = \sqrt{\lambda_{\max}\{\mathbf{A}^{\text{H}}\mathbf{A}\}}, \tag{8.1}$$

where $||\cdot||_2$ denotes the spectral norm, the superscript $^{\text{H}}$ denotes a Hermitian transpose, and $\lambda_{\max}\{\cdot\}$ denotes the largest eigenvalue. The spectral norm of the difference between $\mathbf{p}(t)$ and $\lim_{t\to\infty} \mathbf{p}(t)$ satisfies a triangle inequality

$$||\mathbf{p}(0)\mathbf{T}^t - \mathbf{p}(0)\mathbf{\Pi}||_2 \le ||\mathbf{p}(0)||_2$$
$$\le ||\mathbf{T}^t - \mathbf{\Pi}||_2,$$
$$\le ||\mathbf{T}^t - \mathbf{\Pi}||_2,$$

where we have used the fact that $||\mathbf{p}(0)||_2 \equiv 1$. The quantity $||\mathbf{T}^t - \mathbf{\Pi}||_2$ is an upper bound for the magnitude of the difference between $\mathbf{p}(t)$ and $\lim_{t \to \infty} \mathbf{p}(t)$ at any time t.

To quantify this upper bound, we note that, because $\mathbf{T}$ is symmetric, it is always diagonalisable [124], giving

$$\mathbf{\Pi} = \lim_{t \to \infty} \mathbf{T}^t,$$
$$= \lim_{t \to \infty} \mathbf{V} \mathbf{D}^t \mathbf{V}^{-1}.$$

Furthermore, because $\mathbf{T}$ is doubly stochastic, the eigenvalues of $\mathbf{T}$ are all real and satisfy $|\lambda_k| \leq 1$, for $k = 1, 2, 3, \ldots$. We arrange these eigenvalues by magnitude so that $\lambda_1 > \lambda_2 > \lambda_3 > \cdots$, with $\lambda_1 = 1$. The long time limit is therefore given by $\mathbf{\Pi} = \mathbf{V} \mathbf{D}^\infty \mathbf{V}^{-1}$, where $\mathbf{D}^\infty = \lim_{t \to \infty} \mathbf{D}^t = \text{diag}\{1, 0, \cdots, 0\}$. This allows us to write

$$\mathbf{T}^t - \mathbf{\Pi} = \mathbf{V} \left(\mathbf{D}^t - \mathbf{D}^\infty \right) \mathbf{V}^{-1},$$
$$= \mathbf{V} \mathbf{D}_a \mathbf{V}^{-1},$$

where $\mathbf{D}_a = \text{diag}\{0, \lambda_2^t, \cdots, \lambda_{n-1}^t\}$. Since $\mathbf{T}$ is symmetric, its eigenvectors form an orthonormal basis for $\mathbb{R}^{n \times n}$, where n is the number of vacant lattice sites. This also means that $\mathbf{V}$ is unitary [124] and satisfies $\mathbf{V}^\mathrm{H} = \mathbf{V}^{-1}$. Using these properties we can write

$$\left(\mathbf{T}^t - \mathbf{\Pi} \right)^\mathrm{H} \left(\mathbf{T}^t - \mathbf{\Pi} \right) = \mathbf{V}^{-\mathrm{H}} \mathbf{D}_a \mathbf{V}^\mathrm{H} \mathbf{V} \mathbf{D}_a \mathbf{V}^{-1},$$
$$= \mathbf{V} \mathbf{D}_a^2 \mathbf{V}^{-1}. \tag{8.2}$$

The largest eigenvalue of $\mathbf{V} \mathbf{D}_a^2 \mathbf{V}^{-1}$ is given by the second diagonal element of the diagonal matrix, λ_2^{2t}. Combining Equations (8.1)–(8.2) gives

$$||\mathbf{p}(0) \mathbf{T}^t - \mathbf{p}(0) \mathbf{\Pi}||_2 \leq \lambda_2^t.$$

For modest sized lattices λ_2 can be calculated using the power-iteration method [124].

Chapter 9

Additional results for Chapter 7: Part II

In this appendix we briefly review the theory of Mean Action Time that was developed by McNabb and Wake [45, 46]. To demonstrate the theory of mean action time, we consider

$$\frac{\mathrm{d}z}{\mathrm{d}t} = -kz(t),$$

with $k > 0$, which is a model of exponential decay. McNabb and Wake [45] define

$$F(t) = 1 - \frac{z(t)}{z(0)},$$

which is a monotonically increasing function of t that satisfies $F(0) = 0$ and $\lim_{t\to\infty} F(t) = 1^-$. If we consider $F(t)$ to act like a cumulative distribution function, the associated probability density function is

$$f(t) = -\frac{1}{z(0)} \frac{\mathrm{d}z}{\mathrm{d}t}.$$

The mean of this distribution can be thought of as a measure of the amount of time required for $z(t)$ to effectively asymptote to the long time limit, $\lim_{t\to\infty} z(t) = 0$. The mean of this probability density function, called the mean action time, is

$$M = -\frac{1}{z(0)} \int_0^\infty t \frac{\mathrm{d}z}{\mathrm{d}t}\, \mathrm{d}t.$$

For the exponential decay model we obtain $M = 1/k$.

Higher moments can be used to quantify the width of the distribution [49]. The variance is

given by

$$V = -\frac{1}{z(0)} \int_0^\infty t^2 \frac{\mathrm{d}z}{\mathrm{d}t}\, \mathrm{d}t,$$

where V represents the variance. For the exponential decay model we have $V = 1/k^2$. A useful definition of the amount of time required for $z(t)$ to effectively asymptote to the long time limit, accounting for the mean and width of the distribution, is $M + \sqrt{V}$. Previous analysis of exponentially decaying laboratory data confirms that this definition leads to very useful results that are simple to implement [126]. Therefore, a mathematically motivated finite estimate of the amount of time required for the decay process to effectively reach the long time limit is

$$C = M + \sqrt{V}.$$

Or, for the exponential decay model,

$$C = 2/k.$$

Chapter 10

An analytical method for disentangling the roles of adhesion and crowding for random walk models on a crowded lattice

10.1   Abstract

Migration of cells and molecules in vivo is affected by interactions with obstacles. These interactions can include crowding effects, as well as adhesion / repulsion between the motile cell / molecule and the obstacles. Here we present an analytical framework that can be used to separately quantify the roles of crowding and adhesion / repulsion using a lattice-based random walk model. Our method leads to an exact calculation of the long time Fickian diffusivity, and avoids the need for computationally expensive stochastic simulations

10.2   Simulations and Analysis

Motion of cells and molecules through *in vivo* biological environments is affected by the presence of other cells and scaffolds that can act as obstacles [11, 52–54]. Interactions between

cells and obstacles can include both crowding effects [55, 56], as well as adhesion/repulsion effects [57, 58]. A great deal of theoretical progress has been made in terms of developing mathematical insight into how adhesion between motile cells impacts *in vitro* experiments without any obstacles present [59–62]. However, mathematical models describing the impact of both crowding and adhesion/repulsion *in vivo* with obstacles present are predominantly based on simulation studies, without any underlying analysis [11, 13, 25, 55].

While we anticipate that both crowding and adhesion act to impede the motion of cells *in vivo*, it is not possible to quantify the relative roles of these two mechanisms based on intuition alone. Although it is possible to perform simulations that include both crowding and adhesion, simulation studies can be time consuming, and can fail to provide more general insight. To address these limitations we consider a stochastic, lattice-based model describing the motion of an agent (e.g. a cell or biological molecule) through an environment that is randomly populated by immobile obstacles at density $\phi \in [0, 1]$. The motion of the agent is affected by crowding and adhesion/repulsion between the agent and the obstacles. Since the model involves just a single agent moving amongst a population of obstacles, there is no adhesion/repulsion between agents. The strength of adhesion/repulsion is measured by $\zeta \in [-1, 1]$: setting $\zeta = 0$ corresponds to pure crowding with no adhesion/repulsion; $\zeta > 0$ corresponds to combined adhesion and crowding; and $\zeta < 0$ corresponds to combined repulsion and crowding. We present an exact method that can be used to quantify the relative roles of crowding and adhesion/repulsion by producing exact calculations of the long time Fickian diffusivity, D, of the motile agent. Using this method we calculate $D(\phi, \zeta)$ so that we are able to quantify the roles of both crowding and adhesion/repulsion in terms of the long time Fickian diffusivity. Our results suggest that there is a threshold density of obstacles ($\phi \approx 0.3$) below which adhesion/repulsion has a negligible impact on the long time Fickian diffusivity. In contrast, above this threshold ($\phi > 0.3$), adhesion/repulsion interactions have a significant influence on the long time Fickian diffusivity. The accuracy of our exact calculations is tested using random walk simulations, and although we present results for a two-dimensional square lattice, our approach applies to any regular lattice in two or three dimensions.

We consider a square lattice with unit lattice spacing, $\Delta = 1$, and dimension $X \times Y$. Sites are indexed (i, j) so that each site has location $(x, y) = (i\Delta, j\Delta)$ with $0 \leq x \leq X - 1$ and $0 \leq y \leq Y - 1$. To initiate a simulation, lattice sites are randomly populated with immobile and impenetrable obstacles to a spatially uniform density, ϕ, with, at most, one obstacle per site. A

motile agent is placed on a vacant site, and allowed to undergo a nearest neighbor random walk in which all potential motility events that would place the agent on a site that is occupied by an obstacle are aborted.

During each discrete time step, of duration $\tau = 1$, the probability that the motile agent attempts to step to a randomly chosen nearest neighbor lattice site is

$$\frac{p_m}{4}\left(1 - \frac{\zeta}{4}N\right), \tag{10.1}$$

where $p_m \in [0, 1]$ is the probability that an isolated agent will attempt to move during a time interval of duration τ, $N = 0, 1, 2, 3$ or 4, is the number of nearest neighbor sites occupied by obstacles, and $\zeta \in [-1, 1]$ is the adhesion/repulsion parameter. Note that, to ensure that both the net probability of movement and the net probability of remaining stationary during any time step are always greater or equal to zero, and less than or equal to unity, we consider five different situations. In these situations the agent in question is adjacent to either $N = 0, 1, 2, 3$ or 4 obstacles. Solving the resulting set of inequalities for these five different situations leads us to write the adhesion/repulsion factor in Equation 10.1 as $(1 - \eta N/4)$, with $\eta \in [-1, 1]$.

(a)

(b)
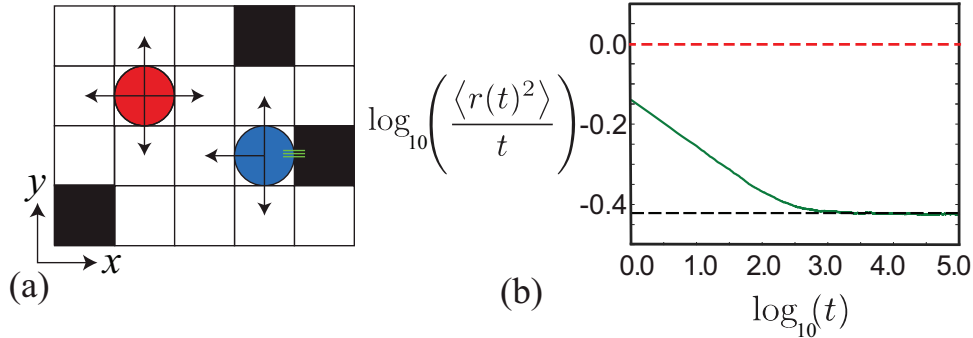
Figure 10.1: (a) Lattice schematic illustrating how crowding and adhesion/repulsion are incorporated into the random walk model. Circles represent motile agents and the squares represent immobile obstacles. The green lines between the agent and obstacle indicates that the model incorporates adhesion/repulsion between the motile agent and immotile obstacles. (b) Plot of $\log_{10}\left(\langle r^2(t)\rangle / t\right)$ as a function of $\log_{10}(t)$ (green solid) from a suite of simulations with $p_m = 1.0$, $\zeta = 0$, $\phi = 0.2$, $X = 10$ and $Y = 10$. The ensemble average is obtained by averaging over 100,000 identically prepared realizations. The lower horizontal line (black dashed) shows $\log_{10}\left(4\bar{D}\right)$, where $\bar{D} = 0.095$ is the exact calculation of the Fickian diffusivity. The upper horizontal line (red dashed) shows $\log_{10}\left(4D_0\right)$, for comparison.

The schematic in Figure 10.1(a) illustrates how crowding and adhesion/repulsion are incorporated into the model. The lattice site containing the red agent is not adjacent to any obstacles

($N = 0$) and the probability that the red agent will move during a time step of duration τ is simply p_m, which is independent of ζ. Since there are no obstacles surrounding the red agent, it is able to move to any of the four nearest neighbor sites, with the target site being chosen at random. In contrast, the blue agent is adjacent to one obstacle ($N = 1$) and the probability that the blue agent will move during a time step of duration τ is $p_m \left(1 - \zeta/4\right)$, which depends on the strength of adhesion/repulsion. Therefore, the motility of agents that are adjacent to one or more obstacles are affected by the strength of adhesion/repulsion to those obstacles. If the blue agent attempts to move, the direction of movement will be chosen at random. If, in this case, the blue agent attempts to move in the positive x direction, the potential movement event will be aborted due to crowding effects caused by the obstacle.

To quantify how crowding and adhesion/repulsion affect the motility of a single motile agent, we consider performing a stochastic simulation in which we record the agent's squared displacement, $r^2(t) = x^2(t) + y^2(t)$, where $x^2(t)$ and $y^2(t)$ represent the components of the squared displacement in the x and y directions, respectively. Following earlier studies [11, 13, 25, 55] we assume that the mean squared displacement follows a power law

$$\left\langle r^2(t) \right\rangle = (2d)\bar{D}\, t^\alpha, \tag{10.2}$$

where $d = 2, 3$ is the physical dimension, $\langle \cdot \rangle$ denotes the average over a large ensemble of identically prepared realizations, and $\bar{D}$ is a generalized diffusivity with units $[L^2/T^\alpha]$ which is less than the diffusivity when no obstacles are present, $D_0 = p_m \Delta^2/(2\, d\, \tau)$. The exponent α is a positive constant that can be used to classify the type of transport process taking place, with $\alpha = 1$ corresponding to Fickian diffusion and $\alpha < 1$ corresponding to subdiffusion [11, 13, 25, 55]. Rearranging Equation (10.2) gives

$$\log_{10}\left(\left\langle r^2(t) \right\rangle /t\right) = \log_{10}\left((2d)\bar{D}\right) + (\alpha - 1)\log_{10}\left(t\right). \tag{10.3}$$

This means that if the power law in Equation (10.2) accurately describes the evolution of the mean squared displacement data, a plot of $\log_{10}\left(\left\langle r^2(t) \right\rangle /t\right)$ as a function of $\log_{10}\left(t\right)$ will be a straight line for all $t > 0$. If the transport process is Fickian diffusion ($\alpha = 1$) the straight line will be horizontal, with zero slope. In contrast, if the transport process is subdiffusion ($\alpha < 1$) the straight line will have negative slope.

To demonstrate these ideas we perform an ensemble of simulations without adhesion/repulsion and with $\phi = 0.2$ on a lattice with periodic boundary conditions, and we plot $\log_{10}\left(\langle r^2(t)\rangle /t\right)$ as a function of $\log_{10}(t)$ in Figure 10.1(b). Consistent with many previous simulation studies [1, 3, 11, 13, 25, 55, 127], we observe that $\log_{10}\left(\langle r^2(t)\rangle /t\right)$ follows a curve. Initially the curve has a negative slope, and the curve tends to a horizontal asymptote as $t \to \infty$. This suggests that the transport process becomes Fickian in the long time limit, $t \to \infty$, with a reduced Fickian diffusivity, $\bar{D}$. For the data in Figure 10.1(b), we fit a horizontal line to the data in the interval $10^3 \le t \le 10^4$, giving $\bar{D} \approx 0.095$. This means that the obstacles have reduced the long time Fickian diffusivity compared to the case where there are no obstacles present, $D_0 = p_m \Delta^2 / (2\, d\, \tau) = 0.25$, in this case.

Unfortunately, using stochastic simulations to compute the long time Fickian diffusivity like we did in Figure 10.1(b) is problematic for two reasons. First, a very large number of identically prepared realizations of the stochastic process are required to produce sufficiently smooth mean squared displacement data. Second, the Fickian diffusion regime is only reached in the long time limit, $t \to \infty$, meaning that we must perform a very large number of identically prepared realizations over a very long period of time to obtain a reasonable approximation of $\bar{D}$. These two issues motivate us to develop an exact calculation of $\bar{D}$ that does not rely on stochastic data. To calculate the long time Fickian diffusivity we modify a method originally proposed by Mercier and Slater [2, 42, 43, 128]. Our modification to their method is to incorporate the effects of adhesion/repulsion. We will describe how to apply the method to calculate the long time Fickian diffusivity in each component direction. All of the details are given for the x Cartesian direction, and adapting the method to apply to the y and z Cartesian directions is straightforward.

To begin with we apply the Nernst-Einstein relationship, which is a special case of the fluctuation-dissipation theorem [129],

$$\bar{D}_x = D_0 \frac{\mu(\epsilon)}{\mu_0}, \tag{10.4}$$

where $\mu(\epsilon)$ represents the probability of movement in the positive x direction when the motion includes a bias of strength $\epsilon \ll 1$, and μ_0 is the probability of movement in the positive x

direction where there is no bias. The motility is given by

$$\mu(\epsilon) = \frac{\mathbf{v} \cdot \hat{\mathbf{n}}}{\epsilon}, \tag{10.5}$$

where $\mathbf{v}$ and $\hat{\mathbf{n}}$ are vectors whose k^{th} elements denote the (local) velocity at the kth site, and the long time limit of the probability of locating the agent at the kth site, respectively. In practice, we calculate $\hat{\mathbf{n}}$ by constructing the transition matrix associated with the lattice, $\mathbf{T}$, and then solving $\mathbf{T} \, \mathbf{n} = \mathbf{n}$ for $\mathbf{n}$, from which we calculate $\hat{\mathbf{n}} = \mathbf{n}/|\mathbf{n}|$. The elements of $\mathbf{T}$, $T_{a,b}$, denote the probability that the agent will step from site a to site b per time step. Therefore, $\mathbf{T}$ encodes details about the strength of adhesion/repulsion, the effects of crowding, and the effects of different boundary conditions [2].

The velocity vector, $\mathbf{v}$, can be calculated element-wise using $v(k) = p_+ L_+ - p_- L_-$, where $v(k)$ is the kth element of $\mathbf{v}$, $p_\pm$ are the probabilities of movement in the positive and negative x directions, $L_\pm = 1$ if the relevant target site is vacant and $L_\pm = 0$ if the relevant target site is occupied by an obstacle. Once we have applied this method to calculate $\bar{D}_x$, we perform analogous calculations in the y and z directions to give $\bar{D}_y$ and $\bar{D}_z$, respectively. Calculating the long time Fickian diffusivity in each direction allows us to investigate the possibility of any anisotropy in the system. For our calculations here, in two dimensions with randomly placed obstacles, we observe no anisotropy and we have $\bar{D}_x \approx \bar{D}_y$ on a sufficiently large lattice. Therefore, we report our results in terms of the total diffusivity, $\bar{D} = \bar{D}_x + \bar{D}_y$ [2]. To demonstrate the accuracy of our calculation, we apply it to the lattice configuration previously considered in Figure 10.1(b) and find that $\bar{D} = 0.095$, which is identical to the result obtained using stochastic simulations. To visualise the match between the exact calculation and the simulation results, we superimpose a horizontal line at $\log_{10}\left(4\bar{D}\right)$ in Figure 10.1(b), where $\bar{D} = 0.095$ is the exact calculation of the long time Fickian diffusivity. To emphasize the differences between the transport process where obstacles are present $(\phi > 0)$ from when obstacles are absent $(\phi = 0)$, we plot a horizontal line at $\log_{10}\left(4D_0\right)$ in Figure 10.1(b).

It is important to note that certain arrangements of obstacles lead to $\bar{D} = 0$. Any situation where obstacles form a closed loop and the motile agent is placed inside the closed loop will lead to $\bar{D} = 0$, as discussed in Section 2.1 of Ellery et al. [2]. This situation can occur for any value of $\phi > 0$. One way of dealing with these special cases would be to apply the exact calculation to a suite of identically-prepared lattices and to exclude those lattices which contain

closed loops of obstacles, leading to $\bar{D} = 0$. We could then calculate an average diffusivity by averaging $\bar{D}$ for the remaining lattices where $\bar{D} > 0$. Instead of excluding these cases, we take a simpler, unbiased approach by calculating $\bar{D}$ for a number of identically-prepared lattices and report the average value of $\bar{D}$ across all randomly-populated lattices. We acknowledge that some of these lattices may contain closed loops of obstacles, meaning that we may have $\bar{D} = 0$ for some of these lattices [2]. Furthermore, we note that the distinction between situations where we obtain $\bar{D} = 0$ and $\bar{D} > 0$ is independent of the percolation threshold [67, 129]. Indeed, our calculations confirm that we can have situations where $\bar{D} = 0$ on a finite sized lattice where ϕ is below the percolation threshold as well as other situations where $\bar{D} > 0$ on a finite sized lattice where ϕ is above the percolation threshold.

Now that we have explained how the exact calculation of the long time Fickian diffusivity can be performed, we apply the calculation to a family of lattices with different obstacle densities, ϕ. By repeating our calculations of the long time Fickian diffusivity with different values of ζ, we can construct the function $\bar{D}(\phi, \zeta)$, showing how the long time Fickian diffusivity varies with both the obstacle density and the strength of adhesion/repulsion. A contour plot of $\bar{D}(\phi, \zeta)$ is shown in Figure 10.2(a) for $\zeta \in [-0.9, 0.9]$ and $\phi \in [0, 0.5]$. When $\phi = 0$ and there are no obstacles, we obtain $\bar{D}(0, \zeta) = D_0$, as expected. Comparing the slope of $\bar{D}(\phi, \zeta)$ in each of the ϕ and ζ directions indicates that, in general, the long time Fickian diffusivity is far more sensitive to ϕ than ζ. In particular, for small values of ϕ, the diffusivity appears, at this scale, to be relatively insensitive to the strength of adhesion/repulsion. However, at larger values of ϕ, there is an significant dependence on ζ.

To further explore the effects of adhesion/repulsion, Figure 10.2(b) shows the ratio $\bar{D}(\phi, \zeta)/\bar{D}(\phi, 0)$ for different values of ζ. This ratio is approximately unity for all values of ζ when $\phi < 0.3$. For $\phi > 0.3$ the affect of adhesion ($\zeta > 0$) is to decrease $\bar{D}(\phi, \zeta)/\bar{D}(\phi, 0)$, whereas the affect of repulsion ($\zeta < 0$) is to increase $\bar{D}(\phi, \zeta)/\bar{D}(\phi, 0)$, as we might anticipate. The increase in $\bar{D}(\phi, \zeta)$ due to repulsion can be as great as 1100% for the values of ϕ and ζ that we consider.

In summary, we present a method that allows us to quantify the roles of both crowding and adhesion/repulsion by quantifying the long time Fickian diffusivity of a motile agent moving through a crowded environment. A key feature of our approach is that it avoids the needs for performing stochastic simulations. Our calculations allow us to examine how the long time Fickian

diffusivity depends both on the density of obstacles, ϕ, and the strength of adhesion/repulsion, ζ. Additional results (not presented) confirm the accuracy of our method since the maximum deviation between the exact calculations and estimates based on repeated stochastic simulation results is less than 0.1% for the range of ϕ and ζ considered in Figure 10.2(a). A key feature of our results is that the long time impact of adhesion/repulsion is negligible for sufficiently small obstacle densities, $\phi < 0.3$, when the mean free diffusion time between two collisions is small. Therefore, our results suggest that estimates of the long time Fickian diffusivity for low obstacle densities can neglect the affect of adhesion/repulsion. In contrast, for moderate to high obstacle densities, $\phi > 0.3$, our calculations show that adhesion/repulsion has an important impact that ought to be accounted for.
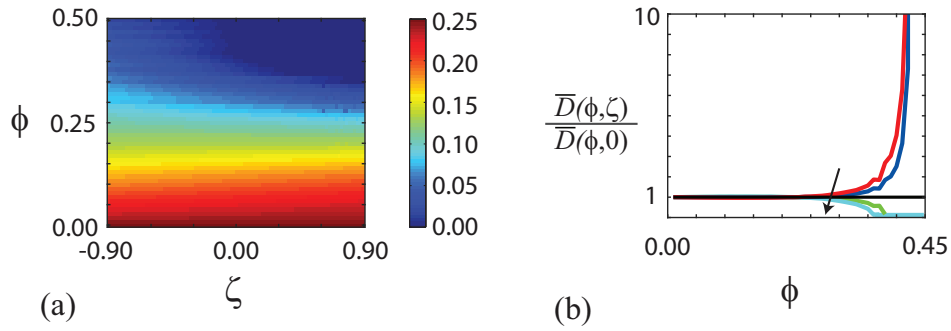
Figure 10.2: (a) Plot of $\bar{D}(\phi, \zeta)$ for $\phi \in [0, 0.5]$ and $\zeta \in [-0.9, 0.9]$ with $p_m = 1.0$ and $X = 100$, $Y = 100$. The surface plot of $\bar{D}(\phi, \zeta)$ is constructed by discretizing the (ϕ, ζ) parameter space into a square grid with 50 equally spaced intervals in the ϕ direction and 100 equally spaced intervals in the ζ direction. Values of $\bar{D}(\phi, \zeta)$ are calculated at each discrete (ϕ, ζ) value, and the surface plot is constructed using MATLAB. All exact calculations of $\bar{D}(\phi, \zeta)$ are repeated using 10 identically prepared lattices, randomly populated to density ϕ, and the values of $\bar{D}(\phi, \zeta)$ are averaged over the suite of lattices considered to give the results in (a). Curves in (b) show the ratio $\bar{D}(\phi, \zeta)/\bar{D}(\phi, 0)$ for $\zeta = -0.90\,(\text{red}), -0.45\,(\text{dark blue}), 0.00\,(\text{black}), 0.45\,(\text{green}), 0.90\,(\text{light blue})$, with the arrow indicating the direction of increasing ζ.

Chapter 11

Additional results for Chapter 10

In this appendix we provide details of three example calculations. In these examples we consider the lattice in Figure 11.1. We calculate the long time diffusivity by considering the x–direction only and in all cases we apply periodic boundary conditions. For each worked example we have apply a bias in the positive x direction of ϵ and we set $p_m = 1$. The three example calculations presented here correspond to three different choices of ζ. Our method can also be used to calculate the long time diffusivity in the y–direction by applying the bias in the y–direction.
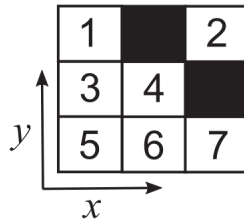
Figure 11.1: A lattice for which $\phi = 2/9$. Obstacles are shown as black squares. The lattice sites are numbered as indicated.

Example 1: No adhesion/repulsion, $\zeta = 0$.

We first consider a case in which there is no adhesion/repulsion ($\zeta = 0$). For this example

112 CHAPTER 11.

the transition matrix is given by

$$\mathbf{T} = \begin{pmatrix} \frac{1+\epsilon}{4} & \frac{1+\epsilon}{4} & \frac{1}{4} & 0 & \frac{1}{4} & 0 & 0 \\ \frac{1-\epsilon}{4} & \frac{2-\epsilon}{4} & 0 & 0 & 0 & 0 & \frac{1}{4} \\ \frac{1}{4} & 0 & \frac{1-\epsilon}{4} & \frac{1-\epsilon}{4} & \frac{1}{4} & 0 & 0 \\ 0 & 0 & \frac{1+\epsilon}{4} & \frac{2+\epsilon}{4} & 0 & \frac{1}{4} & 0 \\ \frac{1}{4} & 0 & \frac{1}{4} & 0 & 0 & \frac{1-\epsilon}{4} & \frac{1+\epsilon}{4} \\ 0 & 0 & 0 & \frac{1}{4} & \frac{1+\epsilon}{4} & \frac{1}{4} & \frac{1-\epsilon}{4} \\ 0 & \frac{1}{4} & 0 & 0 & \frac{1-\epsilon}{4} & \frac{1+\epsilon}{4} & \frac{1}{4} \end{pmatrix}.$$

The probability that the agent will be at the nth site in the long time limit is given by solving $\mathbf{Tn} = \mathbf{n}$, and then normalizing to give $\hat{\mathbf{n}}$. The velocity vector can be calculated element-wise using

$$v(i) = p_+ L_+ - p_- L_-,$$

where $p_\pm$ denotes the probability of moving in the positive and negative x directions and $L_\pm = 1$ if the site is vacant and $L_\pm = 0$ otherwise. For this example these vectors are given by

$$\hat{\mathbf{n}} = \begin{pmatrix} \frac{1}{7} \\ \frac{1}{7} \\ \frac{1}{7} \\ \frac{1}{7} \\ \frac{1}{7} \\ \frac{1}{7} \\ \frac{1}{7} \end{pmatrix} + \epsilon \begin{pmatrix} \frac{1}{28} \\ -\frac{1}{7} \\ -\frac{1}{28} \\ \frac{1}{7} \\ 0 \\ \frac{1}{28} \\ -\frac{1}{28} \end{pmatrix}, \qquad \mathbf{v} = \begin{pmatrix} -\frac{1}{4} \\ \frac{1}{4} \\ \frac{1}{4} \\ -\frac{1}{4} \\ 0 \\ 0 \\ 0 \end{pmatrix} + \epsilon \begin{pmatrix} \frac{1}{4} \\ \frac{1}{4} \\ \frac{1}{4} \\ \frac{1}{4} \\ \frac{1}{2} \\ \frac{1}{2} \\ \frac{1}{2} \end{pmatrix}.$$

From these vectors we can directly calculate the long–time diffusivity, using the formula [3,

127]

$$\bar{D}_x = \frac{\mathbf{v}_\epsilon \, \mathbf{n}_I + \mathbf{v}_I \, \mathbf{n}_\epsilon}{D_{x0}} = 0.13,$$

where the subscripts ϵ and I denote the ϵ dependent and independent components of the vectors and D_{x0} denotes the diffusivity in the x direction when $\phi = 0$. To test the veracity of this exact calculation we also performed stochastic simulations and analysed the long time diffusivity in the same way as described in the main paper which gives $\bar{D}_x = 0.13$. The stochastic approximation of $\bar{D}_x$ used an ensemble of 100,000 identically prepared realizations of the random walk algorithm over the interval $0 \le t \le 10^6$.

Example 2: Repulsion, $\zeta = -0.1$.

The second case we consider involves repulsion with $\zeta = -0.1$. In this case the transition matrix is given by

$$\mathbf{T} = \begin{pmatrix}
\frac{7+11\epsilon}{40} & \frac{11+11\epsilon}{40} & \frac{11}{40} & 0 & \frac{11}{40} & 0 & 0 \\[2mm]
\frac{3-3\epsilon}{10} & \frac{4-3\epsilon}{10} & 0 & 0 & 0 & 0 & \frac{3}{10} \\[2mm]
\frac{11}{40} & 0 & \frac{7-11\epsilon}{40} & \frac{11-11\epsilon}{40} & \frac{11}{40} & 0 & 0 \\[2mm]
0 & 0 & \frac{3+3\epsilon}{10} & \frac{4+3\epsilon}{10} & 0 & \frac{3}{10} & 0 \\[2mm]
\frac{1}{4} & 0 & \frac{1}{4} & 0 & 0 & \frac{10-10\epsilon}{40} & \frac{10+10\epsilon}{40} \\[2mm]
0 & 0 & 0 & \frac{11}{40} & \frac{11+11\epsilon}{40} & \frac{7}{40} & \frac{11-11\epsilon}{40} \\[2mm]
0 & \frac{11}{40} & 0 & 0 & \frac{11-11\epsilon}{40} & \frac{11+11\epsilon}{40} & \frac{7}{40}
\end{pmatrix},$$

and $\hat{\mathbf{n}}$ and $\mathbf{v}$ are given by

$$
\hat{\mathbf{n}} = \begin{pmatrix} \frac{1}{7} \\ \frac{1}{7} \\ \frac{1}{7} \\ \frac{1}{7} \\ \frac{1}{7} \\ \frac{1}{7} \\ \frac{1}{7} \end{pmatrix} + \epsilon \begin{pmatrix} \frac{1}{28} \\ -\frac{1}{7} \\ -\frac{1}{28} \\ \frac{1}{7} \\ 0 \\ \frac{1}{28} \\ -\frac{1}{28} \end{pmatrix}, \qquad \mathbf{v} = \begin{pmatrix} -\frac{11}{40} \\ \frac{12}{40} \\ \frac{11}{40} \\ -\frac{12}{40} \\ 0 \\ 0 \\ 0 \end{pmatrix} + \epsilon \begin{pmatrix} \frac{11}{40} \\ \frac{12}{40} \\ \frac{11}{40} \\ \frac{12}{40} \\ \frac{20}{40} \\ \frac{22}{40} \\ \frac{22}{40} \end{pmatrix},
$$

giving

$$
\bar{D}_x = \frac{\mathbf{v}_\epsilon \, \mathbf{n}_I + \mathbf{v}_I \, \mathbf{n}_\epsilon}{D_{x0}} = 0.14.
$$

To test the veracity of this exact calculation we also performed stochastic simulations and analysed the long time diffusivity in the same way as described in the main paper which gives $\bar{D}_x = 0.14$. The stochastic approximation of $\bar{D}_x$ used an ensemble of 100,000 identically prepared realizations of the random walk algorithm over the interval $0 \le t \le 10^6$. We note that the diffusivity in Example 2, with repulsion, is greater than the diffusivity in Example 1 without any adhesion or repulsion.

Example 3: Adhesion, $\zeta = 0.1$.

The third case we consider involves adhesion with $\zeta = 0.1$. In this case the transition matrix

is given by

$$
\mathbf{T} = \begin{pmatrix}
\frac{13+9\epsilon}{40} & \frac{9+9\epsilon}{40} & \frac{9}{40} & 0 & \frac{9}{40} & 0 & 0 \\
\frac{8-8\epsilon}{40} & \frac{24-8\epsilon}{40} & 0 & 0 & 0 & 0 & \frac{8}{40} \\
\frac{9}{40} & 0 & \frac{13-9\epsilon}{40} & \frac{9-9\epsilon}{40} & \frac{9}{40} & 0 & 0 \\
0 & 0 & \frac{8+8\epsilon}{40} & \frac{24+8\epsilon}{40} & 0 & \frac{8}{40} & 0 \\
\frac{10}{40} & 0 & \frac{10}{40} & 0 & 0 & \frac{10-10\epsilon}{40} & \frac{10-10\epsilon}{40} \\
0 & 0 & 0 & \frac{9}{40} & \frac{9+9\epsilon}{40} & \frac{13}{40} & \frac{9-9\epsilon}{40} \\
0 & \frac{9}{40} & 0 & 0 & \frac{9-9\epsilon}{40} & \frac{9+9\epsilon}{40} & \frac{13}{40}
\end{pmatrix},
$$

and $\hat{\mathbf{n}}$ and $\mathbf{v}$ are given by

$$
\hat{\mathbf{n}} = \begin{pmatrix} \frac{1}{7} \\ \frac{1}{7} \\ \frac{1}{7} \\ \frac{1}{7} \\ \frac{1}{7} \\ \frac{1}{7} \\ \frac{1}{7} \end{pmatrix} + \epsilon \begin{pmatrix} \frac{1}{28} \\ -\frac{1}{7} \\ -\frac{1}{28} \\ \frac{1}{7} \\ 0 \\ \frac{1}{28} \\ -\frac{1}{28} \end{pmatrix}, \qquad
\mathbf{v} = \begin{pmatrix} -\frac{9}{40} \\ \frac{8}{40} \\ \frac{9}{40} \\ -\frac{8}{40} \\ 0 \\ 0 \\ 0 \end{pmatrix} + \epsilon \begin{pmatrix} \frac{9}{40} \\ \frac{8}{40} \\ \frac{9}{40} \\ \frac{8}{40} \\ \frac{20}{40} \\ \frac{18}{40} \\ \frac{18}{40} \end{pmatrix},
$$

which gives

$$
\bar{D}_x = \frac{\mathbf{v}_\epsilon\, \mathbf{n}_I + \mathbf{v}_I\, \mathbf{n}_\epsilon}{D_{x0}} = 0.12.
$$

To test the veracity of this exact calculation we also performed stochastic simulations and analysed the long time diffusivity in the same way as described in the main paper which gives $\bar{D}_x = 0.12$. The stochastic approximation of $\bar{D}_x$ used an ensemble of 100,000 identically prepared realizations of the random walk algorithm over the interval $0 \le t \le 10^6$. We note that

the diffusivity in Example 3, with adhesion, is less than the diffusivity in Example 1 without any adhesion or repulsion.

Chapter 12

Conclusions and Recommendations

In this chapter we summarise the main results and contributions of this work and discuss potential avenues for further investigation.

12.1 Summary of the research

This study uses numerical data from a stochastic model of crowded transport to assess the accuracy of a related FDE model. We show that one of the underlying assumptions of FDE models, that the order of the fractional derivative, α, is constant, is not true for this particular stochastic process. This leads us to conclude that FDE models must be applied with great care and motivates us to develop a new modelling framework of transport through crowded environments. Our new modelling framework enables us to model the early to intermediate time behaviour of a motile agent; to calculate the reduced diffusivity of the motile agent in the long time limit; and to calculate the crossover time of an agent undergoing transport through a crowded environment.

The principle aims of this thesis are to:

- Compare an FDE with population density data from a CTRW to determine the role that crowding plays in determining the type of transport process taking place.

- Extend existing models to include environments that are densely crowded with obstacles of different shapes and sizes to determine how different distributions of obstacles affect the transport process.

- Develop a new modelling methodology that describes the early time behaviour of an agent undergoing transport through a crowded environment.

- Develop a new modelling methodology that allows the calculation of the long time diffusivity of an agent undergoing transport through a crowded environment as well as the calculation of the crossover time associated with a crowded environment.

In the literature [7, 10, 18, 20, 28–30, 36–38], CTRW models and FDE models are often assumed, without justification, to be equivalent and interchangeable. In Chapter 2 we compare a CTRW with the analytical solution of a related FDE. Specifically, we track the MSD of a motile agent undergoing a nearest neighbour random walk on a lattice that contains obstacles and use this data to provide an estimate of a parameter α, which describes the type of transport process taking place. Then, we simulate the transport of a population of motile agents through a crowded environment using the same CTRW model and use these simulations to generate population density data. We match the solution of a related FDE to this data to provide an alternative estimate of α. An underlying assumption of FDE models is that α, the order of the fractional derivative, is a constant. We show that this assumption is not true for our systems and conclude that FDE models must be used with great care. We also examine the relationship between these two independent estimates of α and the properties of the obstacle field for both a single agent and a population of agents; and for both types of models; and we show that in both cases, α decreases as the obstacle density increases and that the rate of decrease is greater for smaller obstacles than for larger obstacles.

In Chapter 4 we extend our analysis to an environment in which there are several different types of obstacles present on the lattice, of various shapes, sizes and densities. Specifically, we consider three different distributions of obstacles: (i) the first contains relatively more smaller obstacles than larger ones; (ii) the second contains relatively more larger obstacles than smaller ones and; (iii) the third contains the same number of occupied lattice sites for each type of obstacle considered. The inclusion of multiple obstacle types allows us to create radically different environments in which the density of obstacles, ϕ, is a constant. We again track and use the MSD of a single agent to provide an estimate of α and then match population density information to a related FDE to provide a second independent estimate of α. By comparing these two independent estimates of α we find that the distribution of obstacle shapes and sizes also play an important role in determining the type of transport process taking place and we

investigate these effects. We conclude that the density of obstacles, alone, is not sufficient to describe the type of transport process taking place and that unless researchers include additional information about the size, shape and relative densities of different obstacle types, their results may be difficult to reproduce.

These new results lead us to consider alternative models of transport through crowded environments. Specifically, we consider (i) how to model the early to intermediate time behaviour of a single motile agent moving through a crowded environment; (ii) how to determine the diffusivity of the motile agent in the long time limit, after the transport process has become Fickian and; (iii) the length of time an experimentalist must wait until they can treat the transport process as Fickian diffusion.

We begin by examining an algorithm proposed in a different context by Mercier and Slater [42–44] for calculating the long time diffusivity in a crowded environment in Chapter 5, and modify it so that it can be applied to our new system. Our new algorithm allows a researcher to take a lattice of interest and directly calculate the diffusivity of a motile agent in the long time (Fickian) regime without performing any computationally expensive and time consuming stochastic simulations. The ease with which our new method can be applied allows us to examine a larger set of environments than those considered by earlier studies [11, 12] which were limited to considering computationally expensive CTRW models. Our new method allows us to confirm the qualitative trends of our data from Chapters 2–4 and present new quantitative results.

To model the early to intermediate time behaviour of our system we outline a new modelling framework which is motivated by the theory of Markov chains. The application of our new method involves several practical difficulties and we outline and provide solutions to these problems in Chapter 7. Unlike stochastic models which provide noisy stochastic data that is only useful if it is averaged over a large ensemble, our new model allows researchers to perform a single exact calculation that typically takes less time than CTRW simulations. We compare our exact calculation of the MSD of a motile agent with MSD data from a related stochastic model to demonstrate the ease with which our new method can be applied.

We then propose another new method, motivated by the MAT proposed by McNabb and Wake [45, 46] and expanded by others [47–51], to provide experimentalists with a 'rule-of-thumb' measurement of the amount of time they must wait until they can safely assume that a

motile agent undergoing transport in a crowded environment is undergoing Fickian diffusion, called the crossover time [11, 12]. Unlike the crossover time proposed by Saxton [11, 12], our new definition of the crossover time can be exactly calculated for a given lattice of interest without performing time consuming and expensive stochastic simulations. Additionally, unlike the method proposed by Saxton, our new method is both objective and reproducible.

Finally, we extend our variation of the Mercier–Slater algorithm to include interactions between the motile agent and the obstacles, such as adhesion and repulsion in Chapter 10. Our results suggest that there is a threshold density of obstacles ($\phi \approx 0.30$) below which the affect of adhesion and repulsion is negligible in the long time limit as $t \rightarrow \infty$. For obstacle densities above this threshold ($\phi > 0.30$) cellular interactions play a major role.

12.2   Future work

There are multiple avenues for future investigation that have arisen from this thesis. We consider some of them below:

- **Models of crowded transport with motile obstacles.**
  All of the work in this thesis assumes that the obstacles acting as blockages are stationary. Experimental data indicates that this assumption is physically unrealistic for both biological environments [34, 39, 105, 108] and analogous non–biological physical systems [53, 54]. Although it is trivial to extend a CTRW model to include motile obstacles, it is non–trivial to extend the Markovian framework developed in Chapter 5 or the modified Mercier–Slater algorithm developed in Chapter 7 to include this level of complexity.

  In Chapter 5 we calculated the long time diffusivity associated with each member a set of lattices occupied with randomly placed obstacles to density ϕ. We show that the distribution of these diffusivities depends on the density, shape, size and distribution of obstacles present on the lattice.

- **Extension to analogous non–biological systems.**
  This work was motivated by the problem of accurately modelling cellular motility. However, there are several other fields in which crowded transport is of theoretical interest including models of the transportation of charge in amorphous semiconductors [22, 130,

131], nuclear magnetic resonance diffusometry [132, 133] and the transport of contaminants in certain porous geological media [134], amongst many others.

Unlike biological systems, these systems have the advantage that collecting large data sets is relatively simple and cheap so that a direct comparison of the theoretical predictions of this research with experimental data is possible. An extension of the ideas developed in this work to other fields would be of wide interest within the mathematics and physics communities.

- **Development of image processing software**

  The application of this research may be difficult for non-mathematicians to understand and implement. This motivates the development of software tools that simplify its application. Such software might take, as input, a photograph of a colony of cells in a Petri dish and output various parameters of interest such as the crossover time and long time diffusivity.

  An example algorithm for such a software package is as follows:

  1. Input a photograph of a Petri dish.

  2. We associate each pixel with an individual lattice site. Utilising image segmentation techniques we can distinguish the pixels in the image that represent cells from the pixels that represent vacant space.

  3. We generate the transition matrix, $\mathbf{T}$, that is associated with this lattice.

  4. From the transition matrix, $\mathbf{T}$, we calculate the crossover time, C, and the long time diffusivity, $\bar{D}$, using the theory outlined in Chapters 5–7.

  5. We output C and $\bar{D}$ to the user.

  The software might include a tool that enables the user to adjust the adhesion parameter, ζ, and the size of the motile agent.

  One disadvantage of this approach is that it does not take into consideration the fact that cells do not move on a lattice. It may be necessary to make a correction in order to account for these differences. This would require further research into how to extend the results of this thesis to a lattice–free environment.

12.3   Final remarks

Mathematical modelling has the ability to provide valuable insight into transport processes that occur in crowded environments. In this study, we investigate the standard models of crowded transport that are utilised throughout the literature, FDE models and CTRW models, and show that they are not equivalent. Specifically, we show that FDE models must be used with great care as one of the underlying assumptions of these models is that the quantity α that describes the type of transport taking place is a constant and this may not be true for all systems. We also showed that the size, shape and density of obstacles in the environment can significantly impact the value of α and suggested that experimentalists include this additional information when reporting their results.

This motivates us to develop a new model that allows us to model the early time behaviour of an agent undergoing transport through a crowded environment and to develop an algorithm that allows researchers to calculate both the long time diffusivity and the crossover time of the agent. This new methodology provides new information that is of great value to experimentalists and opens up several new avenues for investigation by future researchers.

Literature Cited

[1] A. J. Ellery, M. J. Simpson, S. W. McCue, and R. E. Baker, "Characterizing transport through a crowded environment with different obstacle sizes," *The Journal of Chemical Physics*, vol. 140, no. 5, p. 054108, 2014.

[2] A. J. Ellery, R. E. Baker, and M. J. Simpson, "Calculating the fickian diffusivity for a lattice-based random walk with agents and obstacles of different shapes and sizes," *Physical Biology*, vol. 12, no. 6, p. 066010, 2015.

[3] A. J. Ellery, R. E. Baker, S. W. McCue, and M. J. Simpson, "Modeling transport through an environment crowded by a mixture of obstacles of different shapes and sizes," *Physica A: Statistical Mechanics and its Applications*, vol. 449, p. 74, 2016.

[4] R. J. Ellis, "Macromolecular crowding: obvious but underappreciated," *Trends in Biochemical Sciences*, vol. 26, no. 10, p. 597, 2001.

[5] A. P. Minton, "The influence of macromolecular crowding and macromolecular confinement on biochemical reactions in physiological media," *Journal of Biological Chemistry*, vol. 276, no. 14, p. 10577, 2001.

[6] M. Weiss, M. Elsner, F. Kartberg, and T. Nilsson, "Anomalous subdiffusion is a measure for cytoplasmic crowding in living cells," *Biophysical Journal*, vol. 87, no. 5, p. 3518, 2004.

[7] I. M. Sokolov, J. Klafter, and A. Blumen, "Fractional kinetics," *Physics Today*, vol. 55, no. 11, p. 48, 2002.

[8] I. M. Sokolov, "Models of anomalous diffusion in crowded environments," *Soft Matter*, vol. 8, no. 35, p. 9043, 2012.

[9] J. A. Dix and A. S. Verkman, "Crowding effects on diffusion in solutions and cells," *Annual Review of Biophysics*, vol. 37, p. 247, 2008.

[10] R. Metzler and J. Klafter, "The random walk's guide to anomalous diffusion: a fractional dynamics approach," *Physics Reports*, vol. 339, no. 1, p. 1, 2000.

[11] M. J. Saxton, "Anomalous diffusion due to obstacles: a monte carlo study," *Biophysical Journal*, vol. 66, no. 2 Pt 1, p. 394, 1994.

[12] M. J. Saxton, "Single-particle tracking: the distribution of diffusion coefficients," *Biophysical Journal*, vol. 72, no. 4, p. 1744, 1997.

[13] E. Vilaseca, A. Isvoran, S. Madurga, I. Pastor, J. L. Garcs, and F. Mas, "New insights into diffusion in 3d crowded media by monte carlo simulations: effect of size, mobility and spatial distribution of obstacles," *Physical Chemistry Chemical Physics*, vol. 13, no. 16, p. 7396, 2011.

[14] E. Vilaseca, I. Pastor, A. Isvoran, S. Madurga, J.-L. Garcs, and F. Mas, "Diffusion in macromolecular crowded media: Monte carlo simulation of obstructed diffusion vs. frap experiments," *Theoretical Chemistry Accounts*, vol. 128, no. 4, p. 795, 2011.

[15] A. Isvoran, E. Vilaseca, J. L. Garces, L. Unipan, and F. Mas, "Simulation of diffusion in two-dimensional crowded media," in *Sixth International Conference of the Balkan Physical Union*, vol. 899, p. 469, AIP Publishing, 1997.

[16] A. Isvoran, E. Vilaseca, F. Ortega, M. Cascante, and F. Mas, "About implementing a monte carlo simulation algorithm for enzymatic reactions in crowded media," *Journal of the Serbian Chemical Society*, vol. 71, no. 1, p. 75, 2006.

[17] A. Isvoran, E. Vilaseca, L. Unipan, J.-L. Garces, and F. Mas, "Computational study of diffusion in cellular two-dimensional crowded media modeled as mixtures of mobile and immobile obstacles," *Revue Roumaine de Chimie*, vol. 53, no. 5, p. 415, 2008.

[18] S. B. Yuste, E. Abad, and K. Lindenberg, "Reaction-subdiffusion model of morphogen gradient formation," *Physical Review E*, vol. 82, no. 6, p. 061123, 2010.

[19] A. Yadav and W. Horsthemke, "Kinetic equations for reaction-subdiffusion systems: Derivation and stability analysis," *Physical Review E*, vol. 74, no. 6, p. 066118, 2006.

[20] T. A. M. Langlands and B. I. Henry, "The accuracy and stability of an implicit solution method for the fractional diffusion equation," *Journal of Computational Physics*, vol. 205, no. 2, p. 719, 2005.

[21] E. W. Montroll and G. H. Weiss, "Random walks on lattices. ii," *Journal of Mathematical Physics*, vol. 6, no. 2, p. 167, 1965.

[22] H. Scher and M. Lax, "Stochastic transport in a disordered solid. i. theory," *Physical Review B*, vol. 7, no. 10, p. 4491, 1973.

[23] A. Wedemeier, H. Merlitz, C.-X. Wu, and J. Langowski, "Modeling diffusional transport in the interphase cell nucleus," *The Journal of Chemical Physics*, vol. 127, no. 4, p. 045102, 2007.

[24] A. Wedemeier, T. Zhang, H. Merlitz, C.-X. Wu, and J. Langowski, "The role of chromatin conformations in diffusional transport of chromatin-binding proteins: Cartesian lattice simulations," *The Journal of Chemical Physics*, vol. 128, no. 15, p. 155101, 2008.

[25] A. Wedemeier, H. Merlitz, and J. Langowski, "Anomalous diffusion in the presence of mobile obstacles," *EPL (Europhysics Letters)*, vol. 88, no. 3, p. 38004, 2009.

[26] A. Wedemeier, H. Merlitz, C.-X. Wu, and J. Langowski, "How proteins squeeze through polymer networks: a cartesian lattice study," *The Journal of Chemical Physics*, vol. 131, no. 6, p. 064905, 2009.

[27] T. Liggett, *Interacting Particle Systems*, vol. 276. Springer Science & Business Media, 2012.

[28] S. B. Yuste and K. Lindenberg, "Subdiffusion-limited reactions," *Chemical Physics*, vol. 284, no. 1, p. 169, 2002.

[29] S. B. Yuste and K. Lindenberg, "Subdiffusion-limited a+ a reactions," *Physical Review Letters*, vol. 87, no. 11, p. 118301, 2001.

[30] S. B. Yuste, L. Acedo, and K. Lindenberg, "Reaction front in an a+ b c reaction-subdiffusion process," *Physical Review E*, vol. 69, no. 3, p. 036126, 2004.

[31] K. B. Oldham and J. Spanier, *The Fractional Calculus: Theory and Applications of Differentiation and Integration to Arbitrary Order*. Academic Press, 1974.

[32] I. Podlubny, *Fractional Differential Equations: An Introduction to Fractional Derivatives, Fractional Differential Equations, to Methods of their Solution and some of their Applications.* Academic press, 1998.

[33] H. Sanabria, Y. Kubota, and M. N. Waxham, "Multiple diffusion mechanisms due to nanostructuring in crowded environments," *Biophysical Journal*, vol. 92, no. 1, p. 313, 2007.

[34] D. S. Banks and C. Fradin, "Anomalous diffusion of proteins due to molecular crowding," *Biophysical Journal*, vol. 89, no. 5, p. 2960, 2005.

[35] G. Guigas, C. Kalla, and M. Weiss, "Probing the nanoscale viscoelasticity of intracellular fluids in living cells," *Biophysical Journal*, vol. 93, no. 1, p. 316, 2007.

[36] E. Abad, S. B. Yuste, and K. Lindenberg, "Reaction-subdiffusion and reaction-superdiffusion equations for evanescent particles performing continuous-time random walks," *Physical Review E*, vol. 81, no. 3, p. 031115, 2010.

[37] B. I. Henry, T. A. M. Langlands, and S. L. Wearne, "Anomalous diffusion with linear reaction dynamics: from continuous time random walks to fractional reaction-diffusion equations," *Physical Review E*, vol. 74, no. 3, p. 031116, 2006.

[38] J. Gajda and A. Wyomaska, "Fokkerplanck type equations associated with fractional brownian motion controlled by infinitely divisible processes," *Physica A: Statistical Mechanics and its Applications*, vol. 405, p. 104, 2014.

[39] A. Kicheva, P. Pantazis, T. Bollenbach, Y. Kalaidzidis, T. Bittig, F. Jlicher, and M. Gonzalez-Gaitan, "Kinetics of morphogen gradient formation," *Science*, vol. 315, no. 5811, p. 521, 2007.

[40] D. Lepzelter and M. Zaman, "Subdiffusion of proteins and oligomers on membranes," *The Journal of Chemical Physics*, vol. 137, no. 17, p. 175102, 2012.

[41] A. A. Like and W. L. Chick, "Studies in the diabetic mutant mouse: Ii. electron microscopy of pancreatic islets," *Diabetologia*, vol. 6, no. 3, p. 216, 1970.

[42] J.-F. Mercier, G. W. Slater, and H. L. Guo, "Numerically exact diffusion coefficients for lattice systems with periodic boundary conditions. i. theory," *The Journal of Chemical Physics*, vol. 110, no. 12, p. 6050, 1999.

[43] J.-F. Mercier and G. W. Slater, "Numerically exact diffusion coefficients for lattice systems with periodic boundary conditions. ii. numerical approach and applications," *The Journal of Chemical Physics*, vol. 110, no. 12, p. 6057, 1999.

[44] J.-F. Mercier and G. W. Slater, "Random walk and diffusion of hard spherical particles in quenched systems: Reaching the continuum limit on a lattice," *The Journal of Chemical Physics*, vol. 113, no. 20, p. 9109, 2000.

[45] A. McNabb and G. C. Wake, "Heat conduction and finite measures for transition times between steady states," *IMA Journal of Applied Mathematics*, vol. 47, no. 2, p. 193, 1991.

[46] A. McNabb, "Means action times, time lags, and mean first passage times for some diffusion problems," *Mathematical and Computer Modelling*, vol. 18, no. 10, p. 123, 1993.

[47] A. J. Ellery, M. J. Simpson, and S. W. McCue, "Comment on" local accumulation times for source, diffusion, and degradation models in two and three dimensions"[j. chem. phys. 138, 104121 (2013)]," *Journal of Chemical Physics*, vol. 139, no. 017101, pp. 1–2, 2013.

[48] A. J. Ellery, M. J. Simpson, S. W. McCue, and R. E. Baker, "Critical time scales for advection-diffusion-reaction processes," *Physical Review E*, vol. 85, no. 4, p. 041135, 2012.

[49] A. J. Ellery, M. J. Simpson, S. W. McCue, and R. E. Baker, "Moments of action provide insight into critical times for advection-diffusion-reaction processes," *Physical Review E*, vol. 86, no. 3, p. 031136, 2012.

[50] A. J. Ellery, M. J. Simpson, S. W. McCue, and R. E. Baker, "Simplified approach for calculating moments of action for linear reaction-diffusion equations," *Physical Review E*, vol. 88, no. 5, p. 054102, 2013.

[51] K. Landman and M. McGuinness, "Mean action time for diffusive processes," *Advances in Decision Sciences*, vol. 4, no. 2, p. 125, 2000.

[52] W. S. Price, F. Tsuchiya, and Y. Arata, "Lysozyme aggregation and solution properties studied using PGSE NMR diffusion measurements," *Journal of the American Chemical Society*, vol. 121, no. 49, p. 11503, 1999.

[53] D. K. Wilkins, S. B. Grimshaw, V. Receveur, C. M. Dobson, J. A. Jones, and L. J. Smith, "Hydrodynamic radii of native and denatured proteins measured by pulse field gradient nmr techniques," *Biochemistry*, vol. 38, no. 50, p. 16424, 1999.

[54] T. Pirzer, M. Geisler, T. Scheibel, and T. Hugel, "Single molecule force measurements delineate salt, ph and surface effects on biopolymer adhesion," *Physical Biology*, vol. 6, no. 2, p. 025004, 2009.

[55] D. V. Nicolau, J. F. Hancock, and K. Burrage, "Sources of anomalous diffusion on cell membranes: a monte carlo study," *Biophysical Journal*, vol. 92, no. 6, p. 1975, 2007.

[56] D. Lepzelter and M. H. Zaman, "Clustered diffusion of integrins," *Biophysical Journal*, vol. 99, no. 12, pp. L106–L108, 2010.

[57] M. J. Simpson, C. Towne, D. L. S. McElwain, and Z. Upton, "Migration of breast cancer cells: understanding the roles of volume exclusion and cell-to-cell adhesion," *Physical Review E*, vol. 82, no. 4, p. 041901, 2010.

[58] K. K. Treloar, M. J. Simpson, P. Haridas, K. J. Manton, D. I. Leavesley, D. L. S. McElwain, and R. E. Baker, "Multiple types of data are required to identify the mechanisms influencing the spatial expansion of melanoma cell colonies," *BMC Systems Biology*, vol. 7, no. 1, p. 137, 2013.

[59] C. Deroulers, M. Aubert, M. Badoual, and B. Grammaticos, "Modeling tumor cell migration: from microscopic to macroscopic models," *Physical Review E*, vol. 79, no. 3, p. 031917, 2009.

[60] K. Anguige and C. Schmeiser, "A one-dimensional model of cell diffusion and aggregation, incorporating volume filling and cell-to-cell adhesion," *Journal of Mathematical Biology*, vol. 58, no. 3, p. 395, 2009.

[61] R. N. Thompson, C. A. Yates, and R. E. Baker, "Modelling cell migration and adhesion during development," *Bulletin of Mathematical Biology*, vol. 74, no. 12, p. 2793, 2012.

[62] A. E. Fernando, K. A. Landman, and M. J. Simpson, "Nonlinear diffusion and exclusion processes with contact interactions," *Physical Review E*, vol. 81, no. 1, p. 011903, 2010.

[63] D. T. Gillespie, "Exact stochastic simulation of coupled chemical reactions," *The Journal of Physical Chemistry*, vol. 81, no. 25, p. 2340, 1977.

[64] D. Chandler and J. K. Percus, "Introduction to modern statistical mechanics," *Physics Today*, vol. 41, no. 12, p. 114, 2008.

[65] S. B. Zimmerman and S. O. Trach, "Estimation of macromolecule concentrations and excluded volume effects for the cytoplasm of escherichia coli," *Journal of Molecular Biology*, vol. 222, no. 3, p. 599, 1991.

[66] J.-P. Bouchaud and A. Georges, "Anomalous diffusion in disordered media: statistical mechanisms, models and physical applications," *Physics Reports*, vol. 195, no. 4, p. 127, 1990.

[67] B. D. Hughes, *Random Walks and Random Environments*. Clarendon Press Oxford, 1996.

[68] D. Stauffer and A. Aharony, *Introduction to Percolation Theory*. CRC press, 1994.

[69] E. A. Codling, M. J. Plank, and S. Benhamou, "Random walk models in biology," *Journal of the Royal Society Interface*, vol. 5, no. 25, p. 813, 2008.

[70] X. Yu and D. M. Leitner, "Anomalous diffusion of vibrational energy in proteins," *The Journal of Chemical Physics*, vol. 119, no. 23, p. 12673, 2003.

[71] U. Schmidt and M. Weiss, "Anomalous diffusion of oligomerized transmembrane proteins," *The Journal of Chemical Physics*, vol. 134, no. 16, p. 165101, 2011.

[72] K. J. Foster and S. J. Miklavcic, "On the competitive uptake and transport of ions through differentiated root tissues," *Journal of Theoretical Biology*, vol. 340, p. 1, 2014.

[73] J. A. Sherratt and J. D. Murray, "Models of epidermal wound healing," *Proceedings of the Royal Society of London B: Biological Sciences*, vol. 241, no. 1300, p. 29, 1990.

[74] P. K. Maini, D. L. S. McElwain, and D. I. Leavesley, "Traveling wave model to interpret a wound-healing cell migration assay for human peritoneal mesothelial cells," *Tissue Engineering*, vol. 10, no. 3, p. 475, 2004.

[75] M. J. Simpson, D. C. Zhang, M. Mariani, K. A. Landman, and D. F. Newgreen, "Cell proliferation drives neural crest cell invasion of the intestine," *Developmental Biology*, vol. 302, no. 2, p. 553, 2007.

[76] C. Nishiyama, T. Uesaka, T. Manabe, Y. Yonekura, T. Nagasawa, D. Newgreen, H. Young, and H. Enomoto, "Trans-mesenteric neural crest cells are the principal source of the colonic enteric nervous system," *Nature Neuroscience*, vol. 15, no. 9, p. 1211, 2012.

[77] M. J. Simpson, K. K. Treloar, B. J. Binder, P. Haridas, K. J. Manton, D. I. Leavesley, D. L. S. McElwain, and R. E. Baker, "Quantifying the roles of cell motility and cell proliferation in a circular barrier assay," *Journal of The Royal Society Interface*, vol. 10, no. 82, p. 20130007, 2013.

[78] M. J. Simpson, K. A. Landman, and B. D. Hughes, "Multi-species simple exclusion processes," *Physica A: Statistical Mechanics and its Applications*, vol. 388, no. 4, p. 399, 2009.

[79] R. Haberman, *Applied Partial Differential Equations: With Fourier Series and Boundary Value Problems*. Pearson Prentice Hall, 2004.

[80] K. Levenberg, "A method for the solution of certain nonlinear problems in least squares," *Quarterly of Applied Mathematics*, vol. 2, p. 164, 1944.

[81] D. W. Marquardt, "An algorithm for least-squares estimation of nonlinear parameters," *SIAM Journal on Applied Mathematics*, vol. 11, p. 431, 1963.

[82] M. Weiss, "Crowding, diffusion, and biochemical reactions," *New Models of the Cell Nucleus: Crowding, Entropic Forces, Phase Separation, and Fractals*, vol. 307, p. 383, 2013.

[83] M. J. Saxton, "Wanted: a positive control for anomalous subdiffusion," *Biophysical Journal*, vol. 103, no. 12, p. 2411, 2012.

[84] F. Hfling and T. Franosch, "Anomalous transport in the crowded world of biological cells," *Reports on Progress in Physics*, vol. 76, no. 4, p. 046602, 2013.

[85] J. Mittal, J. R. Errington, and T. M. Truskett, "Using available volume to predict fluid diffusivity in random media," *Physical Review E*, vol. 74, no. 4, p. 040102, 2006.

[86] M. Ganjeh-Ghazvini, M. Masihi, and M. Ghaedi, "Random walkpercolation-based modeling of two-phase flow in porous media: Breakthrough time and net to gross ratio

estimation," *Physica A: Statistical Mechanics and its Applications*, vol. 406, p. 214, 2014.

[87] M. A. A. da Silva, G. M. Viswanathan, and J. C. Cressoni, "A two-dimensional non-markovian random walk leading to anomalous diffusion," *Physica A: Statistical Mechanics and its Applications*, vol. 421, p. 522, 2015.

[88] T. Bauer, F. Hfling, T. Munk, E. Frey, and T. Franosch, "The localization transition of the two-dimensional lorentz model," *The European Physical Journal Special Topics*, vol. 189, no. 1, p. 103, 2010.

[89] M. M. Meerschaert, D. A. Benson, H.-P. Scheffler, and B. Baeumer, "Stochastic solution of space-time fractional diffusion equations," *Physical Review E*, vol. 65, no. 4, p. 041103, 2002.

[90] M. M. Meerschaert and P. Straka, "Fractional dynamics at multiple times," *Journal of Statistical Physics*, vol. 149, no. 5, p. 878, 2012.

[91] M. M. Meerschaert and P. Straka, "Inverse stable subordinators," *Mathematical Modelling of Natural Phenomena*, vol. 8, no. 02, p. 1, 2013.

[92] H. W. Cho, G. Kwon, B. J. Sung, and A. Yethiraj, "Effect of polydispersity on diffusion in random obstacle matrices," *Physical Review Letters*, vol. 109, no. 15, p. 155901, 2012.

[93] T. Ando and J. Skolnick, "Crowding and hydrodynamic interactions likely dominate in vivo macromolecular motion," *Proceedings of the National Academy of Sciences*, vol. 107, no. 43, p. 18457, 2010.

[94] S. R. McGuffee and A. H. Elcock, "Diffusion, crowding & protein stability in a dynamic molecular model of the bacterial cytoplasm," *PLoS Computational Biology*, vol. 6, no. 3, p. e1000694, 2010.

[95] M. J. Skaug, R. Faller, and M. L. Longo, "Correlating anomalous diffusion with lipid bilayer membrane structure using single molecule tracking and atomic force microscopy," *The Journal of Chemical Physics*, vol. 134, no. 21, p. 215101, 2011.

[96] B. J. Sung and A. Yethiraj, "Lateral diffusion and percolation in membranes," *Physical Review Letters*, vol. 96, no. 22, p. 228103, 2006.

[97] F. Hfling, T. Munk, E. Frey, and T. Franosch, "Critical dynamics of ballistic and brownian particles in a heterogeneous environment," *The Journal of Chemical Physics*, vol. 128, no. 16, p. 164517, 2008.

[98] M. Ciela, E. G-N, F. Sagus, and I. M. Sokolov, "Tracer diffusion inside fibrinogen layers," *The Journal of Chemical Physics*, vol. 140, no. 4, p. 044706, 2014.

[99] C. Scholz, F. Wirner, J. Gtz, U. Rde, G. E. Schrder-Turk, K. Mecke, and C. Bechinger, "Permeability of porous materials determined from the euler characteristic," *Physical Review Letters*, vol. 109, no. 26, p. 264504, 2012.

[100] K. Murase, T. Fujiwara, Y. Umemura, K. Suzuki, R. Iino, H. Yamashita, M. Saito, H. Murakoshi, K. Ritchie, and A. Kusumi, "Ultrafine membrane compartments for molecular diffusion as revealed by single molecule techniques," *Biophysical Journal*, vol. 86, no. 6, p. 4075, 2004.

[101] T. Andreescu, D. Andrica, and I. Cucurezeanu, *An Introduction to Diophantine equations: a Problem-Based Approach*. Springer Science & Business Media, 2010.

[102] K. W. Kehr and R. Kutner, "Random walk on a random walk," *Physica A: Statistical Mechanics and its Applications*, vol. 110, no. 3, p. 535, 1982.

[103] M. J. Simpson, K. A. Landman, and B. D. Hughes, "Pathlines in exclusion processes," *Physical Review E*, vol. 79, no. 3, p. 031920, 2009.

[104] K. A. Sharp, "Analysis of the size dependence of macromolecular crowding shows that smaller is better," *Proceedings of the National Academy of Sciences*, vol. 112, no. 26, p. 7990, 2015.

[105] C. A. Athale, A. Dinarina, F. Nedelec, and E. Karsenti, "Collective behavior of minus-ended motors in mitotic microtubule asters gliding toward dna," *Physical Biology*, vol. 11, no. 1, p. 016008, 2014.

[106] H. Yin, X. Wen, and T. Zhou, "Local accumulation time for the formation of morphogen gradients from a lvy diffusion process," *Physical Biology*, vol. 10, no. 5, p. 056012, 2013.

[107] P. R. Taylor, R. E. Baker, and C. A. Yates, "Deriving appropriate boundary conditions, and accelerating position-jump simulations, of diffusion using non-local jumping," *Physical Biology*, vol. 12, no. 1, p. 016006, 2015.

[108] A. Q. Cai, K. A. Landman, and B. D. Hughes, "Multi-scale modeling of a wound-healing cell migration assay," *Journal of Theoretical Biology*, vol. 245, no. 3, p. 576, 2007.

[109] K. K. Treloar, M. J. Simpson, D. L. S. McElwain, and R. E. Baker, "Are in vitro estimates of cell diffusivity and cell proliferation rate sensitive to assay geometry?," *Journal of Theoretical Biology*, vol. 356, p. 71, 2014.

[110] S. T. Johnston, M. J. Simpson, and D. L. S. McElwain, "How much information can be obtained from tracking the position of the leading edge in a scratch assay?," *Journal of The Royal Society Interface*, vol. 11, no. 97, p. 20140325, 2014.

[111] T. Alarcn, H. M. Byrne, and P. K. Maini, "A cellular automaton model for tumour growth in inhomogeneous environment," *Journal of Theoretical Biology*, vol. 225, no. 2, p. 257, 2003.

[112] H. M. Young, A. J. Bergner, M. J. Simpson, S. J. McKeown, M. M. Hao, C. R. Anderson, and H. Enomoto, "Colonizing while migrating: how do individual enteric neural crest cells behave?," *BMC Biology*, vol. 12, no. 1, p. 23, 2014.

[113] D. S. Dean, I. T. Drummond, R. R. Horgan, and A. Lefevre, "Perturbation theory for the effective diffusion constant in a medium of random scatterers," *Journal of Physics A: Mathematical and General*, vol. 37, no. 44, p. 10459, 2004.

[114] A. B. Harris, Y. Meir, and A. Aharony, "Diffusion on percolating clusters," *Physical Review B*, vol. 36, no. 16, p. 8752, 1987.

[115] A. Giacometti, H. Nakanishi, A. Maritan, and N. H. Fuchs, "Ideal chain on a two-dimensional critical percolation cluster," *Journal of Physics A: Mathematical and General*, vol. 25, no. 8, p. L461, 1992.

[116] N. H. Fuchs and H. Nakanishi, "Eigenvalue spectrum of hopping transport on critical percolation clusters," *Physical Review A*, vol. 43, no. 4, p. 1721, 1991.

[117] A. Giacometti and H. Nakanishi, "Eigenspectrum and localization for diffusion with traps," *Physical Review E*, vol. 50, no. 2, p. 1093, 1994.

[118] L. G. Bowden, M. J. Simpson, and R. E. Baker, "Design and interpretation of cell trajectory assays," *Journal of The Royal Society Interface*, vol. 10, no. 88, p. 20130630, 2013.

[119] Y. Saad, *Iterative Methods for Sparse Linear Systems*. Siam, 2003.

[120] S. K. Ghosh, A. G. Cherstvy, D. S. Grebenkov, and R. Metzler, "Anomalous, non-gaussian tracer diffusion in crowded two-dimensional environments," *New Journal of Physics*, vol. 18, no. 1, p. 013027, 2016.

[121] H. M. Taylor and S. Karlin, *An Introduction to Stochastic Modeling*. Academic press, 2014.

[122] R. Serfozo, *Basics of Applied Stochastic Processes*. Springer Science & Business Media, 2009.

[123] J. S. Rosenthal, "Convergence rates for markov chains," *Siam Review*, vol. 37, no. 3, p. 387, 1995.

[124] G. H. Golub and C. F. Van Loan, *Matrix Computations*, vol. 3. JHU Press, 2012.

[125] I. S. Gradshteyn and I. M. Ryzhik, *Table of Integrals, Series and Products (Corrected and Enlarged Edition prepared by A. Jeffrey and D. Zwillinger)*. Academic Press, New York, 2000.

[126] M. J. Simpson, F. Jazaei, and T. P. Clement, "How long does it take for aquifer recharge or aquifer discharge processes to reach steady state?," *Journal of Hydrology*, vol. 501, p. 241, 2013.

[127] A. J. Ellery, R. E. Baker, and M. J. Simpson, "Communication: Distinguishing between short-time non-fickian diffusion and long-time fickian diffusion for a random walk on a crowded lattice," *The Journal of Chemical Physics*, vol. 144, no. 17, p. 171104, 2016.

[128] G. W. Slater and H. L. Guo, "An exactly solvable ogston model of gel electrophoresis: I. the role of the symmetry and randomness of the gel structure," *Electrophoresis*, vol. 17, no. 6, pp. 977–988, 1996.

[129] D. Chandler and J. K. Percus, "Introduction to modern statistical mechanics," *Physics Today*, vol. 41, p. 114, 1988.

[130] H. Scher and E. W. Montroll, "Anomalous transit-time dispersion in amorphous solids," *Physical Review B*, vol. 12, no. 6, p. 2455, 1975.

[131] G. Pfister and H. Scher, "Dispersive (non-gaussian) transient transport in disordered solids," *Advances in Physics*, vol. 27, no. 5, p. 747, 1978.

[132] A. Klemm, H.-P. Müller, and R. Kimmich, "Nmr microscopy of pore-space backbones in rock, sponge, and sand in comparison with random percolation model objects," *Physical Review E*, vol. 55, no. 4, p. 4413, 1997.

[133] A. Klemm, H.-P. Müller, and R. Kimmich, "Evaluation of fractal parameters of percolation model objects and natural porous media by means of nmr microscopy," *Physica A: Statistical Mechanics and its Applications*, vol. 266, no. 1, p. 242, 1999.

[134] M. Bromly and C. Hinz, "Non-fickian transport in homogeneous unsaturated repacked sand," *Water Resources Research*, vol. 40, no. 7, 2004.